8-2015

FEASIBILITY ANALYSIS OF STEAM VENTILATION IN SUPERCAVITATION DESIGN

Austin Culberson
Clemson University, aculber@clemson.edu

FEASIBILITY ANALYSIS OF STEAM VENTILATION IN SUPERCAVITATION DESIGN

A Thesis
Presented to
the Graduate School of
Clemson University

In Partial Fulfillment
of the Requirements for the Degree
Master of Science
Mechanical Engineering

---

by
Austin Culberson
August 2015

Accepted by:
Dr. Jay M. Ochterbeck, Committee Chair
Dr. Chenning Tong
Dr. Xiangchun Xuan

ABSTRACT

The complete envelopment of a submerged object by a continuous cavity, or supercavity, results in significant reduction of the skin drag acting on the object, allowing for substantial increases in the maximum speeds of underwater devices. The formation of supercavities often requires supplemental ventilation, traditionally by non-condensable gasses, as natural supercavitation occurs at relative speeds between the object and liquid medium that are infeasible for the device to reach without supercavitation itself. The aim of this research is to investigate the feasibility of vaporous ventilation in supercavitation design with the hope of reducing non-condensable ventilation requirements which are inherently limited in their supply for submerged devices. Specifically, the partial or complete replacement of non-condensable gasses with steam for ventilated supercavitation was investigated to determine the effect on cavity development and ventilation requirements.

While the use of vaporous ventilation gasses was unfound throughout the extensive literature review, a theoretical analysis which drew from various ventilation scenarios of steam insertion into liquid pools or flows suggested limited potential for the sole use of steam as a ventilation gas. In addition to a theoretical evaluation, cavitator systems were designed and tested to obtain both qualitative and quantitative results. Modest increases in the cavity volume and length were seen for very specific combinations of concurrent ventilation of steam and air relative to air only ventilation. The overall advantages appear extremely limited, however, as the ventilation requirements for steam addition are

roughly an order of magnitude larger compared to the required increases of non-condensable ventilation for the production of similar results. Steam alone was shown to be entirely incapable of generating continuous cavitation structures for the range of steam flowrates tested, the upper limit being over three orders of magnitude larger than the critical air ventilation flowrate needed for successful creation of a continuous attached cavity. As such, the advantages of steam ventilation in supercavitation design appear very limited at best when compared to the relative ease of ventilated supercavity development by non-condensable gasses.

ACKNOWLEDGMENTS

Special thanks to Dr. Jay M. Ochterbeck for his continued support, encouragement, and friendship.

TABLE OF CONTENTS

LIST OF FIGURES

NOMENCLATURE

Symbols

ρ	-	density at bulk flow temperature [M/L^3]
σ	-	cavitation number [dimensionless]
A	-	cross-sectional area [L]
D	-	cavitator diameter [L]
d	-	diameter/spacing between wall and offset jet [L]
K	-	geometry constant [dimensionless]
$\dot{m}$	-	mass flowrate [M/t]
P	-	pressure [M/Lt^2]
Q	-	volumetric flowrate [L^3/t]
Q^*	-	air-entrainment coefficient [dimensionless]
R	-	radius of cavitation nuclei [L]
S	-	surface tension [M/t^2]
T	-	temperature [T]
U	-	relative velocity [L^2/t]
w	-	height of jet nozzle [L]
x	-	downstream distance [L]

Subscripts

a	-	ambient or local value of parameter
b	-	parameter value for bubble
c	-	choked condition/parameter value for cavity
cp	-	combine point of wall and offset jet
l	-	parameter value for liquid phase
mp	-	initial merge point of wall and offset jet
r	-	reference value
s	-	steam
T	-	parameter value for tunnel
v	-	parameter value for vapor phase
w	-	water
∞	-	free stream value

CHAPTER 1: FUNDAMENTALS OF CAVITATION

Cavitation refers to the formation of cavities within an initially homogeneous liquid as a result of the local pressure dropping below a critical threshold, generally taken as the vapor pressure of the liquid. Such cavities are comprised of a mixture of vaporized liquid and non-condensable gasses diffused through the liquid-vapor interface from the bulk liquid [1]. Cavities that result from cavitation alone are often assumed to be purely vaporous as they result from the vaporization of the liquid itself, which in many applications has limited concentrations of non-condensable gasses. Cavities can also be achieved through the artificial ventilation of gasses in order to create a mostly gaseous cavity, where gaseous is used here and in all subsequent occasions to refer to a non-vaporous, non-condensable gas. Although little to no actual cavitation of the flow may occur in such cases, this is a common cavitation design practice referred to as ventilated cavitation.

The extent of cavitation can vary depending on the fluid properties, flow characteristics, and geometry. Supercavitation refers to the extreme case of complete and sustained envelopment of a submerged object by a continuous gaseous or vaporous cavity. Only the nose, commonly referred to as the cavitator, and any control surfaces of the supercavitating device remain in contact with the liquid, resulting in a significant reduction of the object's wetted surface area and thus a reduction of the skin drag acting on the object [2]. Between sixty and seventy percent total drag reduction is commonly

cited for supercavitating devices with some researchers quoting up to ninety percent reduction of drag, resulting in significant increases in the maximum speeds of underwater objects and associated gains in acceleration and range [3, 4, 5].

Similarly, the presence of cavities along the hulls of ships also provides a means by which skin drag can be significantly reduced. It is common for such ships, referred to as air cavity ships or ACS, to have recesses in the hull in which a partial, stable cavity can be maintained at minimal ventilation requirements. Total drag reduction of between ten and thirty percent is commonly cited for such designs with ventilation requirements consuming less than two percent of total power generation[1] [6].

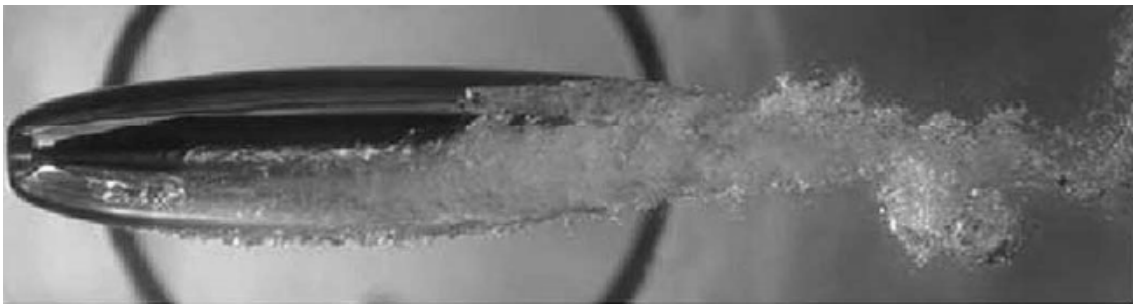

Figure 1. Example of supercavitation at Saint Anthony Falls Laboratory. Taken from Arndt et al. [7].

The fundamentals of cavitation will be discussed below with specific regard to development and behavior of attached cavitation structures. Additional details of the cavitation process not directly relevant to the present research can be found in the books

[1] This method should not be confused with micro-bubble drag reduction techniques which rely on small bubbles along the hull to reduce skin drag.

of Franc and Michel, Knapp, Daily and Hammitt, and Brennen as well as the extensive literature concerning cavitation [8, 2, 9].

A. The Cavitation Process

From a conventional thermodynamic viewpoint, traversal of the liquid-vapor curve from an initial liquid state results in vaporization of the liquid. For approximately isobaric heating, this phase change is referred to as boiling while the term cavitation is used to describe vaporization resulting from approximately isothermal pressure reduction. Expanding this definition, cavitation is distinguished from boiling in that, for cavitation, vaporization occurs primarily as a result of pressure reduction as opposed to heat addition. For cavitation, the point of traversal between liquid and vapor is defined by the saturated vapor pressure at a given temperature, $T_{sat,}$ of the liquid, explaining the common definition of cavitation as the vaporization of a fluid due to local pressure reduction below the vapor pressure. A detailed analysis using conventional hydrostatic principles and macroscopic properties supports this assumption while allowing for often predictable departures from this model to be accounted for [10].

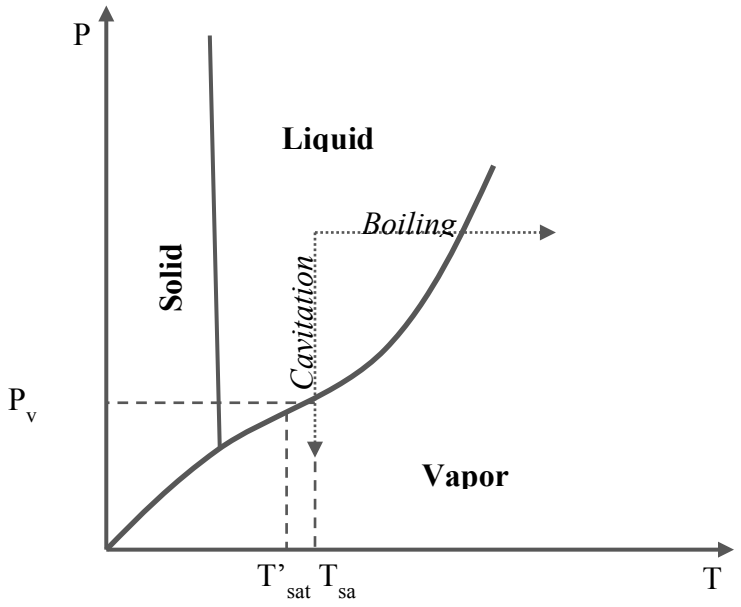

Figure 2. Pressure vs. temperature plot with phase regions showing primary difference between cavitation and boiling as well as the temperature depression resulting from the cavitation process.

Microscopically, cavitation can be thought of as the breakdown of the liquid medium as a result of pressure variations in which a critical pressure threshold is exceeded [10, 9]. The pressure threshold below which liquid cohesion is no longer guaranteed has been classically given as the vapor pressure of the fluid. Research has shown that for highly controlled cases, the liquid is significantly stronger than proposed by the assumption of a threshold defined by the vapor pressure, as pressures well below the vapor pressure can be maintained without vaporization occurring, resulting in a metastable superheated liquid. This delay of vaporization is often referred to as the static delay to cavitation [10]. The discrepancy can be accounted for through the inclusion of surface tension effects which increase the theoretical cohesive strength of the liquid.

The theoretical limit of liquid superheat is defined by the combination of a given equation of state and the criteria for thermal, mechanical, and phase equilibrium, all of which combine to give the spinodal limit at a given saturation state [11]. Such calculations often show the theoretical superheat limit to occur at very significant negative pressures, well into the thousands of bars for water, in which case the liquid is in tension. Cavitation research with "real" water as opposed to "ideal" water consistently shows liquid breakdown for pressures well above the theoretical pressure threshold however [12, 10]. This departure from theory can be attributed to a number of factors, the primary of which being the existence of impurities within the liquid in the form of gas or vapor inclusions [13]. These inclusions, known as cavitation nuclei, serve as points of weakness in the flow whose growth in the presence of low pressures is the catalyst for cavitation inception [10, 11, 14].

Turning to a more practical analysis of cavitation in real flows, the aforementioned cavitation nuclei are inherently present in the flow, typically as either gas or vapor bubbles suspended in the flow or along solid surfaces although other sources and theories can also explain their seemingly pandemic existence [12, 13]. The initial growth of these nuclei is referred to as incipient cavitation and is characterized by the formation of individual bubbles within local cavitation zones with the bubbles often collapsing as a result of hydrostatic instability upon exiting the low pressure region. The critical pressure for growth depends on the size of the nuclei with larger nuclei being more susceptible to growth. The flow field also plays an important role in incipient cavitation as bubble

growth requires sufficient time for the nucleation sites to remain within favorable, low pressure regions. Thus, for flows in which the cavitation nuclei transverse the critical pressure region faster than the time required for bubble growth, cavitation may not occur even though the critical pressure exists [2].

Larger concentrations of nuclei and increased local cavitation promote coalescence and the formation of larger cavitation structures. As the cavitation zone is increased and individual bubbles grow and coalesce, developed cavitation is achieved and is characterized by a semi-permanency [10]. In the event of extensive coalescence, a continuous cavity may form. If such a cavity consequently collapses along a surface, it is referred to as partial cavitation whereas supercavitation is achieved if the individual cavity continues to grow, eventually becoming large enough to collapse aft of the surface [15]. As partial and supercavitation are defined relevant to a surface, these forms of cavitation are often, and will here be, referred to as attached cavitation. Cloud cavitation refers to developed cavitation spanning a region while still being characterized by the growth of individual cavitation nuclei which remain largely unique.

Cavitation can also be described by its location relative to an object in the flow as well as by its temporal behavior. For local cavitation, individual cavitation bubbles are often carried along by the flow, a scenario referred to as traveling cavitation. As the bubbles remain largely unique, traveling cavitation is common for the early stages of cavitation. Conversely, attached or fixed cavitation refers to quasi-stable cavitation where the flow detaches from a solid boundary, resulting in a continuous cavity along the solid

boundary, occurring for both partial and super cavities as previously mentioned. Sheet or vortex cavitation may also occur as a result of cavitation in highly turbulent shear layers or in the vortex cores in the wake of a body, respectively. Vibratory cavitation can also occur as the result of pressure fluctuations within a liquid due to high frequency, high amplitude vibrations [2].While the above qualification of cavitation forms and stages appears to clearly distinguish cavitation regimes, cavitating flows are often a compilation of various modes. For example, it is common for traveling cavitation to occur in the flow around fixed cavities, leading to complicated interaction of the two modes.

B. The Cavitation Parameter

Cavitation is dependent on numerous parameters including flow characteristics such as velocity, hydrostatic pressure, turbulence, gas content, and temperature, as well as the geometry of the flow and any objects within it. The complex interaction of these parameters prohibits the creation of a comprehensive cavitation model. A common parameter known as the cavitation number or cavitation parameter is, however, used to quantify the susceptibility and extent of cavitation with the above mentioned parameters resulting in often predictable deviation from the predicted behavior.

The non-dimensional cavitation number is defined as,

$$\sigma = \frac{p_r - p_v(T)}{\Delta p} \tag{1}$$

where p_r is some conveniently defined reference pressure, $p_v(T)$ the vapor pressure at the bulk liquid temperature, T, and Δp a pressure difference that characterizes the

hydrodynamics of the cavitation scenario. The cavitation parameter physically represents a ratio between the pressure opposing the existence of a cavity to that promoting cavity inception and growth [2]. For the case of cavitation in which there is relative motion between an object and the flow Eq. (1) takes the form,

$$\sigma = \frac{p_\infty - p_v(T)}{\frac{1}{2}\rho_L V_\infty^{\,2}} \tag{2}$$

where p_∞ is the freestream static pressure taken sufficiently upstream to avoid any cavitation effects and the denominator is given by the dynamic pressure where ρ_L is the freestream fluid density and U_∞ is the relative velocity between the object and the freestream flow. The dynamic pressure is used as the potential for cavitation due to pressure variations is fundamentally a result of the velocity variation of the flow along the surface of the body as predicted by potential flow theory. Note that Eq. (2) accounts for any relative motion between the object and flow and is thus independent of absolute object motion, allowing for supercavitation research to be performed using flow about a stationary object.

As the above definition does not account for the partial pressure of non-condensable gasses in the cavity, the cavitation parameter has little physical significance for the case of ventilated cavitation. An alternative parameter referred to as the relative underpressure by Franc and Michel is used for describing the ventilated case [10]. Defining the cavity

pressure, p_c, as the sum of the partial pressures of vapor and gas in the cavity, the non-dimensional relative underpressure can be defined as,

$$\sigma_c = \frac{p_r - p_c}{\Delta p} \tag{3}$$

or, for flow about an object,

$$\sigma_c = \frac{p_\infty - p_c}{\frac{1}{2}\rho_L V_\infty^{\,2}} \tag{4}$$

Eq. (4) will be referred to as the ventilated cavitation number, σ_{vent}, and relative underpressure interchangeably for the remainder of this work.

From examination of the cavitation number and relative underpressure definitions, we see that the difference is in the assumed composition of the cavity and subsequently, the cavity pressure. In fact, the relative underpressure is also valid for the case of natural cavitation as it accounts for the presence of non-condensable gas in the cavity, whether through diffusion from the free-stream or gaseous bubbles initially trapped along the solid surface. The concentration of such gases is often neglected in the case of natural supercavitation, however. This simplification combined with the theoretical assumption that cavitation occurs for pressures approaching the vapor pressure results in the assumption that the cavity pressure can be approximated by the vapor pressure as seen in Eq. (1). This assumption has been experimentally proven to be valid for a majority of circumstances and is thus commonly used in the definition of the cavitation number. Similarly, the partial pressure of vapor is often neglected for ventilated cavities in which

the conditions for incipient cavitation are not met and vapor diffusion across the cavity interface can be neglected [10].

The cavitation number is useful in that it allows for a quantification of both the likelihood and extent of cavitation development for a flow. For flow about an object, the cavitation number is based on the flow itself while its interpretation is dependent on the object configuration. Consequently, the response of a system corresponding to a cavitation number is specific to the system itself. In other words, for two systems in flows of identical cavitation numbers, the extent and type of cavitation experienced may vary drastically based on the geometry of the objects and the composition of the flow.

The likelihood and extent of cavitation is maximized for decreasing cavitation numbers with supercavitation occurring for very low cavitation numbers, often less than 0.1 [7]. The largest cavitation number for which supercavitation occurs is commonly identified for a given geometry to serve as a benchmark. Upon the creation of a supercavity, further reduction of the cavitation number signifies a reduction in the pressure difference between the cavity and the ambient flow, consequently reducing the cavity curvature resulting in an increase in the cavity length [10].

For natural cavitation, the incipient cavitation number, denoted by σ_i, which quantifies the maximum cavitation number for which local cavitation can be identified, is also commonly cited. Due to the static delay in cavitation which is highly dependent on the nuclei concentration and other factors such as the smoothness of test section walls and

the flow field, all of which can be extremely difficult to accurately control in experimental setups, the incipient cavitation number can show great variability between various experimental cases. It has been shown that the point at which cavitation disappears, or desinent cavitation number, σ_D, is much less dependent on such factors and can thus be used in place of the incipient cavitation number [2]. Again, these values are a characteristic of the geometry rather than the flow and are thus more or less constant across a range of flow scenarios for a given geometry.

The process by which the cavitation number was defined relied on the assumption that gravitation affects were negligible. In fact, for small cavities or during the formation of individual cavitation bubbles such as in the incipient cavitation stage, gravity will have very little effect at all. As cavity size increases, the effects of gravity do as well, often becoming significant for the supercavitation case; the buoyancy of the cavity results in an upward curving asymmetry of the cavity as seen in Figure 3.

The effect of gravity on cavitation also points to the relationship between cavitation and the Froude number based on the length of the cavity,

$$Fr_l = \frac{U}{\sqrt{gL_c}} \tag{5}$$

where U is the characteristic velocity and L_c is the cavity length. As the Froude number is effectively a ratio between the inertial and gravity effects on a flow, the influence of gravity will be more pronounced for decreasing Froude numbers. It has been shown that

the cavitation number also drops for increasing Froude number; this is to be expected as the cavitation number is inversely dependent on velocity as seen in Eq. (2) with inertial effects dominating for large cavitation numbers corresponding to slower flows [7]. Gravity effects are often very significant in ventilated supercavitation as the ventilation allows for supercavities to be created at significantly reduced velocities, and hence smaller Froude numbers, compared to natural supercavitation.

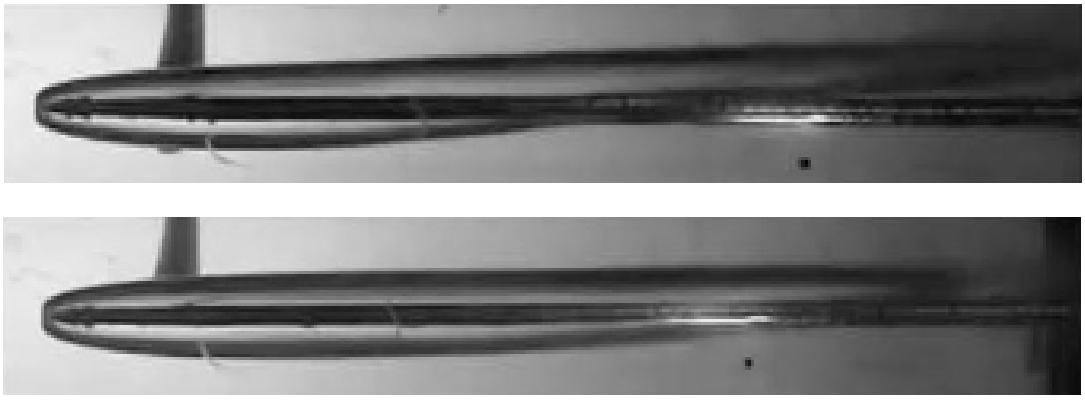

Figure 3. Effect of gravitational forces on cavity shape. The upper picture is for a flow with $\sigma = 0.046$ and $Fr_l = 17.5$ while the bottom is that of a flow with $\sigma = 0.047$ and $Fr_l = 35.0$. Taken from Zhang et al. [16].

Temperature also has a significant impact on natural cavitation as the cavity pressure, and thus the cavitation number, is dependent on the vapor pressure. For temperatures approaching the critical point, the vapor pressure is significantly increased, consequently decreasing the cavitation number and thus the likelihood of cavitation. The increase in cavitation potential for increasing temperature is not unopposed, however. As vaporization is an endothermic process, cavitation requires the energy for vaporization to

be supplied from a thin shell of liquid surrounding the vaporization interface, resulting in a lowering of the local temperature and thus a lowering of the cavity temperature as vaporization proceeds. The saturation pressure is subsequently reduced and the cavitation number increases, leading to a retardation of the cavitation process; this effect is referred to as the thermal delay in cavitation [10, 2]. The overall effect of this thermal delay depends on the thermal sensitivity of the fluid and increases for temperatures approaching the critical temperature. For many fluids such as water, the vapor pressure does not vary drastically for temperatures well below the critical point and thus the thermodynamic effect may be appropriately neglected in cavitation development. Conversely, it often has a substantial effect for cavitation in cryogenic fluids as the critical temperature is commonly approached [15]. This effect can be seen for both large and small scale natural cavitation structures, i.e. supercavities and individual bubbles [9].

In summary, the extent to which cavitation occurs and the mode by which it is achieved varies according to various parameters. A general trend is present, however. Incipient cavitation occurs when the pressure drops below a critical value, whether from static or dynamic effects, and is characterized by the formation of localized cavities in the form of small cavitation bubbles. As the cavitation number is further decreased the extent of cavitation increases through the growth and coalescence of cavitation bubbles leading to the formation of one or more continuous cavities. For sufficiently low cavitation numbers, an attached cavity will develop that partially or completely envelops the body. Again, the cavitation number at which each cavitation stage occurs is dependent on

numerous factors including the flow properties, body geometry, and mode by which cavitation occurs.

C. Behavior of Attached Cavitation Structures

The above discussion developed the fundamentals of cavitation from a thermodynamic perspective with discussion of the important parameters for the cavitation process, as well as outlining the process itself. The following sections focus exclusively on attached, partial and super cavities including traditional cavitation design practices. A brief discussion of experimental procedures in cavitation research concludes the section.

1. Cavity Detachment

The presence of attached cavities, both partial and super, requires detachment of the cavity from the solid surfaces about which they form. Franc and Michel identify two primary models for describing the exact location of this detachment for the case of attached cavities formed by natural cavitation. The Villat-Armstrong detachment criterion, which assumes an inviscid fluid, proposes that the cavity detachment occurs at the point of minimum pressure along a solid surface as the cavity itself is a zone of minimum pressure within the flow. Using this criterion, the detachment location is solved for iteratively with an initial guess based on non-cavitating conditions and subsequent guesses accounting for the presence of cavitation structures as such structures often cause a shift in the pressure field about the object. As attached cavitation requires flow separation, detachment at the point of minimum pressure cannot be completely valid as an adverse pressure gradient does not yet exist as needed for flow separation [10].

Laminar Separation Criterion is an alternative model which takes into account viscous effects, especially the presence of a boundary layer [17]. This model is based on the observation that cavitation inception and development occurs in the recirculation zones following laminar flow separation with Franc and Michel showing that it also applies to supercavities [18, 10]. The model additionally accounts for surface tension effects which serve to curve the detachment interface, resulting in a cavity detachment point slightly behind the boundary layer separation point as shown in Figure 4. The research of Franc and Michel support this model by showing that cavity detachment is always downstream of a separation point; the separation point and subsequent dead zone shield the cavity from the oncoming flow, allowing it to remain attached to the surface rather than being swept away [10].

If the point of minimum pressure and the boundary layer separation point correspond, such as at an abrupt geometry change, there will be little difference between the two models as this also corresponds to the location of cavity detachment, with the Laminar Separation Criterion becoming more accurate for departure of the separation point from the point of minimum pressure [10]. The detachment process of ventilated cavities is often simpler as it generally occurs at the point of ventilation in the case of supercavitating foils or at the edges of a sharp edged cavitator or backward step behind which ventilation occurs for supercavitating projectiles or ACS respectively. It is important to note that cavitation is in no way guaranteed by boundary layer separation as it is still dependent on the absolute pressure rather than the pressure gradient within the

flow, e.g. a sufficiently large adverse pressure gradient may exist such that flow separation occurs, but if the absolute pressure in this separation zone is still higher than the vapor pressure then cavitation will not occur [2].

Brennen notes that the attached cavity is often glassy immediately following the separation point as the separation often occurs while the flow is still laminar about the body. As the flow transitions to turbulent, the cavity interface becomes clouded, appearing as a frothy mixing region [9]. As for the freestream flow, in the transition from laminar to turbulent flow, boundary layer separation is increasingly suppressed and traveling cavitation dominates as steady cavities are incapable of attaching to the wall. Pressure variations resulting from partial cavitation may be significant enough to allow boundary layer separation and thus allow the cavity to become attached [10].

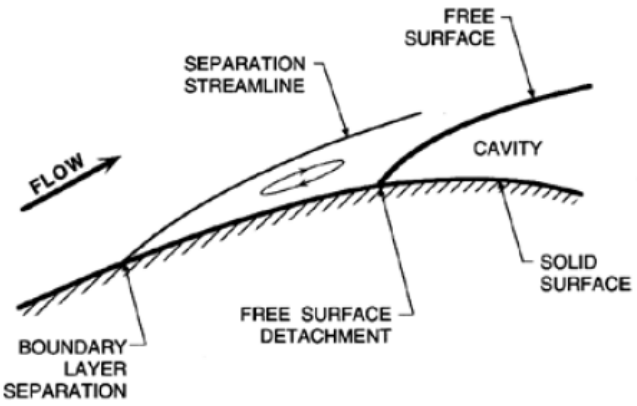

Figure 4. Diagram showing an attached cavity with smooth cavity detachment. Notice the delay of the detachment from the boundary layer separation point. Taken from Brennan [9].

Cavitation nuclei can be activated in the low pressure zone preceding an attached cavity, forming a region of mixed cavitation called the mixed cavitation band where

bubble cavitation occurs upstream of an attached cavity [10]. This region is minimized for increasing seed rate as the bubble regime expands. Saturation can also occur where the concentration of bubbles is large enough to allow for coalescence and formation of a quasi-continuous cavity which is roughly at the vapor pressure and expands upstream for increasing nuclei rates [10]. Briancon-Marjollet also demonstrated that the implosion of cavitation bubbles can result in local turbulence about the cavity interface, potentially causing the boundary layer to reattach, thus destroying the mechanical equilibrium of the cavity and resulting in a portion of the attached cavity being swept outwards and carried along by the flow after which the boundary layer can reattach and an attached cavity reform [19]. If the nuclei concentration becomes excessive, reattachment of the cavity is prohibited by the disturbance of successive traveling bubbles and traveling bubble cavitation will replace attached cavitation altogether [10].

2. Cavity Pressure and Closure Models

While cavity detachment is very similar for both partial and supercavitation, closure models are fundamentally different between the two attached cavitation regimes. In general the cavity pressure is assumed uniform throughout a supercavity. The partial pressure of gas is directly proportional to the amount of gas in the flow and is often neglected for natural cavitation, especially if the fluid is sufficiently de-aerated. Similarly, the vapor pressure is often negligible for ventilated cavitation. Assuming non-negative cavitation numbers in which the pressure about the cavity is higher than the cavity pressure, the cavity becomes curved inward as predicted by Euler's equation

applied normal to a streamline, with the streamlines defined by the cavity interface [10]. The convergence of the streamlines at the closure location is conceptually similar to a stagnation point in which a portion of the flow is carried into the cavity itself; this inward flow being referred to as a re-entrant jet.

Neglecting condensation and diffusion, the cavity's contents are confined to the cavity and cannot escape as a result of cavity closure. In order to maintain mass balance, there must exist some evacuation mode to counter vaporization of the liquid and diffusion of any gasses into the cavity for the case of natural cavitation. The impingement of the afore-mentioned re-entrant jet on the cavity interface causes the portion of the cavity aft of the jet-interface contact location to separate and be swept downstream. Development of the re-entrant jet and shedding of the cavity alternate continuously, resulting in pulsation of the cavity [10]. For high velocity flows and relatively short cavities in which the re-entrant jet has sufficient momentum to reach the front of the cavity, the entire cavity may be released.

For lower velocity flows, the jet may have insufficient momentum to overcome entrainment along the cavity interface, resulting in smaller amplitude, higher frequency pulsations with only portions of the cavity being released [9]. Knapp et al. further describe the mechanism of complete and partial cavity detachment by noting that the impingement of the jet on the interface results in an instantaneous and concentrated pressure increase, allowing for the flow to again follow the guiding surface and thus release the attached cavity [2].

The detached bubble cloud has a large circulation associated with it as a result of the opposing momentum of the jet relative to the cavity interface which serves to maintain a circular structure of the bubble cloud until its eventual, and often violent, collapse [20]. In the event of axisymmetric flow, this circulation and periodic shedding takes the form of periodic toroidal vortices [10]. The cyclic nature of the cavity can be avoided for supercavities of sufficient length where the impingent flow is entrained along the cavity walls, resulting in the quasi-stable characteristics of fully developed supercavities [21].

Brennen notes that the jets are not as clean as the re-entrant model may suggest but are rather a "frothy turbulent mass tumbling back into the cavity" [9]. The wake itself is highly turbulent and often contains alternate vortices which entrain the released gases and vapors, resulting in secondary cavitation structures. It should be noted that while the re-entrant jet closure model is based on numerous experimental observations and is widely accepted, some researchers question its accuracy and offer other explanations ranging from leading edge jet theory by Kubota and a flow recirculation zone that periodically disturbs the cavity as described by Hoekstra [22, 23]. Avellan et al. also provide a model for cavity closure more specific to sheet cavitation, citing instabilities along the cavity interface as the reason for the apparent instability of sheet cavitation [24]. Similarly, Franc and Michel discuss the periodic "jump" of turbulence from the rear to the front part, leading to a periodic shedding of attached cavities about hydrofoils [10].

The non-condensable nature of traditional ventilated supercavitation results in several different modes of evacuation compared to the natural case; the lack of

condensation also increases the potential for secondary cavitation structures downstream of the cavity. For large Froude number and cavity underpressure, the cavity is axisymmetric as gravitational effects are negligible and cavity closure is by an unstable re-entrant jet as discussed above. Consequently, the closure region is filled with foam. The outer foam is entrained and convected away by the outer flow through entrainment while the inner regions move as a counterflow, resulting in the formation of periodic ring, or toroidal, vortices [10].

For moderate Froude numbers and smaller cavity underpressures in which the cavity becomes elongated and the effect of gravity is increased, cavity closure is characterized by two opposing hollow vortex tubes. These tubes are highly effective at removing large concentrations of the ventilation gas continuously and are typically more stable and less turbulent than the re-entrant jet mode [9]. Based on experimental data, Buyvol gives the criterion for this closure model as,

$$\sigma_c^{3/2} Fr^2 < 1.5 \tag{6}$$

with the re-entrant jet closure model applying for values larger that the critical value [25].

As the ventilation rate is further increased, to a point at which ventilation rates are in excess of that which can be removed by the above mentioned closure models, a transition occurs where ventilation gas evacuation occurs through the periodic shedding of large air pockets or bubble clouds [9]. This occurs as variation of the cavity pressure generates undulations along the cavity interface, the meeting of which result in the pinching off of

an air pocket [2]. As mentioned by Franc and Michel, these pockets have been found to consist of small bubbles in alternate vortices rather than being a continuous cavity [10]. The susceptibility of a cavity to instabilities arising from small perturbations is quantified by the stability parameter, β, defined as the ratio of natural to ventilated cavitation numbers or $\beta = \frac{\sigma}{\sigma_v}$. $\beta = 1$ for naturally cavitating flows and increases for increasing ventilation with a critical limit above which any disturbances along the cavity grow unstably [26, 27].

3. Traditional Supercavitation Design Theory

Three primary design tactics have arisen over decades of cavitation research for promoting cavitation in flows. These include reduction of the ambient pressure of the flow, increasing the cavity pressure through artificial ventilation of non-condensable gasses, and increasing the relative velocity between the flow and the object, each largely corresponding to the three terms found in the definition of the cavitation parameter. The opposite corollaries of these tactics are used to prevent cavitation from occurring, such as in the design of turbo-machinery in which cavitation erosion should be minimized.

Recall that the cavitation parameter for relative flow between a liquid and an object is given by,

$$\sigma_c \widehat{=} \frac{P_\infty - P_c}{\frac{1}{2}\rho_L {U_\infty}^2}$$

with the likelihood and extent of cavitation increasing for decreasing cavitation numbers. Also recall that due to the dimensionless properties of the cavitation parameter, physically similar cavitation responses can be achieved regardless of technique assuming consistent cavitation numbers and appropriate scaling of flow parameters.

Let us first consider the reduction of the freestream or reference pressure term, P_∞. According to cavitation theory, the likelihood and extent of cavitation increases for decreasing pressure about the object. Such an adjustment is generally only possible in the controlled environment of experimental testing in which the reference pressure can be artificially controlled, typically through the use of a vacuum component as commonly found in cavitation tunnels. For flow in an open channel or infinite flow field, the pressure is simply a function of the ambient pressure and depth of the object, and thus largely out of the designer's control. Consequently, this process is largely constrained to experimental testing but is an extremely important technique as it allows for cavitation research to be performed at reduced velocities compared to the actual application.

Conversely, increasing the cavity pressure, P_c, serves to reduce the cavitation number. Such is the premise for ventilated cavitation where non-condensable gases are used to artificially increase the cavity pressure. This is a rather common design practice for supercavitating devices, the Russian Shkval torpedo being perhaps the most famous example. Typical sources of the ventilation gas include exhaust gasses from propulsion systems or onboard gas tanks [28]. A simple air compressor is often used for experimental setups or for surface vessels with ventilation technology.

For the case of a naturally cavitating object in an open flow in which the pressure terms are largely fixed and no ventilation is present, maximization of the relative velocity between an object and the flow, U_∞, becomes the dominant design parameter as the cavitation number decreases with the square of the freestream velocity. Unfortunately, this technique is often limited by propulsion capabilities and the presence of large skin drags prior to cavity development, prohibiting the ability of the object to reach the speeds required for natural cavitation, much less supercavitation [21]. The variation of velocity has little effect in and of itself. Rather, it is the variation of the dynamic pressure term as given by $\frac{1}{2}\rho U^2$ resulting from the increased velocity of the flow about an object that explains the increase in cavitation potential. From fundamental fluid mechanics, the hydrostatic pressure distribution around a body is a function of the flow velocity, with higher velocities resulting in larger dynamic pressure variations corresponding to reductions of the static fluid pressure about the body. In the event of local hydrostatic pressure reduction below the critical pressure, natural cavitation will occur with expansion of the low pressure region allowing for the growth of cavitation nuclei and subsequent formation of larger cavitation structures. The use of ventilation can also assist this process through the provision of excess cavitation nuclei.

As seen from the above discussion, the three primary techniques for increasing hydrodynamic cavitation are all quite limited. Rather than focusing solely on the reduction of the cavitation number of the flow, it is also possible to reduce the critical cavitation number for which a given geometry will experience cavitation however. Take

for instance a streamlined body and a blunt body subjected to an identical flow in which the free stream velocity is continually increased. The static pressure reduction about the streamlined body will be minimal compared to the blunt body. Consequently, the streamlined body will require a lower cavitation number of the flow before incipient cavitation is achieved. In other words, the blunt body will experience a larger fluid pressure drop and hence reach the critical pressure for cavitation before the streamlined body. Even in the event of cavitation initiation, attached cavities may not form along the streamlined body due to the lack of boundary layer separation whereas the blunt body will likely experience attached cavitation as a result of flow separation and/or vortex cavitation in its wake.

The effect of geometry on pressure variation resulting in cavitation development highlights the reason that cavitator design is an essential aspect of supercavitation design. Cavitators, often in the form of a disc with its symmetric axis parallel to the flow, are designed to maximize the pressure variation along its surface or in its wake, resulting in sufficiently low pressures to allow for nucleation site growth at considerably lower velocities of the free flow [1]. In the case of ventilated supercavitation, the ventilation gas is capable of overcoming the recirculation momentum caused by the adverse pressure gradient in the cavitator wake for sufficient ventilation momentum fluxes, pushing the closure point downstream and allowing for the formation of a gaseous cavity [29].

It has been shown that supercavitating bodies are inherently unstable within the cavity due to the location of the center of pressure at or near the cavitator, resulting in

translation and rotation of the body within the cavity with the tail of the body periodically touching or even resting on the cavity interface. This greatly hinders the maneuverability of such devices, with turning angles already limited due to the requirement for the body to remain within the relatively thin cavity. Control surfaces extending into the liquid flow can provide some control as well as adaptive cavitator designs which allow for angled orientation relative to the oncoming flow [28, 30].

4. Ventilated Supercavitation Design Theory

The above discussion has largely assumed vaporization of the fluid itself due to pressure variations, resulting in a vaporous cavity, a process referred to as natural cavitation. The formation of a single, continuous cavity closing aft of the object through this process is subsequently referred to as natural supercavitation and generally occurs for high relative velocities between the object and the flow. Take for example an object submerged 1 meter below a free surface at 1 atm in 20°C water. Assuming supercavitation to occur for $\sigma \leq 0.1$, a velocity in excess of 46 m/s would be required with increases in depth leading to further increases in the required speed. For larger objects, such as torpedoes or submarines, the ability to accelerate to the speeds required for natural supercavitation ironically requires supercavitation itself. Ventilated cavitation, however, relies on gases inserted about a body to artificially produce a cavity, allowing for attached cavitation structures to be realized at much lower speeds than for naturally cavitating devices. While the general appearance and overall behavior of ventilated cavities varies little compared to the naturally cavitating case, the mode of development

is fundamentally different as well as the differences in cavity closure and gravity effects as previously discussed [9].

One of the most commonly used techniques in applied ventilated supercavitation design is to route high pressure exhaust gases through the body of the supercavitating device and out of the cavitator, generally through orifices on the backside of the cavitator. This method is extremely useful for rocket propelled devices as an abundance of exhaust gases are created. The use of a compressed gas source is also possible such as is thought to be used in the design of the supercavitating pontoons of the *Ghost* and in ACS designs [31]. For surface ships, compressed air can be continually produced with a compressor, the power requirements of which must be less than the gains that result from ventilation to be advantageous. For submerged devices without exhaust gas ventilation, this is infeasible, requiring either a pre-filled compressed gas tank or the use of a chemical reaction to produce the gases in flight, both circumstances having considerable supply limitations considering the size constraints generally associated with such a device.

The cavitation number is related to the ventilation flowrate as a function of flow velocity and cavitator diameter by the dimensionless ventilation flux or air entrainment coefficient, Q^*, defined as,

$$Q^* = \frac{Q}{D_c^2 U_\infty} \tag{7}$$

where D_c is the cavitator diameter and Q is the volumetric flowrate of ventilation gases with smaller cavitation numbers corresponding to larger air entrainment coefficients as shown in Figure 5. The dimensionless ventilation rate serves as a key parameter for describing a ventilated supercavity with specific ventilation rates corresponding to specific cavitation numbers.

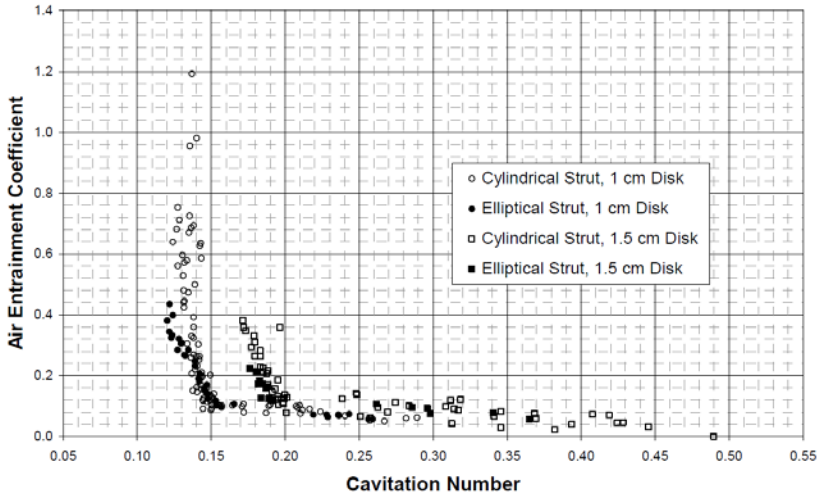

Figure 5. Variation of the air entrainment coefficient vs. cavitation number based on the experimental results of Wosnik et. al. Note the apparent asymptote for a minimum cavitation number. Taken from Wosnik et al [32].

The relationship between air entrainment coefficient and cavitation number is far from linear, having an apparent asymptote at infinity for a minimum cavitation number [33]. Swanson and O'Neill attribute this limit to the transition from the somewhat inefficient cavity evacuation through re-entrant jets to the much more efficient evacuation by either opposing twin vortices or large scale pulsations [34]. This explanation is supported by the results of Kawakami and Arndt which show a decrease in the necessary ventilation rate until the transformation from the reentrant model to the twin vortices

model, after which a minimum cavitation number is quickly achieved and increases in the ventilation rate have minimal effect on cavity behavior and thus little effect on the cavitation number [33, 35]. Similarly, Franc and Michel note that for the re-entrant jet regime, a small increase in the ventilation flux will result in a significant increase in the cavity pressure due to the inability of the reentrant evacuation mode to effectively accommodate the increased ventilation, resulting in a dramatic lowering of the ventilated cavitation number [10]. The limited response of the cavitation number to ventilation changes at low cavitation numbers may also be partially attributed to the choked flow condition in circumstances where such an assumption might apply; however, Kawakami and Arndt point out the difficulty of separating cavity closure and blockage effects [36, 35].

At first glance, this trend appears to be contrary to a physical understanding of the flow as natural cavitation would be expected to increasingly dominate for decreasing cavitation numbers, eventually allowing for the required ventilation flux to go to zero [35]. While this may indeed occur and is useful in that it allows for the production of an initial gaseous cavity by ventilation, and, as the object is able to accelerate to higher speeds at the reduced drag, transition from ventilated to natural supercavitation, it is not guaranteed and highlights the difference between the ventilated and natural cavitation numbers. The development of natural cavitation is linked to the cavitation number as defined for the flow, largely in terms of the vapor pressure. Ventilated cavitation, however, relies on modification of the partial pressure of gas in the cavity due to

ventilation, the effects of which will only remain while ventilation remains, allowing for the creation of identical cavities with respect to size and shape but at much lower velocities, and thus higher cavitation numbers of the flow, than required for natural cavitation. Hence the ventilated cavitation number does not correspond to the cavitation number of the flow and thus has no direct use in determining the likelihood of natural cavitation occurring save for the effect of velocity which serves as the link between ventilated and natural cavitation assuming identical pressure environments. The ventilated cavitation number thus represents an equivalent quantification of cavity development to the natural case.

The proposed decrease in required ventilation flux due to the transition to natural cavitation for decreasing cavitation number is therefor only valid from the standpoint of the flow cavitation number. This transition can in fact occur in the event that ventilation allows for increases in the relative velocity between the object and the flow, effectively lowering the cavitation number of the flow; the natural cavitation number will still remain larger than the ventilated cavitation number as discussed for the effect of ventilation on cavity pressure. Arndt et al. recognize this important distinction and provide a more comprehensive model to account for the transition from ventilated to natural cavitation as a function of the ventilation rate Q,

$$\frac{Q}{A_c U_\infty} = K\left(1 - \frac{\sigma}{\sigma_{vent}}\right) \tag{8}$$

where K is a constant of the geometry [37]. Figure 6 shows a general result of this theory for arbitrary values with the anticipated increase in ventilation flux up to a certain point after which natural cavitation increasingly dominates until no ventilation flux is required. Note that required ventilation flux reaches a maximum after which it is assumed the velocity is sufficient to allow for transition to natural cavitation, eventually requiring no ventilation for the case of a naturally cavitating flow. A hysteretic effect is also common for both 2D and 3D ventilated cavities, requiring lower ventilation rates for the maintenance of a successfully created cavity compared to the required flux for initial cavity creation [21, 10, 37].

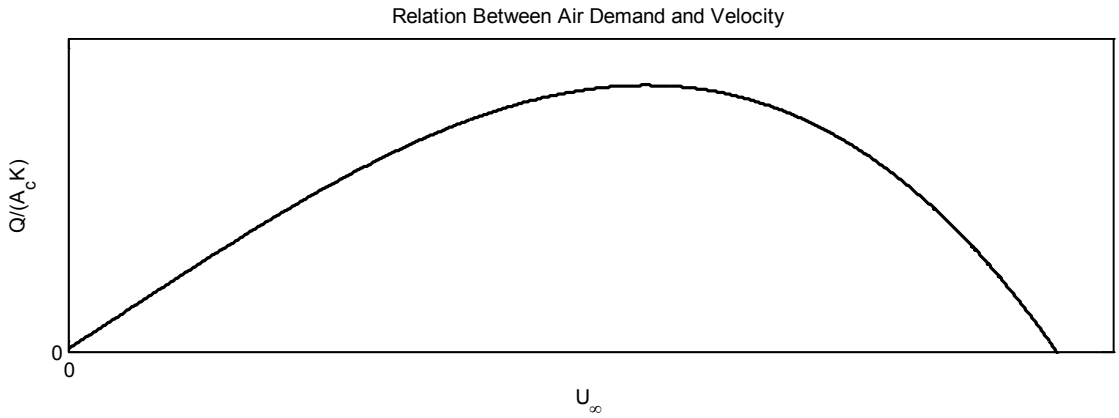

Figure 6. Generalized result of the relation between ventilated and natural cavitation number with respect to flow velocity for a given cavitation number as given by Arndt et al [37].

Cavitation also provides a means of drag reduction for surface ships through the creation of steady, ventilated cavities along recesses in the hull leading to a reduction of the wetted surface area; such ships are referred to as air cavity ships (ACS). As surface ships travel at speeds significantly below that needed for even incipient cavitation,

ventilation serves as the primary means by which partial cavities along the hull are developed. In contrast to the case of supercavitation about a fully submerged body, ACS often exhibit negative cavitation numbers in which the cavity pressure actually exceeds the flow pressure, resulting in a lift force which serves to further reduce the ship displacement and consequently the drag [38]. The power consumption needed for ventilation is typically less than 2% of the total propulsion power with drag reduction typically between 15-30%, showing the potential value of such a design [38, 39]. The development of such cavities is by no means trivial and is the subject of extensive research. Optimization of the hull is a key component of ACS design as it relates to cavity development and stability while the basics of seaworthiness, maneuverability, and propulsion must be maintained [30].

Four basic cavity shapes encountered in ACS design can be seen in Figure 7. Shape 1 is one in which a re-entrant jet is present as seen in supercavitation; this jet is confined to the rear part of the cavity with the forward section remaining largely stable. Shape 2 occurs for the case of smooth cavity closure and reattachment to the body, theoretically requiring no ventilation to be sustained. Shape 3 occurs for high gas ventilation fluxes and results in strong pulsations along the length of the cavity. Shape 4 occurs for even higher ventilation fluxes allowing for avoidance of cavity closure along the body; ventilation fluxes needed for this case far surpass those economic to ACS design however [6, 38].

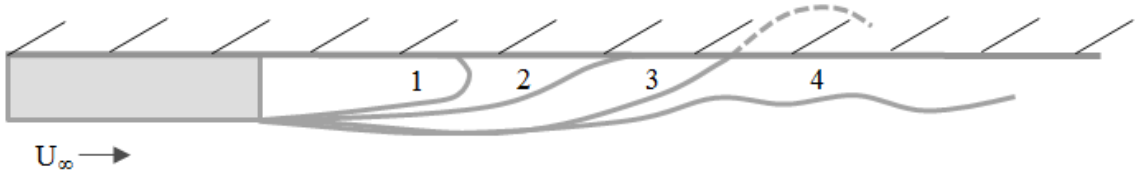

Figure 7. Cavity closure shapes for a reverse step as commonly seen in ACS design. Recreated from Matveev [6].

The amount of ventilation gas escaping the cavity decreases for decreasing closure angle of the cavity, β, measured through the cavity from the solid surface to the cavity interface, with the limiting case of β approaching zero allowing for theoretically zero ventilation flux needed for cavity maintenance [38, 40]. This case represents the optimal design as it corresponds to no power requirements. The development of this limiting case still requires initial ventilation in order to traverse the reentrant jet regime unless air is initially trapped in the hull recess [38]. For slower flows in which the cavity length is limited for ventilation fluxes within the optimal range of shape 2, a progression of steps along the hull may be required to completely cover the hull in a series of cavities [38]. The theoretical limit of cavity length, L_{lim}, for smooth reattachment of a stable, 2D partial cavity is given by Matveev,

$$L_{\text{lim}} \approx 0.37\lambda \tag{9}$$

where λ is the free-surface water wavelength,

$$\lambda = 2\pi U^2 / g \tag{10}$$

[6].

As with ventilated supercavitation, the ventilation flux is a key parameter for development and stability of the cavity as well as the flow velocity, the cavity length

being proportional to its square as seen in Eq. (10) [41]. Upon successful development, increases of up to five times the ventilation flux result in only minimal effects on the main part of the cavity, having a large impact in the exit mode behavior at the cavity tail instead, causing a general instability and increase in air leakage [6, 38].

The angle of inclination also becomes a critical factor as the gravitational effects are much more significant for the lower velocities of ACS designs compared to supercavitation. Matveev et al. showed that a maximum in cavity length occurs for small positive angles of inclination of the hull recess surface relative to the flow for a reverse step recess, the length varying by several times over a range of only several degrees. For small positive trim angles, the buoyant force of the ventilation gas is opposed by the slope of the surface thus decreasing the escape of gases from the tail of the cavity. As the trim angle increases, an inflection of the cavity length occurs as the buoyant force results in the escape of gasses from the front and/or sides of the recess [6]. The optimal combination of ventilation rate, step depth, and trim angle is dependent on the speed of the vessel and stability of its motion.

D. Experimental Practices in Cavitation Research

Knowledge of the cavitation number is essential for communication of cavitation research, whether experimental or computational. The most straightforward method of determining the cavitation number is through direct calculation according the Eq. (2). This requires knowledge of the static and cavity pressures, liquid density, and relative velocity between the liquid and the body. Measurement of the cavity pressure is far from

trivial, however, due to the dynamic nature of many cavities. For example, accurate pressure readings of a continuous cavity require that pressure measurement devices remain fully within the cavity, upstream of cavity closure and any dynamic cavity structures such as re-entrant jets. Any uncertainty in the temperature measurement will also be propagated through the calculation of the vapor pressure and density terms as well. These complications are often unavoidable, requiring alternative methods to be used [32, 21].

The most common alternative is through back calculation based on the cavity shape using appropriate shape relations. Such is the method as pioneered by Schevkohvs and used by many such as Wosnik, Arndt et al., and Zhang et al. [42, 21, 16]. The shape relations are generally of the form,

$$\frac{l}{c} \cong A\sigma^{-n} \tag{11}$$

where l is the cavity length and c some characteristic length of the body; this form is to be expected due to the inverse relationship of cavity development to cavitation number. As the cavity shape for naturally and ventilated cavities have been found to be safely approximated as similar, formulas for cavity shape can be used for determining the cavitation number for natural and ventilated cavities alike [16, 43]. Extra care must be taken to account for gravity deformation as the Froude numbers of ventilated cases are often much smaller due to the reduced velocity. The exact cavity shape is dependent on the ambient and cavity pressures as well as geometry of the flow and body; for

axisymmetric cavities, the cavity shape is generally approximated as an ellipsoid with exact dimensions given by numerous authors.

Relations between cavitation number and the drag coefficient, such as,

$$C_D(\sigma) \approx (1+\sigma)C_D(0) \tag{12}$$

also allow for the cavitation number to be reverse calculated assuming the drag coefficient can be accurately determined [44, 10]. In fact, many of the shape relations mentioned above are derived from application of this theory for specific geometries. The reader is referred to the works of Waid, Savchenko et al, Franc and Michel, Vaslin, and additional authors referenced by May for more detailed discussion of empirical shape and drag relations including their respective derivations and application examples [45, 46, 10, 47, 48].

Even careful determination of the cavitation number using the above mentioned methods can result in flawed values if wall effects and cavitation nuclei are not accounted for. Wall effects, caused by the presence of solid surfaces, as is common in experimental setups, as well as proximity of free surfaces, result in variations of cavity shape and device drag when compared to unbounded flow conditions. This consequently results in a departure of cavity behavior as a function of cavitation number from that seen in unbounded flow conditions, introducing an error in the calculated cavitation number relative to the physical cavitation response. Chen et al. document the trend of increasing cavity length and diameter for decreasing tunnel area for a given specimen area as well as

a decrease in the critical ventilation rate for supercavitation [9, 49]. In fact, the cavity length increases monotonically as the tunnel to cavity ratio approaches unity. More generally, wall effects increase as the tunnel to cavity area ratio tends toward unity.

The importance of correcting for wall effects can be seen from the comparison of the drag coefficient as a function of cavitation number as given by Brennen. From initial experimental results, it appears that for similar flows, lower drag forces are seen for the confined flow case as compared to the free flow case [9]. The difference arises from determination of the cavitation number based on cavity shape and size. As the presence of wall effects increase the size of the cavity, the drag coefficient is reduced as compared to the unbounded flow [2]. Adjusting experimental data to account for wall effects resolves the conflict as discussed by Brennen [9]. Chen et al document additional trends relating the wall effect to various cavity parameters [49].

Wall effects can also result in a choked flow condition and a corresponding minimum cavitation number for a given flow and geometric scenario. This choking phenomenon is analogous to that of a compressible flow as it represents an upper limit to the flow velocity; any attempts to exceed this limit result in an increase in the flow pressure to maintain a constant cavitation number [9]. The chocked cavitation number, σ_c, is related to the area ratio according to,

$$\frac{A_c}{A_T} = 1 - \left(1 + \sigma_c\right)^{-1/2} \tag{13}$$

where A_c and A_T represent the limiting cavity area and tunnel area respectively [9]. From Eq. (13) it can be seen that the chocked cavitation number, σ_c, will increase as the area ratio tends toward unity, becoming potentially large enough to prevent the onset of supercavitation altogether and must thus be considered in the experimental design [32]. Further details concerning wall effects and procedures by which they can be corrected can be found in the works of Brennen, Wu et. al, Chen et. al, and Karlikov and Sholomovich [50, 49, 51, 52].

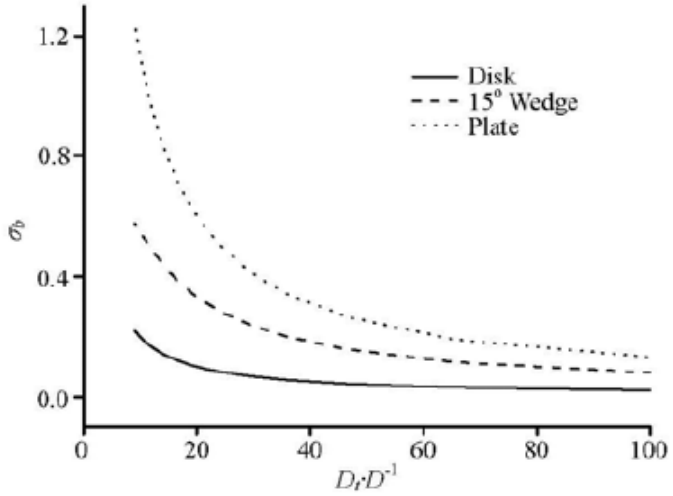

Figure 8. Plot of the chocked cavitation number, σ_c, or σ_b as used here for the blockage effect, as a function of tunnel to model diameter ratio for various geometries. Taken from Chen et al. [53].

The presence of cavitation nuclei can greatly affect the development of cavitation and thus skew the results of cavitation number calculations which neglect to directly consider their presence. Gas and vapor inclusions in the flow or along surfaces serve as nuclei sources, and for insufficient NPSH, any pumps used in the experimental setup will also result in cavitation, generating large cavitation nuclei concentrations often without

the possibility of removal prior to the test section. The flow loop and test specimen should also be as smooth as possible with smooth geometric transitions to reduce nuclei being trapped along the surfaces or cavitation occurring in the low pressure recirculation zones following abrupt geometry changes. Ideally, pure water in a flow loop with sufficient degassing capabilities downstream of any pumps should be used. Degassing also becomes essential as testing progresses due to the recirculation of cavitation nuclei created or activated in previous circuits.

The factors for which nuclei will become unstable and grow to initiate incipient cavitation include the nuclei composition of the flow as well as temperature, pressure, and flow speed; all of which are difficult to ensure consistency amongst, thus presenting one of the greatest difficulties in scaling amongst cavitation experimentation [2]. While back calculation of the cavitation number using shape or drag relations inherently includes the effect of cavitation nuclei, their effect on the cavity shape skews the final cavitation number. It can thus be seen that nuclei concentrations should also accompany cavitation number reporting in results when possible. Given these observations, any experimental results should be interpreted with the understanding that they are highly dependent on the exact testing scenario and are not directly transferable among different test scenarios unless great care is taken to correct for known conditions and precisely recreate all testing parameters.

CHAPTER 2: THEORETICAL EVALUATION OF STEAM VENTILATION

At a fundamental level, supercavitation design is related to the minimization of the flow cavitation number and/or optimization of the cavitation number at which different cavitation regimes occur for a given body. Externally powered projectiles such as underwater bolts may have sufficient velocity to create a natural cavity while larger systems require artificial ventilation, at least for initial cavity development. Various propulsion systems have been proposed for such devices such as ram jets with the potential for using the surrounding water as the oxidizer for a metal fuel [54]. Solid rockets have been successfully used as a propulsion source with the exhaust serving as the ventilation source. More traditional propulsion is also feasible assuming the propulsor is in contact with water to allow for the required thrust development and thus must be located before the supercavity or otherwise aft of cavity closure, the latter case being complicated by interaction of the propulsor with the cavity itself and any evacuated gases remaining in the wake [30].

Throughout the background information, ventilated cavities were assumed to be produced through the use of non-condensable gases. This assumption is based on an extensive literature review of techniques and research in ventilated supercavitation where air was the most common gas used. The use of exhaust gases from propulsion systems used in supercavitating devices largely conforms to this assumption as the exhaust would contain many non-condensable components such as hydrocarbons, H2, N2, CO, CO2, ect., although a significant amount of vapor may also be present. The use of non-

condensable gasses as the ventilation source for fully submerged devices introduces limitations in the range of supercavitating operation due to the discrete amount of ventilation gasses stored by the device [55].

The aim of this research is to determine the potential of vapor, specifically steam, as a ventilation gas. The potential for ventilated supercavitation design using vapor may allow for simplification of the ventilation systems currently used as well as increases in the range of the device through prolonged supercavitation. Replacing the non-condensable gases with vapor would allow for significant increases in range compared to the above mentioned designs as limits on compressed gas storage or generation would no longer be present. The vapor could be supplied by directly boiling the flow itself, assuming sufficient heat could be supplied by the propulsion system or supplementary heaters. Such a scenario could be imaged for a small supercavitating submarine, as proposed by the U.S. Navy, for which a compact nuclear reactor might provide sufficient heating capabilities [56].

The specific claim is as follows:

> *The addition of vapor to a non-condensable ventilation source will reduce the required non-condensable ventilation flux for cavity creation and maintenance by a meaningful amount while maintaining similar ventilated supercavitation operating characteristics. The extreme case is that for which vapor could be used as the sole ventilation gas, completely replacing the traditional use of non-*

condensable gasses as the ventilation source while maintaining similar ventilated supercavitation characteristics.

For natural cavitation, vaporization of the flow results in a depression of the cavity temperature below that of the bulk flow. In reality, this depression is generally negligible for water but does in theory reduce the condensation potential as the thermal energy flux is directed into the cavity. For the case of vapor ventilation, assuming vapor temperatures above that of the bulk flow as would be the case for ambient or pressurized boiling, this flux would be reversed, with a significant thermal gradient developing at the cavity interface affecting the rate of condensation along the cavity. The subsequent condensation resulting from this energy imbalance must be accounted for by increases in the required ventilation rate compared to that as given by non-condensable cavitation theory. Assuming saturated vapor, any energy loss to the surrounding flow will result in a lowering of the quality of the cavity. In other words, at best, the required ventilation rate for obtaining a given cavitation number is expected to be higher for vapor ventilation than for gaseous ventilation due to parasitic losses of vapor through condensation along the cavity interface, and possibly along the body as well; a general correlation for the required vapor ventilation flux being one of the key objectives of this research assuming successful creation of a vaporous cavity is possible to start with. In theory venting superheated vapor would serve to offset the required increases in ventilation rate for vapor through reduction of the condensation rate as sensible cooling would delay condensation; the overall gains of superheating are expected to be negligible for the

testing ranges considered here as the Jakob number for water at superheats of only tens of degrees Celsius is much less than one.

Although no open source research with direct regard to vaporous ventilated supercavitation could be found, the feasibility of steam venting can be evaluated in comparison to other two-phase scenarios involving ventilation of a gas into a pool or flow of liquid. The following discussion will draw from several such scenarios, applying relevant results in relation to vaporous venting in the hopes of distilling practical design guidelines to maximize the potential for successful vaporous ventilation. More importantly, this review serves as a general feasibility analysis with regard to the potential of vaporous ventilation with both qualitative and quantitative arguments.

A. Comparison to Direct Contact Condensation

Condensation within the cavity is precluded by the assumption that a continuous cavity can be successfully developed using vapor ventilation alone. The creation of a vaporous supercavity through steam ventilation is physically similar to direct contact condensation, the fundamentals of which are presented here along with other relevant condensation considerations useful to the evaluation of this assumption. While the reduced density and viscosity of a two-phase mixture or even heated liquid alone present a potential for drag reduction, this study is concerned only with the drag reduction resulting from continuous cavities attached to the body of interest. Consequently, the only region of DCC jets that will be considered is the steam plume which is assumed to be a continuous region of saturated or even superheated steam. It is interesting to note that the

viscosity of steam can be less than that of air for certain combinations of temperature and pressure, and would thus result in slight reductions in drag; this difference is negligible compared to the multiple order of magnitude reduction compared to liquid water however. While conventional DCC research aims to maximize heat transfer, formation of a vaporous ventilated supercavity requires the minimization of condensation, and thus the minimization of heat transfer. As such, many of DCC design practices will be purposefully contradicted for application to supercavitation design.

Let us assume a supercavitating device traveling through water with the ability to independently sustain steam generation for a meaningful period of time through some on-board steam generation system, potentially even using the oncoming flow as the water source. For successful supercavitation, the length of the device must be less than the maximum achievable plume length for steam injected into water. Table 1 gives estimated steam plume lengths for various steam flowrates assuming a single nozzle normal to a solid surface; values are approximate. The sample ranges were chosen to be representative of future experimental testing which saw steam flowrates up to 4 g/s at sub-cooling in excess of 75°C. Comparison to DCC literature required calculation of several dimensionless parameters including the steam inflowrate, G_0, defined as the ratio of the mass flux of steam to the nozzle exit area,

$$G_o = \frac{\dot{m}}{A_{nozzle}} \tag{14}$$

and the condensation potential as given by the dimensionless Jakob number,

$$B = \frac{c_{p_l}}{h_{fg}} \Delta T = \frac{c_{p_l}}{h_{fg}} (T_{steam} - T_{water}) \tag{15}$$

where c_{pl} is of the water at ambient pressure [57]. The Reynolds number of the steam as a function of the nozzle exit diameter was also determined according to,

$$\mathrm{Re}_D = \frac{\rho V D}{\mu} = \frac{G_o D}{\mu} \tag{16}$$

Table 1. DCC behavior for various injection rates of steam at 100°C (unless otherwise noted) injected into stagnant water at 25°C and 75°C corresponding to Jakob numbers of 0.14 and 0.05 respectively. Interpolation of DCC regimes from de With et al. with length data interpolated from de With. [58, 59].

Steam Mass Flux, $\dot{m}$ [kg/s]	Diameter, D [mm]	Steam Influx, G_0 [kg/m^{2}s]	Reynolds Number, Re_D	Water Sub-cooling (T_s-T_w) [°C]	DCC Regime	Estimated Plume Length, L [cm]
5E-5	1	6.4E+1	5.2E+3	25	Bubbling	Negligible
				75	Conical Jetting	Negligible
5E-3	1	6.4E+3	5.2E+5	25	Ellipsoidal Jetting	6
				75	Ellipsoidal Jetting	3
	10	6.4E+1	5.2E+4	25	Conical Jetting	Negligible
				75	Conical Jetting	Negligible
1E-1	10	1.3E+3	1.0E+6	25	Ellipsoidal Jetting	12
				75	Ellipsoidal Jetting	6
			9.0E+5[2]	125	Ellipsoidal Jetting	2[3]

Based on these assumptions, the creation of a significant cavity is not feasible even for extreme steam fluxes, much larger than what would be feasible for a compact supercavitating device. Even for the case of effectively infinite ventilation capabilities, the upper range of plume lengths found in DCC literature is roughly 15 cm, occurring for

[2] Calculated for steam at 150°C and stagnant water at 25°C corresponding to a Jakob number of 0.23.
[3] Extrapolated from de With graph at Re_D = 1.05E+6 [59].

flowrates in excess of 100 kg/m^{2}s and for minimal sub-cooling [58]. When inspected with regard to supercavitation design, this would only result in supercavitation for a rather small body for which the steam generation capabilities would be far insufficient, likely orders of magnitude less than what is needed for this maximum plume length. For larger devices in which the required steam flux might be feasibly created, the plume length would be of little consequence in terms of the creation of a pure vaporous supercavity. The need for minimal sub-cooling in order to create a maximum cavity length is also unfeasible for applied supercavitation design in marine environments as the ambient temperature is largely fixed and has significant sub-cooling. Even if the device could artificially increase the oncoming flow temperature, this would require a substantial amount of thermal energy, energy needed for the generation of the steam.

It is interesting to note that the continuous cavity lengths for direct insertion of a non-condensable gas into a stagnant water pool are also significantly limited. Harby et al. performed extensive experimental testing for air inserted into a stagnant water pool for varying flowrates and nozzle diameters, corresponding to a range of Froude numbers and momentum fluxes. In the absence of condensation, the continuous regime corresponding to the plume is further decomposed to momentum and buoyant jetting regimes, after which instabilities result in the creation of a two-phase turbulent zone of gas bubbles. The combined length of these regions increases for increasing mass flux as well as for increasing Froude number, as instabilities are reduced for increasing Froude number. Even for the maximum flowrates tested of 0.03 kg/s air (~60 cfm), the total cavity length

remains well below 0.5 meters (30 cm for 0.03 kg/s air assuming summation of momentum and buoyant regions). Thus the maximum length for steam ventilation in which condensation must be considered will expectantly be much less as predicted in the above analysis [60]. Thus for direct venting of steam normal to the flow through a single nozzle, the creation of a useful cavity appears infeasible.

A more likely configuration of venting for supercavitation design would be an array of vents as is common in ventilated design, such a configuration being geometrically similar to a sparger. Cho et al. investigated DCC for varying sparger designs and found small pitch to hole diameter ratios (P/D) and staggered orientations resulted in an increase in the individual jet interaction. Such an interaction decreases the kinetic energy of the individual steam jets, which, as this energy is largely responsible for thermal mixing with the surrounding water, decreases thermal mixing and results in temperature increases in the local region around the sparger. The resulting decrease in condensation potential allows for the formation of larger and more stable steam plumes; the length of these plumes is still largely a function of the amount of sub-cooling [57]. While little quantitative data with respect to plume lengths could be found for sparger venting, it is still assumed that such a case would be of little significance to supercavity development as prohibitive condensation would still occur.

The applicability of DCC principles in high velocity bulk flows is uncertain as DCC literature makes only limited mention of ventilation into a flow, largely focusing on the more common scenario of ventilation into a stagnant pool. It has been shown, however,

that venting into a flow of water serves to increase the heat transfer rate and thus further limit the steam plume length; de With et al. showed roughly 65% reduction in plume length for injection of steam normal to a 1.9 m/s flow of water for $\Delta T = 85°C$ with the anticipation of even larger reductions for increasing flowrates of water [59]. This knowledge, combined with the already improbable creation of a significant steam cavity assuming stagnant venting, suggests that the creation of a purely vaporous supercavity is unlikely for direct ventilation into the flow.

Other aspects of DCC theory can still be used to provide crucial insight into the potential of a mixed ventilation system. Specifically, the presence of non-condensable gases in DCC applications results in a significant reduction of the heat transfer due to the development of a non-condensable boundary layer at the DCC interface. Assuming the non-condensable gases are fully mixed with the steam, natural convection, or even momentum transfer for the case of flowing steam, serves to carry the non-condensables to the condensation interface where they can only cross through diffusion, resulting in the development of a large NC concentration which serves as a barrier to further condensation [61]. This process is both self-initiating and self-sustaining, with the rate of development of the high NC concentration depending on the rate of mass transfer to the condensation interface and the NC mass faction of the ventilation flow.

The effect of non-condensable gases on condensation can also be seen for other condensation scenarios including individual bubbles and film condensation. Larger reductions in heat transfer and condensation rates are seen for similar NC concentrations

in film concentrations compared to DCC applications. This suggests the importance of allowing for the NC concentration layer to develop. This is further supported by the delay in the decrease of the heat transfer coefficient seen for film condensation in the presence of NC's as it takes time for the layer to develop. For the case of a stagnant steam-air mixture in direct contact with a falling liquid film inside a vertical tube, the initial decrease of the heat transfer coefficient took approximately one tube diameter with the limiting value being reached after approximately 4 tube diameters, the exact distances depending heavily on the liquid film flowrate [62].

The time required for the NC boundary layer to develop is dependent on both the mass fraction of non-condensable gas in the mixture as well as the condensation rate which is itself dependent on the sub-cooling of the wall, or bulk flow, compared to the mixture temperature and other parameters such as the Reynolds number of the film as determined by the ventilation rate. As the ventilation flowrate increases, interfacial shear increases, resulting in thinner liquid films and subsequent increases in heat transfer due the reduced thermal resistance. More importantly for the present research is the development of interfacial waves and earlier transition from a laminar to turbulent boundary layer for increasing ventilation fluxes, both serving to increase the interfacial area over which heat transfer occurs as well as turbulent mixing, reducing the effect of NC gasses on condensation rate [63, 64, 65]. Interestingly, faster condensation increases the rate of NC B.L. development by increasing the rate at which N.C. gasses are

delivered to the interface, complicating the effects of NC concentrations in condensing flows [66].

While a majority of film condensation literature is concerned with condensation along a flat plate, Oh and Revankar investigated film condensation in a vertical cylindrical pipe submerged in a water pool. The condensation heat transfer coefficient and condensation rate were both shown to decrease for increasing NC concentrations, the relationship being roughly linear for small NC concentrations with approximately 30% reduction in condensation at 10% NC concentration [63]. Asymptotic behavior is expected for larger NC concentrations with the condensation HTC and condensation rate both converging to zero for NC concentrations approaching one.

Continuation of these theories lends itself to the idea of artificially creating a non-condensable boundary layer through the insertion of non-condensable gases with vaporous ventilation underneath, along the body of the device, forming an annular vapor region with a material surface interior and a non-condensable boundary layer exterior. Similar to the disturbance of the non-condensable boundary layer by waves mentioned by Park et al, it is believed that the incidence angle of the steam relative to the CA should be designed such that the CA boundary can be formed with minimal disturbance [65]. Fundamental fluid mechanics dictates that this will occur in the absence of pressure and velocity gradients which would otherwise result in circulation of the flow as predicted by viscous flow theory (velocity gradient would result in shear stresses, resulting in mixing turbulence, and pressure gradients which would serve to bend the flow) as well as

interfacial instabilities. The ventilation nozzles should be designed to allow for these conditions to be met, presenting a significant challenge for non-constant ventilation supply rates and requiring an extensive optimization study. Even if such a layer could be successfully created, mass diffusion would still occur, leading to condensation along the gaseous interface. The effect of this condensation is unknown for the case of horizontal flows in which gravity would likely cause the condensation to fall out rather than creating a condensate film as shown for condensation along a vertical solid surface; annular flow is unlikely for realistic ventilation fluxes as will be later shown.

It is interesting to note that compressed air venting normal to the flow is capable of generating a supercavity, as will be shown in Chapter IV and thus the case of steam ventilation normal to the flow will still be experimentally investigated. While no discussion of the ventilation dynamics around the cavitator could be found in the open literature, a rather simple model for the behavior of the gases immediately following ventilation is here proposed. Assuming a sharp edge cavitator, the flow will separate at the sharp edge, creating a low-pressure wake surrounded by a higher pressure potential flow. It is this low pressure wake that is replaced by the ventilation gases, which themselves create a cavity at a lower pressure relative to the potential flow. The lower pressure causes the ventilation gases to bend back towards the surface, developing a mean velocity tangent to the flow along the surface of the device, thus behaving similar to a wall jet. For the case of steam ventilation, however, the advancing front will

continually condense and be swept downstream, preventing the creation of a continuous cavity.

B. Comparison to Wall and Offset Jet Theory

As the potential for vapor venting based on direct insertion normal to the device surfaces and flow is theoretically infeasible, we turn to the potential for the creation of a film of vapor along the surface of the body. Film boiling could serve as a potential method for the creation of such a film, using the body of the device as the heat transfer surface itself. Kuklinski proposed a variant of this theory, suggesting the boiling of a thin layer along the surface of a torpedo using waste heat from a thermal engine, or even an auxiliary heating unit. A key realization of the patent was that as the surface temperature of the torpedo increases, so will the heat transfer coefficient, potentially prohibitively so assuming the heat flux required for boiling is above that provided by the heat source. If regions of boiling can be successfully developed, a significant reduction of the heat transfer coefficient will occur due to the higher thermal resistance posed by the vapor bubbles or vapor film. Kuklinski thus proposes the use of ventilation to generate an initial cavity, allowing time for the surface to become sufficiently superheated, at which point ventilation can be reduced as film boiling develops [67].

Kuklinski's design was numerically evaluated by Wang et al. who showed that vapor void fractions approaching one could be successfully generated using a heated cavitator for cases in which natural cavitation would not be normally seen. Cavitation occurred for temperatures slightly in excess of the saturation temperature corresponding to the flow

pressure at a given point. As expected, cavitation first occurred at locations of minimal pressure along the surface of the body, the range of cavitation increasing for both decreasing flow cavitation number and increasing surface temperature. For combinations of sufficiently low cavitation number and sufficiently high surface temperatures, vapor void fractions approaching one were computed, suggesting the presence of a continuous cavity. The skin friction was also computed and shown to be a minimum for surface temperatures for which the vapor void fraction first approached one. This minimum was approached from lower temperatures due to a combination of decreasing liquid viscosity for increasing temperature and the development of cavitation along the surface. Additional heating past the minimum friction point actually increased the viscosity of the steam, thus increasing the skin friction [68].

The focus of this research is, however, concerned with vapor ventilation, which if directed along the body would be analogous to jetting as seen for the cavity contents in traditional non-condensable ventilation, with the potential for a more centralized and directed boiling of the flow using a specially designed cavitator. In other words, it is possible that if steam venting is directed along the surface of the body, tangent and concurrent to the flow, a film of significant length could be created along the body of the device. This situation could be thought of as wall and/or offset jetting, the fundamentals of which are presented below with hopes of distilling design guidance. Many cavitators for ventilated supercavitating devices use a deflector to direct the flow along the body,

tangent to the flow, suggesting this is in fact a more efficient method of ventilation regardless of the ventilation gas.

For the directional ventilation of pure steam parallel to both the surface of the device and the flow, the steam would still be subjected to the extreme condensation potential of the outer flow as encountered in DCC applications. Energy could be supplied along the solid surface, similar to the design as mentioned by Kuklinski but at reduced quantities, to reduce condensation as a small degree of superheat could be maintained. To further shield the vapor from condensation, however, an insulating layer of non-condensable gas could be developed between the vapor and the bulk flow. The most direct application would be a pre-mixed ventilation supply of steam and CA, allowing for the natural development of the non-condensable gradient along the condensation interface as seen in film condensation. The development time for this layer is supposed to be prohibitive considering the highly dynamic and short characteristic lengths of supercavities. A more elegant solution would be separate venting of steam and CA such that the CA boundary could be engineered for stability and maximum thickness to allow for maximum insulation of the steam. Such a case would resemble parallel venting of wall and offset jets, corresponding to vapor and CA ventilation respectively.

Figure 9 provides a schematic of a wall and offset jet configuration with jet width, w, and offset spacing, d. For a single offset jet, attachment to the wall will occur downstream, the jet then behaving similar to a wall jet; the reattachment point increases for increasing d/w ratios up to a limit at which point no reattachment occurs and the jet

progressively diffuses into the ambient [69]. The addition of a wall jet below an offset jet serves to increase the attachment length of the offset jet due to an increase in the pressure below the jet which in turn reduces the curvature of the jet towards the wall [69]. A recirculation zone develops in the offset between the two jets, extending until the two jets initially begin to merge at some location x_{mp}. The reverse flow region following the vents is shown to decrease in length for decreasing offset ratios as well as for velocity ratios, U_w/U_o, approaching unity [70, 71]. Further downstream, the jet centerlines fully merge, a point referred to as the combined point, x_{cp}; the velocity gradient is here smooth and singularly parabolic and the jets behave largely as a single wall jet, eventually achieving self-similarity [70]. It is unclear if this also dictates complete mixing of the jets, however, especially for two-species flow in which species gradients are desired.

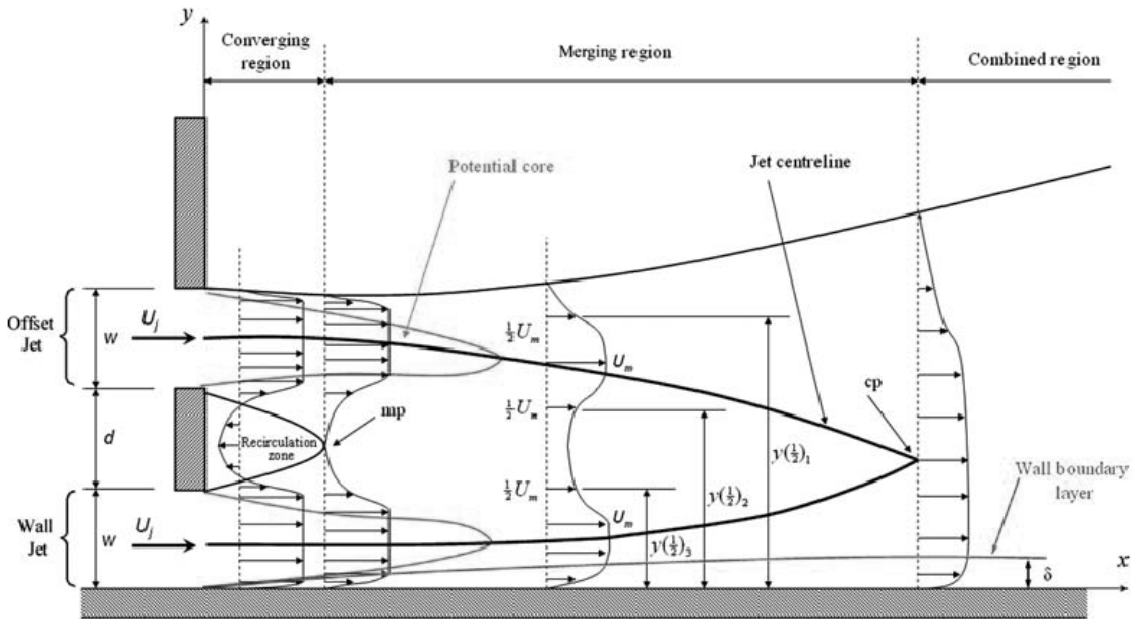

Figure 9. Schematic of the experimental results of Wang and Tan showing the flow patterns including the jet centerlines and various mixing regions for a plane wall jet and parallel offset jet. Taken from Wang and Tan [70].

For $U_w/U_o=1$, the presence of the wall results in a slight inclination of the offset jet toward the wall due to the Coandă effect, exhibiting more of a melding of the jets rather than entrainment of one into the other [71, 69]. This inclination becomes more pronounced for increasing U_w/U_o ratios, the offset jet being completely entrained nearly immediately with its initial momentum carrying it a given distance before actually curving back against the flow; this results in a highly turbulent interaction of the two jets and nearly complete mixing across the jets with significant turbulence remaining downstream [71]. The entrainment direction is reversed for $U_w/U_o<1$, the wall jet being entrained upward into the offset jet. For sufficiently low U_w/U_o ratios, the wall jet may even exhibit separation and reattachment from the wall [71]. These correlations are based

on velocity rather than momentum; for jetting of substances with similar densities and nozzle areas, momentum effects will largely match the velocity behavior [69]. It is here assumed that the densities of steam and CA are sufficiently close and the design ranges wide enough to accommodate any discrepancies this scenario may produce.

Based on the results of Li et al. for parallel and offset jets of $d/w=1$, it is proposed to maintain a velocity ratio range of $0.75<U_w/U_o<1.25$ as these ratios exhibited no wall jet separation and relatively smooth merging of the jets and corresponding minimization of the mixing with both larger and smaller velocity ratios exhibiting increased mixing [71]. As for the offset ratio, we here suggest a ratio of 1. This ratio was also shown by Wang and Tan to have a significantly longer reattachment length of the offset jet (x_{rp}/w=6.7) compared to many other d/w ratios, suggesting a more gradual merging of the two jets [70]. It was also shown that wider spacing results in faster expansion and subsequent mixing of the jets as well as an increase in the large scale pulsations as shown above [72].

Decreased turbulent stresses in the inner shear layer for the addition of a wall jet to an offset jet has also been experimentally shown, as well as the increased distance from the surface at which they occur as a result of the more gradual approach of the offset jet towards the wall; this suggests that mixing of the streams could be largely minimized and relegated to the outer shear layer, not influencing the inner steam layer until far downstream where the turbulent fluctuations were actually seen to increase for the addition of a wall jet [69, 70].

It is well documented that the interface of parallel jets with near equal momentum fluxes results in large scale "flapping" with frequencies much smaller and amplitudes much larger than the instabilities characteristic of Rayleigh-Taylor and Kelvin-Helmholtz structures [69, 70]. The "flapping" phenomenon is a function of the jet spacing and momentum ratio and largely replaces R-T and K-H type roll-up in the offset jet-wall jet and wall jet-wall shear layers [70]. The flapping results in large scale mixing of the jets as compared to the largely interfacial mixing seen for R-T and K-H instabilities. The structures disrupt the flow on a larger scale by inducing circulation of the wall and outer shear layers as the Karman-like vortices periodically shed and move downstream, resulting in a periodic downward motion of the offset jet and upward pull on the wall jet as seen in the vorticity plot of Figure 10, resulting in mixing across the entire jet layer rather than at the interface only [70, 72]. While not directly stated in the literature, it is likely that this "flapping" is largest for nearly equivalent momentum fluxes as mismatched jet momentums are characterized by increasingly violent entrainment of one jet into the other, thus masking or replacing the "flapping" with other turbulent mixing.

It is imperative that such large scale mixing is minimized; even if at the expense of R-T and K-H instabilities which are a function of the density and velocity of each layer, becoming increasingly unstable for divergence of the properties across the interface. As the flapping is largely a result of the recirculation zone between the jets, explaining the similarity to bluff body vortex shedding, reducing the jet spacing serves to reduce the amplitude of flapping "rapidly" [72]. The spacing between the jets, their offset from the

wall, and the momentum ratio between them then become the primary optimization parameters to maximize preservation of the two layers. Interaction with the bulk flow must also be considered, further complicating the scenario.

The above discussion has focused on primarily 2D, planar jetting, the applicability of which must be verified for the case of an axisymmetric cavitator. Axisymmetric jets commonly exhibit toroidal, helical, and streamwise vorticity [10]. Examining an axisymmetric supercavity, the cavity interface could be modeled as either a material or non-material cylindrical boundary with the body itself serving as a material cylindrical boundary with a no-slip wall condition. As such, jetting in an annular cavity with an external boundary moving concurrent to the jetting direction would be most directly applicable to the case of an axisymmetric cavity; no such a case was found in literature however. Nath et al. did investigate jetting into a low-aspect cylindrical cavity [73]. Overall, similar jet behavior relative to the wall was noticed, suggesting that the design information distilled from planar jetting is applicable to axisymmetric supercavitation.

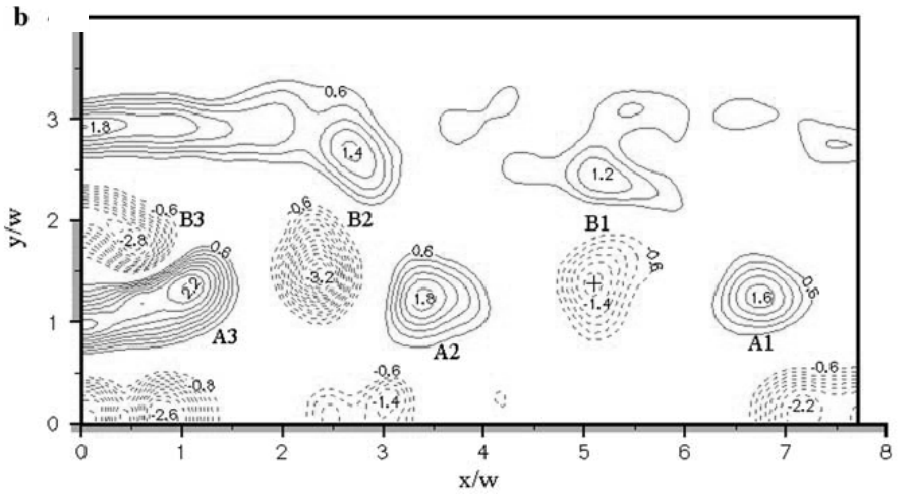

Figure 10. Instantaneous contour plot of vorticity for parallel wall and offset jet with dashed lines representing CW rotation and solid lines CCW rotation. Here *x* is downstream position, *y* vertical height, and *w* the width of the jet at exit. Taken from Wang and Tan [70].

The discussion thus far has not addressed the issue of characteristic lengths. The preservation of distinct layers of steam and air is fundamentally based on the assumption that the characteristic length of turbulent mixing structures is smaller than the layer thicknesses; otherwise, mixing will occur across the entire layer, disrupting the non-condensable boundary layer and subsequently reducing its ability to shield the steam from condensation. This highlights the importance of minimizing larger scale mixing structures such as the flapping characteristic of many wall-offset jetting scenarios as well as smaller scale Rayleigh-Taylor and Kelvin-Helmholtz instabilities. Little quantitative information was found in the literature regarding mixing of the jets although analysis of the shear stress tensors and velocity components suggests that jet merger may allow for preservation of the distinct layers for two-species jetting.

Unfortunately, the literature focused largely on the near field interaction of jets and detailed discussions of species mixing in the far wake were not found. Jet theory does predicts the expansion of jets due to turbulent diffusion and convection for increasing streamwise location, showing that mixing will be eventually inevitable but at unknown lengths. The combine point and mixing length are generally given as several nozzle diameters, suggesting limited merge lengths, considerably less than 1" for the 1/16" ventilation channels used in experimental testing. Again the amount of mixing upon merger and the development of instabilities along the various interfaces for concurrent ventilation severely limit the ability to determine the feasibility of concurrent steam and air ventilation.

C. Comparison to Annular Flow

Additional insight with regard to the potential for pure vaporous ventilation can be gained from an idealized comparison to condensing annular flow within a pipe. For long cavities with minimal gravity deflection in which the cavity curvature is negligible for the greater portion of the cavity length and assuming a cylindrical inner body, the cavity is proposed to be modeled as a pipe. Following this model, the cavity interface is representative of the liquid film that develops due to condensation along the pipe wall during annular two-phase flow with an internal vapor core. This assumption is in-line with the simplification of the cavity interface as a solid wall as used by Franc and Michel in order to determine the heat transfer behavior at the interface [10]. In fact, supercavity modeling is often simplified using free streamline flow theory to model the cavity

interface with the associated assumption of tangential velocity along the interface and the added assumptions of constant and uniform internal pressure as well as negligible shear stress and mass transfer at the cavity interface [2, 10].

These assumptions allow for approximation of the cavity interface velocity according to,

$$\frac{V_c}{V_\infty} = \sqrt{1 + \sigma - \frac{2gy_c}{V_\infty^2}} \tag{17}$$

or for small cavitation number supercavities with minimal gravitation affect,

$$\frac{V_c}{V_\infty} \cong \sqrt{1+\sigma} \cong 1 \tag{18}$$

[10]. Eq. (18) shows that there is a minimal velocity gradient at the cavity interface, substantiating the assumption of negligible shear acting on the cavity. Assuming a mean cavity diameter of 2 cm (an estimate of the cavity thickness seen during experimental testing), Figure 11 gives the required mass flowrates for annular flow for given qualities as interpolated from the regime map for horizontal two-phase flow of Taitel and Dukler [74]. Even for qualities approaching one, over 10 g/s is estimated to be required, a flowrate that exceeds that during experimental testing and is at least two orders of magnitude larger than non-condensable flowrates capable of successful supercavitation. Such flowrates would also result in ventilation gas speeds within the cavity of 32 m/s or larger, several times faster than mean flow velocity encountered during experimental testing and thus invalidating the assumption of negligible interfacial shear. Instabilities

would be expected to develop along the cavity resulting in increased heat transfer and subsequently increasing the condensation potential of the flow. As such, even for the highly idealized assumptions above, excessive steam flowrates are to be expected for vaporous ventilated cavity creation.

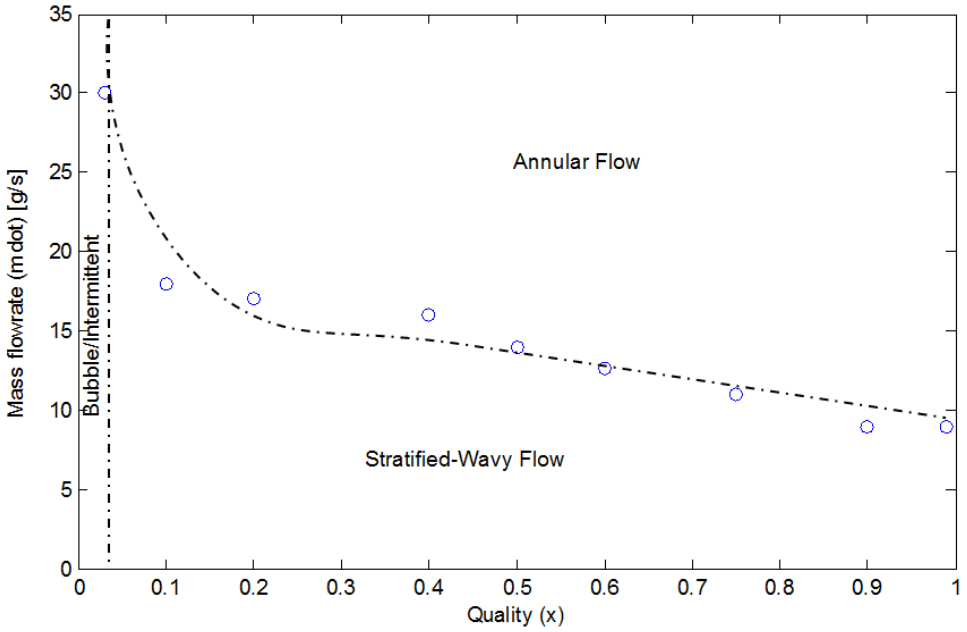

Figure 11. Combinations of quality and mass flowrate for annular flow in hypothetical cylindrical 2 cm diameter cavity. Dotted lines are approximate regime transition curves.

A similar extension can be made to concurrent ventilation although limited literature exists related to the annular flow of a steam/air mixture through a horizontal tube, where condensation occurs along the wall. Ren et al. did investigate this scenario, showing an appreciable decrease in the condensation rate, heat transfer coefficient, and overall heat transfer for increasing non-condensable concentrations with testing going at up to 40% NC mass concentration [64]. The air was unheated and thus the temperature of the

mixture decreased for increasing NC concentration due to the reduced partial pressure of the steam, this partially accounting for the decrease in the heat transfer coefficient. The effect is not linear, being more dramatic for lower NC concentrations. The effect of NC concentration was also shown to be significantly less than for corresponding scenarios in a stagnant vapor; this result being a manifestation of increased mixing as a result of both large and small scale instabilities and turbulence [64, 61]. It was also shown that for increasing gas (steam and air) flowrates, the heat transfer coefficient and overall heat transfer rate increase due to the increased shear effects. This in turn results in waviness and instability of the interface which serve to increase the HT surface area and enhance mixing as well as reduction of the condensate film [64, 63].

Oh and Revankar also investigated the condensation of a steam/air flow through a vertical, 2.66 cm inner diameter tube at flowrates of 2.5-5.5 g/s; these testing parameters are comparable to those used during axisymmetric testing and are thus consulted even for the vertical orientation. Roughly a 30% condensation reduction was realized for the upper range of NC concentrations tested (from 0.9 to 0.6 percent condensation for NC concentrations of 0 and 10% respectively) with the rate of reduction slowing for further increases in the NC concentration [63]. The condensation testing length was 0.984 m with complete condensation not occurring for the tested flowrates. While this appears to suggest the potential creation of a significant cavity for mixed ventilation of steam and air, the testing setup was such that the temperature difference was minimal and thus represents very limited condensation potential. This is vastly different from the case of

steam ventilation into a bulk flow of water with sub-cooling in the tens of degrees Celsius; applicability is also limited due to the vertical rather than horizontal orientation. Even still, the addition of non-condensable gasses to the steam flow may provide a significant reduction in steam condensation, allowing for increases in the net ventilation flux without requiring additional air ventilation.

CHAPTER 3: EXPERIMENTAL DESIGN

In order to experimentally evaluate the potential for vaporous ventilation, two testing setups were used. Initial testing was done in a low velocity (on the order of several tens of in/s) water table with ventilation occurring below a horizontal flat surface. This allowed for modifications of the test specimen to be easily made and allowed for more control of the testing parameters. Final testing was performed in a flow loop with axisymmetric test specimen, this being more analogous to supercavitation applications. The test specimen were designed to allow for testing of steam only ventilation as well as concurrent venting of steam and CA; CA only ventilation served as the baseline for all cases.

Similar steam and compressed air ventilation supply systems were used for both setups. The compressed air was supplied through the laboratory's compressed air network at a temperature of approximately 25°C with unknown dryness. The air flowrate was measured using a series of rotameters with varying measurement ranges (design stage uncertainties of ±0.5, ±0.05, and ±0.025 SCFH). Actual air flowrate adjustments were made according to,

$$Q_{actual} = Q_{s\,\mathrm{tand}\,ard}\left(\frac{T_{actual}}{T_{s\,\mathrm{tan}\,dard}}\right)\left(\frac{P_{s\,\mathrm{tan}\,dard}}{P_{actual}}\right) \tag{19}$$

where standard temperature and pressure were given as 70°F and 14.7 psia respectively with the actual pressure being measured directly upstream of the rotameter bank using a dial gauge. An unknown amount of hysteresis was inherent in the CA flowrate

measurements as the largest rotameter valve did not fully close; this was consistent among all tests except for ventilation at compressed air flowrates above 5 SCFH for which this valve was opened.

Steam was provided by a JR 1.5 kW Reimers steam generator capable 1/6 BHP saturated steam generation. The steam flowrate was determined using a straight section of ¼" pipe over which the pressure drop was measured using a Sensotec differential pressure transducer with 25 psid full scale measurement, allowing for determination of the flowrate according to the Darcy-Weisbach relation. The steam density was determined according to steam tables with the pressure and temperature being measured directly upstream of the flow element using a Sensotec absolute pressure transducer with full scale measurement of 200 psia and T-type thermocouple. Pressure measurements were displayed on a Sensotec GM signal conditioner-indicator while an Omega HH23 microprocessor thermometer meter displayed thermocouple temperature measurements; all pressure ports were either installed above or to the side of the flow tube to prevent condensation from affecting measurement accuracy [75]. Additional details of steam flowrate measurement including justification of measurement techniques can be found in Appendix A. Any liquid in the steam ventilation network, either from the oncoming flow or condensation of un-expelled steam from previous testing was ejected for the initiation of steam ventilation; approximately 10 mL of air was also released upon the initiation of steam ventilation. These ventilation artifacts must be considered in the analysis of testing

results as they may cause unintended changes in the cavity behavior, both initially and permanently.

As both the steam and air ventilation supplies were pressure driven, it was feared that liquid flow turbulence and cavity instabilities would result in pressure fluctuations within the water tunnel and cavity leading to subsequent pulsations in the ventilation supply rate and vice versa. Observance of the rotatmeter readings showed pulsations considerably less than 0.05 SCFH air, suggesting the ventilation rate is nominally affected by the cavity pulsations; this also suggests the cavity pulsations result in minor changes in cavity pressure. A constant flowrate of CA was also maintained regardless of the vapor ventilation rate for concurrent, but unmixed ventilation. As the steam supply pressure was higher than the air supply, the air flowrate was reduced for mixed ventilation cases, ceasing entirely for large steam flowrates. As such, a one-way valve was installed in the air supply line upstream of the combine point for premixed ventilation testing to prevent backflow of steam through the air line and to protect the rotameters. Various combinations of compressed air and steam flowrates were tested for each specimen; detailed testing sequences will be discussed in conjunction with results.

Fully developed flow of the oncoming water and ventilation gases was not a concern considering the large uncertainties and qualitative nature of the testing; fully developed flow is also unrealistic for most practical applications of supercavitation and ventilation is inherently chaotic. Given the limits in available instrumentation, challenges of determining the cavitation number directly from pressure and temperature measurements

as mentioned in the literature, and significant wall effects for the small area ratio between the test chamber and cavitator, specific cavitation numbers were not determined. While shape relations would have allowed an alternative means for cavitation number calculation, the testing speeds were lower than those common in literature and it was feared that shape relations and corrections for asymmetric cavity deflection would not still hold.

Various cameras and lighting configurations were experimented with as capturing the high speed and highly dynamic cavitation events presented a significant challenge, requiring very specific combinations of shutter speed, contrast, aperture, sensitivity, and lighting. Frontal lighting resulted in a glare on the supercavity surface that prevented the cavitator from being seen and also over-exposed the surrounding flow. Backlighting was also troublesome, again due to glare on the viewing window and reflection of the light source itself. A subtle backlight from slightly below or above with the cavitator directly in front of a solid black surface resulted in the clearest photographs; similar setups provided the clearest videos as well. Photographs and videos were captured using a Cannon Rebel T3i and Cannon Vixia HFR-42 respectively. While very fast shutter speeds allowed for individual cavitation structures to be clearly captured, long exposure times allowed for an averaging effect in which the general shape of the cavity could be determined. The use of a CCD system, further reduction of artifacts in the flow, and a planar viewing window would likely allow for significant improvements in visualization of the test specimen.

A. Flat Plate Testing

Low fidelity testing was performed in the Clemson University Mechanical Engineering water table, capable of maximum flow velocities of 5 in/s, unaltered, with a free surface at atmospheric pressure. A nozzle was designed and inserted into the flow, reducing the flow area by 66%; the resulting increase in flow speed allowed for testing at approximately 15 in/s. Such speeds are roughly two orders of magnitude below that needed for natural supercavitation to occur for the given pressure. As little variation in cavity behavior with respect to vapor ventilation was seen for varying flow speeds, all reported results are for 15 in/s flow unless otherwise stated. The conservative flow speed and increased control of the test parameters including in situ modifications allowed for the interaction of ventilation gases to be more clearly observed with the naked eye with various configurations being easily cycled.

The test surface was simplified to that of a flat plate as seen in Figure 12, suspended in the middle of the water table test section. Two ventilation ports were drilled into the specimen to allow for concurrent but independent venting of steam and CA. The vents themselves were in the form of slots spanning the entire width of the test specimen, being bounded by two clear viewing windows attached to the side of the specimen in order to create a continuous cavity spanning the entire width of the specimen. The clear viewing windows extended below the test surface and allowed for clearer observations of a 2D cavity without disturbance from vortices peeling from the sides of the cavity; a silicone sealant was used to ensure all connections and contact points were air and steam tight.

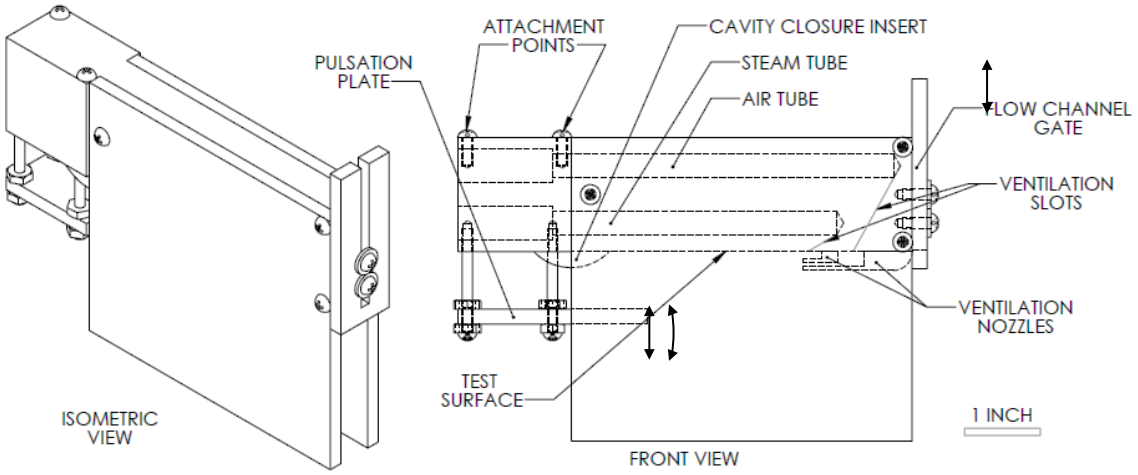

Figure 12. Schematic of flat plate testing specimen including three configurations of ventilation slots at various angles from tangent relative to the flow: 90/45°(not shown), 60/30° as shown, and 0/0° with the addition of the ventilation nozzles.

Upward venting was infeasible as the ventilation gasses would immediately rise to the surface due to the dominance of buoyancy effects given the moderate flow speeds, preventing the creation of a continuous, attached cavity. The specimen were thus suspended such that the vents were downward facing to allow for creation of a continuous cavity along the flat surface as buoyant forces caused the gases to be trapped in the downward facing channel formed by the test surface and viewing windows. Such an orientation is more analogous to hull ventilation of surface ships than axisymmetric, high-speed supercavitation but allowed for general trends in the interaction of steam and air to be identified; brief comparisons to ACS theory will be made in the discussion of results although this is outside of the scope of the present research.

Three major testing configurations were used with respect to the ventilation angle measured from tangent relative to the oncoming flow: 90/45°, 60/30°, and 0/0° for air and steam ventilation respectively. 0/0° testing required the addition of ventilation nozzles below the 60/30° slots to turn the ventilation gasses tangent to the flow; the nozzles were secured directly to the testing surface by epoxy. The outer surface of the nozzle was parabolic to minimize flow separation with the hopes of minimizing interfacial instabilities along the cavity. Air ventilation occurred upstream of the steam vent in order to evaluate the feasibility of engineering a mixed ventilation cavity in which a non-condensable layer serves as a condensation insulator to the steam.

In situ variations were also made to the test specimen to increase the combination of test cases. One such modification was the addition of a gate spanning the width of the flow channel at its entrance; the gate being analogous to rear facing steps as seen in ACS designs and also allowing for comparisons to sharp edged disc cavitators. The gate could be adjusted vertically to increase the step height, allowing for varying wake thicknesses and modification of the recirculation zone length. Introduction of dye upstream of the ventilation channel showed a circulation zone extending past the air ventilation slot but ending before the steam ventilation slot for the gate in the up position. In the down position, the gate extended ¼" below the testing surface resulting in an increase in the recirculation zone length past the steam ventilation slot.

Matveev showed that the addition of a small hydrofoil below the surface of ACS designs can lead to significant cavity lengthening while also increasing the stability of the

cavity [76]. Per this observation, a thin "pulsation plate" was designed that could be suspended below the test surface near the tail of the cavity; the angle and offset distance could be easily adjusted using a series of nuts on the screws from which the plate was suspended to influence the effectiveness of the plate on cavity behavior. Amromin et al. also showed that the addition of an insert at the stern of the testing surface, here referred to as the cavity closure insert, allows for smooth reattachment of the cavity to the surface, increasing the stability of the cavity tail and allowing for potential reductions in the required ventilation flux [77]. A press fit between the viewing windows secured the cavity closure insert against the testing surface; the cavity closure insert and pulsation plate could not be used concurrently. The attitude of the entire specimen could also be varied (±5° from horizontal) by adjusting the angle of the system from which the specimen was suspended.

B. Axisymmetric Testing

In order to better model axisymmetric supercavitation behavior, three axisymmetric cavitators were designed for use in a flow loop capable of much faster speeds than the water table. The flow loop consisted of an IPT-3S5XHR trash pump capable of pumping 300 GPM under ideal conditions through a network of 3" PVC tubing with all connections sealed with rubber compression fittings or PVC cement. A 300 gallon holding tank served as the reservoir for the loop with non-degassed tap water serving as the liquid. In order to simplify result reporting, a single pump power setting was used for all testing, and when combined with an approximate head loss of 14 ft. gave a flowrate of

150 GPM as determined by pump performance curves. This corresponds to an average flow velocity of approximately 4.5 mph.

Considering the flow speed and pressure, the cavitation number of the flow was on the order of ten and was thus significantly higher than that required for natural supercavitation. Due to insufficient suction head, the pump was expected to cavitate; this was confirmed by the presence of bubbles within the flow itself. In order to limit the nuclei concentrations passing through the test chamber, the chamber was installed upstream of the pump in the suction line. The water return was also submerged in the reservoir tank to minimize entrainment of air into the reservoir compared to a free jet return which would increase nuclei concentrations through violent entrainment of bubbles at the free surface. The tank was filled to capacity to maximize the available head and increase the recirculation time of a given fluid element to allow time for bubbles to escape through the free surface due to buoyant effects. Unfortunately bubbles could still be seen in the test section. It is unclear if these are a result of insufficient degassing in the reservoir or as a result of flow cavitation in the suction line itself. While the presence of cavitation nuclei has negligible effect on ventilated supercavitation, excessive nuclei concentrations can impede visualization. Ideally, testing would be performed in a closed loop cavitation tunnel with a degasser to allow for any residual cavitation nuclei to be removed.

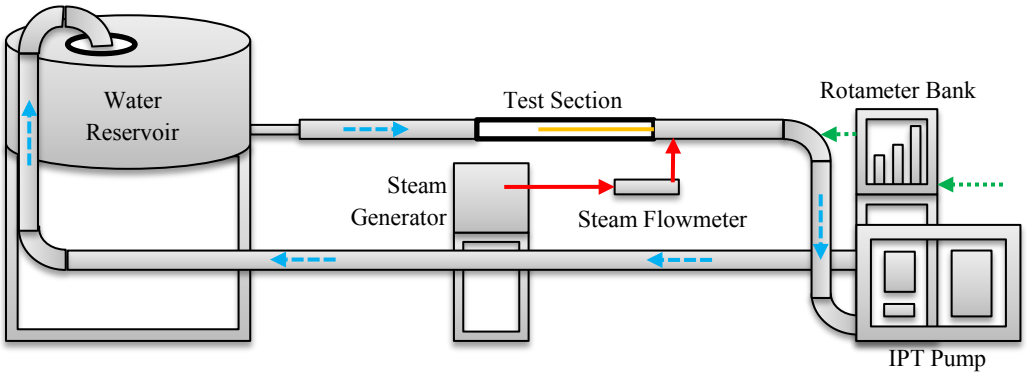

Figure 13. 2D plane view schematic of flow loop for axisymmetric testing. Solid red and dotted green arrows denote steam and CA supply paths respectively; yellow line denotes direct ventilation supply line to test specimen with ventilation gas depending on testing scenario. Broken blue arrow denotes water flow direction.

Through the review of experimental supercavitation research, it was determined that a 1 cm disc cavitator would provide a test specimen for which supercavitation could be relatively easily achieved while allowing for comparison to existing research. The test specimen was constructed of stainless steel to provide a smooth contact surface to promote a smooth and symmetric cavity and minimize corrosion while maintaining structure integrity under the high temperatures of steam ventilation. Twelve holes concentrically drilled directly behind the sharp edged disc served as vents, allowing for ventilation gases to be inserted in the turbulent wake directly behind the cavitator head. The gases traveled from the ventilation source through the hollow support tube and body of the cavitator. This design allowed for independent venting of steam and CA as well as premixed, concurrent ventilation.

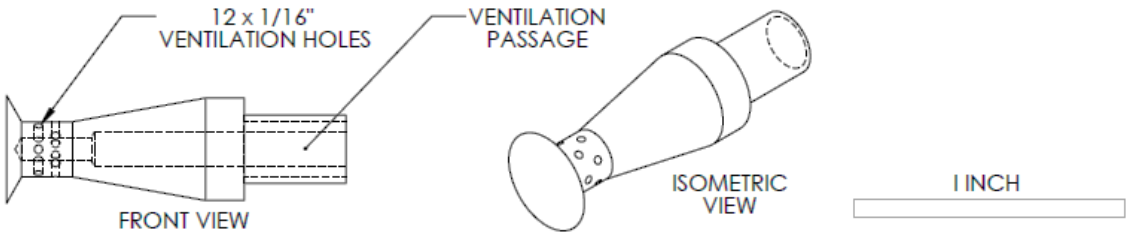

Figure 14. 1 cm, sharp edged disc cavitator used for experimental testing. The body is hollow to allow for ventilation gas transportation with twelve ventilation ports for venting.

A second cavitator (here referred to as the jetting cavitator) was designed to allow for experimental testing of the effect of axisymmetric jetting for combinations of steam and gas on supercavity development. The design consisted of separate and isolated ventilation paths for steam and compressed air with the steam venting interior to the compressed air. The design was motivated by jetting theory in the hopes of artificially creating an insulating non-condensable boundary layer to reduce steam condensation. The design allows for individual ventilation of steam and CA as well as unmixed, concurrent venting. As conventional machining was infeasible due to the complex internal geometries, the cavitator was made of 3D printed ABS.

The vents were concentric with discrete points venting parallel to the axial plane of the cavitator to reduce swirl[4][5]. Discrete points of exit would result in three dimensional

[4] Swirl results in increased dispersion of the jets through the increased vorticity as a result of the swirl increasing the energy of the flow, hence promoting vortex development and mixing [96].

vorticity and subsequent azimuthal and radial mixing, both of which would progress for increasing downstream location and severally compromise the ability for steam layer preservation. The addition of a recessed slot for discrete ventilation nozzles in film cooling of turbine blades has been shown to allow for the creation of a more continuous coolant distribution. The slot or channel allows for circumferential distribution to occur before encountering the main flow with the hope of minimizing any azimuthal mixing of the flows [78, 79, 80]. A similar result was found by Goldstein et al. who noted that the slot decreases the mean velocity of the cooling film, minimizing penetration into the flow and allowing for attachment to the wall as well as better spreading, especially for higher ventilation fluxes [81]. Slots were thus added to the test specimen, extending past the discrete vents to create annular ventilation channels for both the air and steam. An offset ratio of $d/w=1$ was chosen to limit large scale fluctuations as proposed in the theoretical feasibility analysis.

---

[5] Vortex cavitation occurs in low pressure vortex cores [9]. It is possible that a cavitator designed to rotate at such a speed to generate a significant vortex about the body of the device may allow for natural cavitation of the oncoming flow, allowing for supercavitation without the need for ventilation.

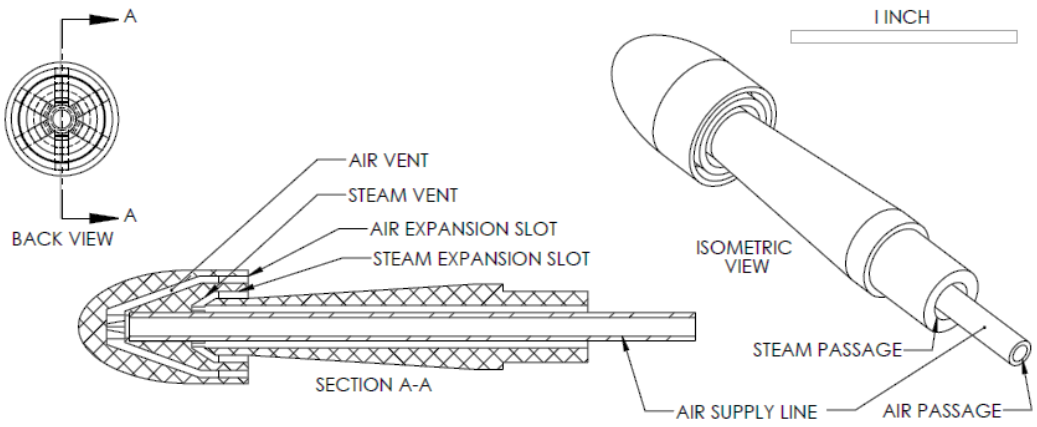

Figure 15. Jetting cavitator design. Note separate ventilation paths for steam and CA with the steam venting interior to the CA. Ventilation channels allow for circumferential mixing before jet exit.

After testing with the disc and jetting cavitator, it became apparent that ventilation off-tangent to the flow and behind an abrupt geometry change as with the disc cavitator allows for the creation of larger cavities, the flow forcing the ventilation gasses toward the cavitator surface but not before the cavity significantly thickens relative to the jetting cavitator. A third cavitator (here referred to as the film cavitator due to the similarity of its steam vents to film cooling nozzles) was then designed to incorporate several of the design features of the first two cavitators. Separate pathways were provided for steam and air, again with air venting before and largely exterior to the steam in hopes of creating an insulating layer of non-condensables to shield the steam during concurrent venting, allowing for an increase in the net ventilation flux.

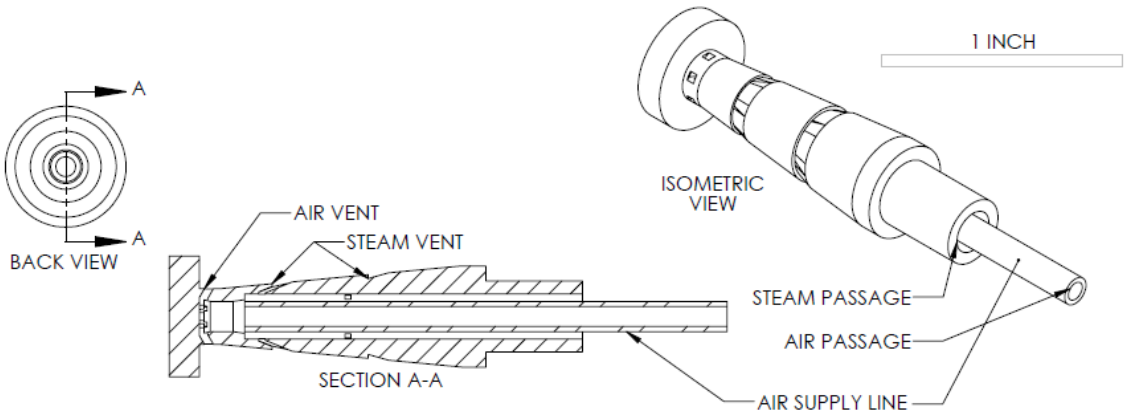

Figure 16. Film cavitator design. Air vents are directly behind disc with steam vents downstream and angled 18° relative to the cavitator surface. Ventilation channels allow for circumferential mixing of steam upon exiting vent.

A disc served as the head of the cavitator with air vents oriented 45° from tangent to the flow. As the goal was to effectively create a film of steam which was itself shielded from the oncoming flow by a film of non-condensable gas, film cooling literature was consulted for design guidance. Film cooling vents are often oriented 20°-35° from tangent to the flow, relying on the mainstream flow to force the jet towards the surface; this effect is somewhat offset for higher ventilation fluxes in which the momentum of the jet allows for further penetration into the bulk flow and potential lift off of the jet from the surface[6] [82]. The steam vents were thus oriented at 18° tangent to the flow, being recessed in thin slots so as to minimize azimuthal mixing after ventilation as discussed

[6] The angle of 20°-35° tangent to the flow appears to be largely a consequence of manufacturing limitations such that the importance from a design optimization standpoint is unclear.

for the jetting cavitator. 3D printing was again used as machining of the very small diameter vents was difficult given their low angle of incidence.

A support tube that also served as a portion of the ventilation path connected directly to the cavitator bodies (threaded connection for sharp edged disc and press-fit sealed with epoxy for jetting and film cavitators) and was connected to the external ventilation sources through watertight connections downstream of the test section. This configuration technically prevented supercavities from forming as cavity closure could not occur aft of all solid surfaces, rather creating partial attached cavities. The behavior of super and partial axisymmetric cavities are very similar however, and it is believed the results can be safely extended to real supercavities. As the jetting cavitator required an air supply interior to the steam supply for unmixed, concurrent ventilation testing, a 1/8" stainless steel pipe was routed through the interior of the cavitator support/steam tube. A press fit secured the hose into the cavitator itself with compression fittings at the downstream ventilation junction fixing all pipes in place and preventing the air supply pipe from backing out of its press-fit in the cavitator head.

The test chamber itself was made of clear, 3' schedule 40 acrylic tube. The cavitator was secured within the test section using a radial array of screws clamped against the support tube. The location of support struts can greatly affect cavity development through upstream effects as discussed by several authors [21, 83]. The small frontal area of the screws minimized effects on the surrounding flow and, as they were placed aft of the cavitator by several inches, upstream effects were assumed negligible. Lock nuts on the

screws were tightened against the test chamber outer surface to provide additional stability for the screws and prevent their loosening. Extreme care was taken to level the specimen within the test section to reduce asymmetric effects on cavity development and shape.

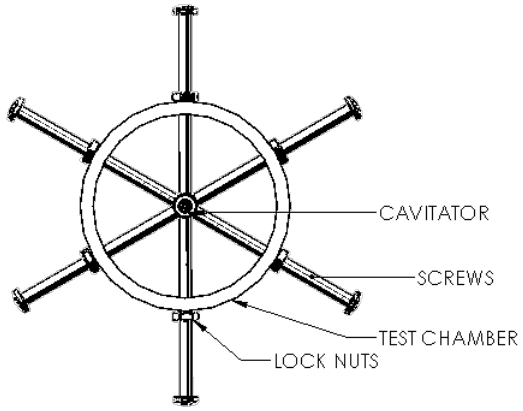

Figure 17. Securing system for cavitator. 6 #10-32x3" machine screws clamp down on cavitator support pipe. Lock nuts secure screws and insure they are square against tubing.

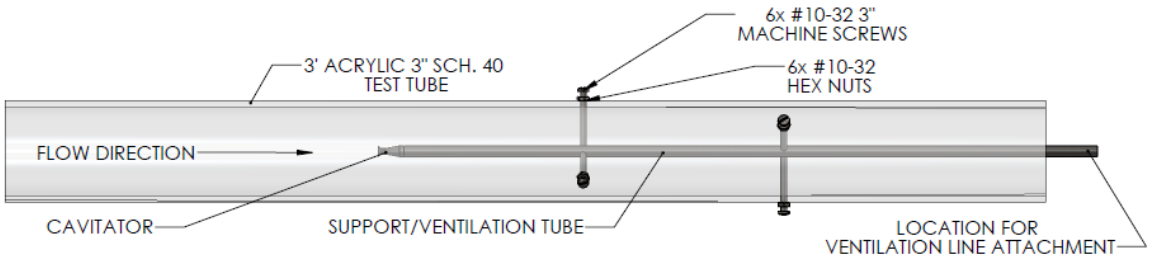

Figure 18. Clear test chamber with cavitator and cavitator securing system. Ventilation gas hoses connect directly to hollow supply/ventilation tube.

For steam ventilation, an initial amount of superheat was obtained by allowing the steam generator to operate at elevated pressures, resulting in superheated steam upon expansion through the flow valve. After measuring the temperature at various positions, it

was determined that significant cooling occurred along the ventilation supply path, especially upon entering the water flow loop, resulting in partial condensation of the steam prior to venting. While the addition of insulation along the ventilation path largely offset this cooling, a 36", 125 W rope heater wrapped around the steam ventilation line allowed for additional superheating to be achieved such that the temperature at the steam flowmeter was maintained at 122°C, allowing for sensible heat loss along the ventilation path without condensation and ensuring superheated steam at the flowmeter such that the quality was of no concern in determining the density of the steam.

Due to limitations in the steam and compressed air supplies and measurements, rather small ranges of flowrates were able to be tested. Fear of condensation required a substantial amount of ventilation such that the range of steam flowrates varied between approximately 1 and 4 g/s (2-8 CFM assuming a steam density of 1 kg/m^3)[7]. The lower bound of this range resulted from the realization that successful steam ventilation was dependent on the steam reaching the cavitator in a superheated or saturated state. Direct measurement of the steam temperature and pressure at ventilation was infeasible for the testing configuration and simple visualization of the steam entering the cavity was incapable of providing any certainty in the ventilation quality, requiring calculation according to heat transfer relations instead. For an initial superheat of 22°C and without

[7] Steam density of 1 kg/m^3 is an estimate that covers the range of densities for the expected ventilation pressures.

insulation along the steam ventilation network, steam flowrates in excess of 290 g/s were required for venting at *x=1*. Two layers of insulation double faced with foil were secured along the ventilation path within the flowloop, allowing for steam flowrates of 14 g/s to maintain vapor saturation; the required flowrate was decreased to 2 and 1 g/s for ventilation at *x=0.9* and *0.5* respectively; while condensation would occur for these cases, it was assumed that the vapor volumetric flux would render the liquid volume flux negligible. Lower steam flowrates were not used during testing as no steam could be seen exiting the vents for ventilation below 1 g/s even though the assumption of negligible liquid volumetric flowrates was expected to still hold. The upper bound of 4 g/s was selected as this was the highest ventilation rate at which the steam generator could maintain pressure and thus sustain ventilation at a given flowrate.

Air ventilation ranged between 0.0005-0.5 CFM, these limits being set by the measurable range of the rotameter bank. Considering the steam and air ventilation ranges, the range of non-condensable mass concentrations, $\dot{m}_{air}/\dot{m}_{total}$, for mixed, concurrent ventilation in which the steam and air flows were passively mixed upstream of the disc cavitator ranged from 0-33 percent. Of course the addition of steam required traversal through steam flowrates below the lowest measured value of 2 CFM; as such the actual non-condensable mass fraction range was from 0-100 percent for the addition of steam to air ventilation. Similarly, the volumetric ventilation ratio, Q_{steam}/Q_{air}, for unmixed concurrent ventilation ranged from 20-1600 for the measured ranges with actual ranges being from 0 to 1600.

Given the traditional use volumetric fluxes in ventilated supercavitation research, all ventilation rates will be given as volumetric flowrates in the discussion of results. Extension to mass flowrates or ventilation fluxes (volumetric flowrate per unit area) will not drastically affect the qualitative trends as the density of steam and air are of the same relative magnitude for the pressures and temperatures seen here. The same holds when considering the results from a momentum or velocity standpoint as the total vent areas are similar.

The relatively low velocity of the water corresponded to a low Froude number condition in which the effect of gravity was large, resulting in significant upward deflection of the cavity. As such, vertical testing orientations were considered to allow for more axisymmetric behavior. An upward flow over a downward oriented cavitator was feared to have undeterminable effects on the cavity due to the buoyant acceleration of the cavity, leading to a potential for artificial lengthening of the cavity and significant changes in the evacuation process compared to horizontal behavior. An upward pointing cavitator in a downflow of water was also considered after the realization of substantial cavity formation for spargers in down flowing pipes [84]. While this may seem advantageous, the cavity creation is not "pure" in the sense that such large, continuous cavities would be unlikely for sparger designs at similar ventilation fluxes in a horizontal flow; it seems that the buoyant motion of the ventilation gases allow for the creation of a large, continuous bubble in the small recirculation zone following the sparger vent rather than the gasses being instantly swept away by the flow.

CHAPTER 4: DISCUSSION OF EXPERIMENTAL RESULTS

A. Flat Plate Testing

The flat plate testing procedure was much less rigid compared to axisymmetric testing with specific ventilation rates being ignored as qualitative observations were of much greater interest. In situ modification and greater control of testing parameters as well as the much less fragile testing specimen allowed for a significant number of combinations to be tested, the ranges of steam and air flowrates being cycled interchangeably and in various sequences. Due to the much shorter steam ventilation network and its limited submersion length, smaller steam flowrates could be tested compared to the axisymmetric case as a result of the much reduced heat transfer rate and corresponding reduction in steam condensation in transit to the test specimen. The reduced lower limit of steam ventilation is significant in that it allowed for ventilation ratios approaching and even receding below one to be tested, and thus allowed for evaluation of the ventilation ratios proposed in the theoretical analysis. Ventilation ratios, Q_{steam}/Q_{air}, on the order of several tens will here be referred to as moderate with smaller and larger ratios being referred to as low and high respectively.

While the pulsation plate did increase the stability of the cavity and allowed for slight increases in its length, overall trends with respect to vapor ventilation did not vary compared to testing without the plate; consequently no distinction will be made between

Table 2. Testing configurations for flat plate testing based on specimen orientation and add on features.

Vent Angle (Air/Steam)	Specimen Angle	Channel Gate	Pulsation Plate	Cavity Closure Insert
90/45°		X	X	
60/30°	±5°	X	X	
0/0°	±5°		X	X

testing results with or without the plate. Addition of the cavity closure insert to the 0/0° specimen allowed for a stable cavity with thickness equal to the nozzle depth to be maintained without any ventilation. Addition of air ventilation to the initially stagnant cavity resulted in a thickening of the cavity with bubbles periodically breaking from the tail. A similar trend was seen for very low flowrates of steam which also resulted in condensation along the viewing windows. Destruction of the cavity occurred for increasing steam ventilation after which steam only venting behavior occurred as will be discussed below; similarly, concurrent ventilation exhibited the same behavior for testing without the closure plate. There are no foreseeable advantages of steam ventilation for this cavity state as it represents the optimal scenario for ACS designs as no ventilation is needed following initial cavity formation; the results of this configuration will not be discussed further.

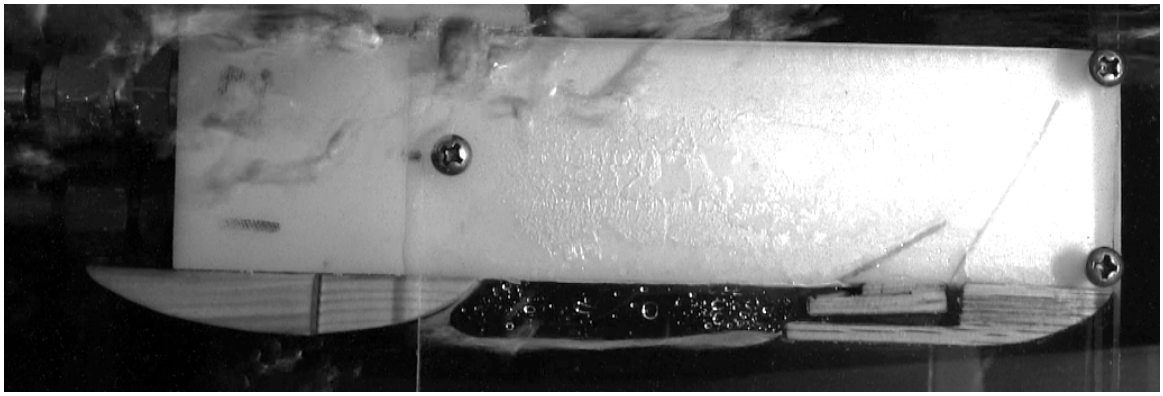

Figure 19. The addition of the cavity closure plate allowed for the existence of a stable cavity without ventilation.

The angle of the test specimen had a significant impact on overall cavity behavior including significant differences in the critical ventilation rates for cavity development, cavity closure, and the effects of steam ventilation. For horizontal orientations, large bubbles of ventilation gases escaped from the front of the specimen rather than being exclusively swept downstream. This resulted in large scale pulsation of the cavity, severely compromising the ability to discern testing results. This issue was magnified for increasingly positive attitudes with ventilation gasses escaping primarily from the front surface for the maximum attitudes tested. Negative attitude orientations served to prevent bubbles from escaping from the front of the specimen but also resulted in an acceleration of ventilation gases along the test surface due to buoyant effects, increasing the required ventilation flux for successful cavity development.

The optimal configuration was found to be a slightly downward specimen orientation with the flow channel gate extended below the flat plate surface. The gate, which is representative of a reverse step in the hull of an ACS or a sharp edged cavitator for

comparison to axisymmetric supercavitation, served as a barricade to prevent air from escaping from the front of the specimen, reducing the pulsation amplitude of the cavity and confining it largely to the cavity tail. The slight negative attitude allowed for the majority of the cavity to be shed upon cessation of ventilation such that a stable, stagnant cavity extending past the immediate recirculation zone downstream of the gate was impossible. This was essential to allow for a pure evaluation of the effects of steam ventilation alone. In the event that steam ventilation would lead to significant increases in the length of an initially unventilated cavity, testing was also done at a horizontal orientation in which an unventilated cavity was able to remain.

1. Air Only Ventilation

For low flowrates of CA alone, the turbulent interaction of the cross flow orientation for the 90/45° specimen severally compromised the ability of a continuous cavity to be formed and resulted in large pulsations along the entire cavity length, with the cavity instability increasing for increasing CA flowrates. High speed video showed the pulsations to initiate along the front of the cavity, traveling its length, and resulting in the pinching off of large bubbles, up to seventy-five percent of the cavity length upon the pulsation wave collapsing to the solid surface of the test specimen. For the upper range of air flowrates tested, cavity closure was actually by cavity detachment as will be discussed below.

The extreme instability of this test specimen limits its usefulness as an ACS design; important insight into the dynamics of ventilation can be gained however. Upon exiting

the vent, the air is carried into the oncoming flow by its momentum, the length of penetration being proportional to the ventilation momentum itself. The flow then serves to turn the gases tangent to the mean flow direction, this direction being itself dependent on ventilation as evident by the curvature of streamlines about the cavity[8]. For very large ventilation fluxes, the ventilation momentum is sufficient enough to actually cause a separation bubble to form within the cavity along the testing surface, this separation being analogous to the liftoff of very high momentum cooling jets as seen in film cooling applications. The separation leads to destruction of the cavity due to periodic shedding of the outer, unattached cavity as shown in Figure 20. Comparison to axisymmetric testing showed that the faster flow speeds result in more rapid curvature of the ventilation gases, allowing for continuous cavities to be formed without detachment for even the highest air ventilation rates tested.

The 60/30° specimen exhibited similar behavior but was generally more stable with the pinch-off pulsation being constrained to the tail of the cavity. The overall cavity thickness was also much reduced as the inertia of the air vent was limited in its ability to penetrate the cross flow before being turned tangent to the flow. For a relatively low flowrate of CA alone, a rather steady cavity of uniform thickness equal to the depth of the channel gate and spanning the entire length of the test surface could be formed with small

---

[8] Bubbles within the flow served as particle tracers, allowing for observation of the general shape of streamlines about the test specimen as well as recirculation zones and wake behavior.

frequency, small amplitude pulsations confined mostly to the rear portion of the cavity. Increasing the air ventilation resulted in increasingly unstable cavities of increasing thickness. Eventual transition to periodic pinch-off and even detachment was observed, but at higher ventilation rates than for the 90/45° specimen.

The 0/0° specimen created very uniform cavities spanning the entire length of the test surface with very limited pulsation as a result of the much smoother flow separation; instabilities were again seen for increasing air ventilation but the overall thickness and length remained largely unaffected. Cavities spanning the entire length of the specimen could be created at much reduced air ventilation rates for the 0/0° specimen compared to the others, apparently as a result of the reduced cavity pulsation and subsequent stability as well as the absence of cavity thickening due to the tangent ventilation. This conclusion is confirmed by the prevalence of venting along the hull recess in ACS designs.

2. Concurrent Steam and Air Ventilation

The behavior of concurrent venting of steam and CA was dependent on the ventilation ratio as well as the individual ventilation rates and even the order and rate at which ventilation was altered. The behavior was similar for both the 90/45° and 60/30° specimen and will be discussed first without distinction between the two cases with the 0/0° results to follow. For low ventilation ratios, the cavity appeared to be filled with both steam and air as condensation occurred along the interior viewing window, anterior to and aft of the vapor vent. The cavity thickness was increased for the addition of steam, but at the expense of magnified cavity instability. It is difficult to determine if the

thickening corresponds to an increase in the cavity volume or if it is a result of the increased amplitude of pulsations as direct comparison of the cavity volume was complicated due to the pulsation of the cavity which drastically varied in both scale and frequency. The individual ventilation rates of both the steam and air were important in that they affected the overall thickness of the cavity as well as the point at which transition to an unstable cavity occurred; larger initial cavities as created by larger air ventilation rates were less sensitive to the addition of steam while very small cavities showed unstable transition at even the lowest ventilation ratios.

For increasing ventilation ratios, interaction of the individual jets was increased, replacing diffusive mixing throughout the largely stable cavity as seen for low flowrates. Due to the large incidence angles of the air vents, an arched cavity anterior to the steam vent location was seen to develop as a result of the air jet being carried away from the surface by its momentum before being entrained by the steam jet. For moderate ventilation fluxes, the cavity was still largely continuous after the entrainment point as seen in Figure 21 with large bubbles breaking off from the cavity tail. Vapor condensation could be seen in the forward cavity, suggesting backflow of the ventilation gasses upon entrainment. This is to be expected as the entrainment is rapid enough to result in the formation of an impinging jet directed towards the test surface and subsequent stagnation point behavior. For high ventilation ratios, the entrainment was so turbulent that no cavity remained aft of the steam vent, the wake being a turbulent mass of smaller bubbles that were consequently swept downstream with great speed. The

thickness of the downstream wake increased for increasing steam ventilation rates for both moderate and high ventilation ratios.

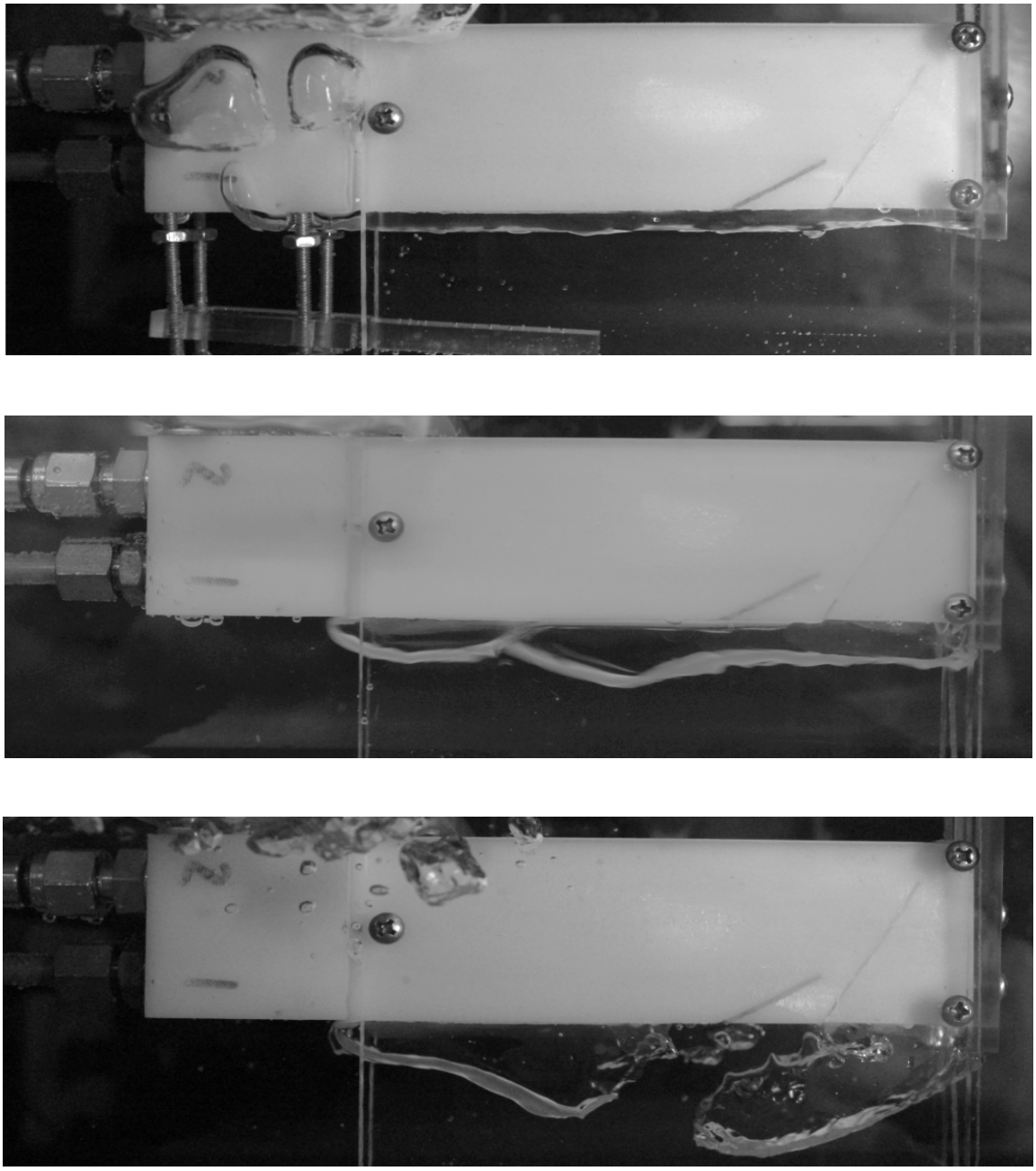

Figure 20. Comparison of cavity thickness and dynamic behavior for CA only ventilation at 1 SCFH with pulsation plate (top) 1 SCFH (middle) and 5 SCFH (bottom). Pictures were taken at moment of cavity pinch-off.

Figure 21. Concurrent steam and CA ventilation showing entrainment of CA by the steam vent; low ventilation ratio. Notice continuation of continuous cavity downstream of steam vent with large scale bubbles breaking from rear of cavity.

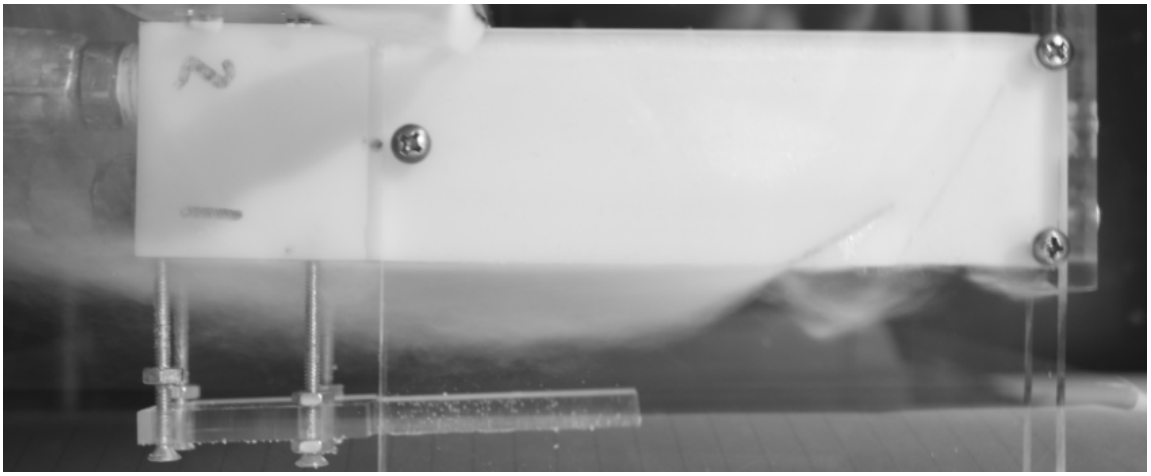

Figure 22. Long exposure photograph of concurrent steam and CA ventilation showing entrainment of CA by the steam vent; moderate ventilation ratio. No continuous cavity remains aft of steam vent but rather a frothy mass of bubbles.

Significant differences were seen for concurrent ventilation using the 0/0° specimen. For very low ventilation ratios, the cavity exhibited very little change save for the

observation of condensation along the viewing windows. For low to moderate ventilation ratios, the cavity aspect ratio was actually decreased. Rather than a thickening of the cavity as seen for the 90/45° and 60/30° cases, the added inertia of the steam jet resulted in partial entrainment of the air jet, resulting in a reduction of the cavity thickness and an increase in the speed of the ventilation gasses within the cavity. This behavior is in fact very similar to that expected by jetting theory although the large vs. small scale instabilities were indistinguishable. The entrainment was partial in that it was a more gradual merging of the jets without the creation of an impinging jet as opposed to the very energetic entrainment seen for higher ventilation ratios as discussed above. As such, a continuous cavity was maintained with large bubbles periodically breaking from its tail. The absolute ventilation rates were also much less critical than for the angled ventilation specimen as the cavity thickness was more uniform, being roughly equal to the depth of the nozzles.

Perhaps most interesting was the release of vapor from the bubbles upon reaching the free surface and imploding, indicating that the bubbles were in fact comprised of both air and steam. This was seen for low to moderate ventilation ratios for all of the test specimen. As the ventilation ratio was increased, the energetic entrainment of the air vent by the steam vent resulted in the destruction of the cavity. The resulting frothy wake was comprised of bubbles whose size varied proportionally to the ventilation ratio, being larger than 1 mm in diameter for moderate fluxes; for low ventilation fluxes, large bubbles were released from the cavity tail. For larger bubbles, the normalized surface

area is small compared to the volume and thus results in reduced heat transfer, allowing for slower condensation and subsequent formation of the NC boundary within the bubble which serves to preserve the steam as it rises to the surface. The smaller bubbles formed by high ventilation ratio testing and steam only ventilation experienced much reduced buoyant effects and were subsequently swept further downstream until they eventually disappeared due to condensation for the case of steam only venting or escaped through the free surface without noticeable vapor expulsion for the case of concurrent ventilation.

The above results were for the addition of steam ventilation to air ventilation. It did appear that the addition of an immeasurable amount of air allowed for the immediate creation of a cavity for initially steam only venting for which no cavity could be achieved; subsequent cessation of steam venting resulted in destruction of the cavity. While this appears to support the idea of steam allowing for cavity creation at smaller CA ventilation requirements, no air flow was seen whatsoever upon cessation of steam ventilation. As such, it appears that this effect is an artifact of the testing scenario rather than a pure result. It is proposed that steam ventilation results in a reduction of the local pressure in the flow channel, initiating an immeasurable increase in the pressure driven flow of CA, this flow ceasing upon cessation of steam ventilation as the pressure difference no longer exists. This explanation is supported by the observance of air bubbles occasionally escaping from the air ventilation chamber during steam only venting.

3. Steam Only Ventilation

Steam ventilation alone was incapable of creating a continuous cavity for any of the test specimen. A small vapor dome similar to that described by DCC theory formed directly at the vent for moderate and larger flowrates. This plume was very small, on the order of 1 mm or less even for the highest flowrates, and was elliptic in nature, indicative of the inertial expansion mentioned in DCC literature. Outside of the plume, rapid condensation occurred, resulting in the formation of a frothy, cloudy wake of very small bubbles. The bubble diameter was much less than 1 mm, substantially smaller than those seen for concurrent ventilation except for at the highest ventilation ratios. For low flowrates, condensation was so rapid that neither a steam plume nor bubble filled wake were seen.

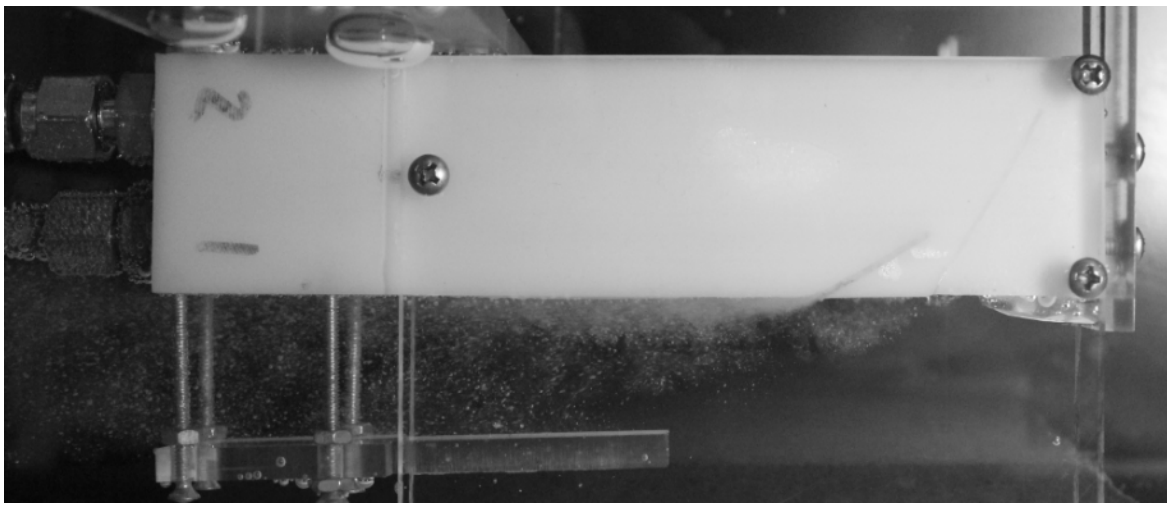

Figure 23. Steam only ventilation showing small steam bubbles; large steam flowrate. Bubbles in front of steam vent are result of failed sealing between viewing windows and test specimen. Small stagnant air bubble remains in wake of gate.

The ventilation of steam was somewhat skewed by the presence of air bubbles of various sources. The initiation of steam ventilation resulted in the release of approximately 10 mL of air into the testing channel, a substantial volume when compared to the volume of the testing channel, as a result of air being present in the vapor generator. This resulted in the apparent creation of a steam cavity when it was indeed just an air cavity. Such a bubble or cavity persisted for very low steam flowrates in which case there was insufficient turbulence to cause detachment of the bubble from the vent edge. Air was also seen entering the steam ventilation channel after cessation of testing for which an air cavity extended below the steam vent, this air adding to the volume of air expelled upon the initiation of steam ventilation. Steam only ventilation testing thus relied on venting at a high enough flowrate to expel air initially in the steam ventilation network and detach any bubbles before results were gathered. While these artifacts were also present during concurrent ventilation, the continuous release of bubbles from the rear of the cavity accounts for the initial, artificial increase in air ventilation.

These testing artifacts also complicated analysis of the interaction of steam with an initially stagnant, unventilated cavity, resulting in an apparent increase in cavity volume due to the addition of steam when this increase was again due to the air artifact. After the initial volume increase, very low steam ventilation rates allowed for a thickening of the cavity with condensation occurring all along the viewing windows suggesting largely diffusive mixing throughout; the cavity remained largely static without any bulk motion. Small increases in the steam ventilation rate resulted in a transition to a cavity whose

contents had a bulk velocity tangent to the flow as a result of the increased inertia of the steam vent. This resulted in a reduction of the cavity aspect ratio, becoming longer and thinner. Further increases in the steam ventilation resulted in destruction of the cavity after which steam only ventilation characteristics followed.

Any air pockets initially upstream of the vapor vent were also affected by steam only ventilation, stably growing in size until their advancing front reached the steam vent at which point they were entrained by the steam jet and swept downstream. It is hypothesized that the initial growth is a combination of a decrease in the surface tension as a result of the increased local temperature for steam ventilation as well the slow expansion of air into the pocket from the air ventilation network. This expansion is likely a combination of the reduced pressure within the testing channel as a result of the steam vent initiating a small pressure driven flow as well as thermal expansion of the air itself due to heating of the air tube by conduction within the test specimen. Vaporization of the flow across the pocket interface as a result of the increased local temperature may also contribute to the pocket growth as condensation could be seen within the pocket as it approached the steam vent. While this is an interesting observation, it has no perceivable effect on overall cavity development and was not investigated further.

4. Conclusions of Flat Plate Testing

These results highlight the advantage of ventilation tangent to the flow and along the surface for ACS designs as stable cavities of significant length can be created at lower ventilation fluxes compared to off tangent ventilation. Unfortunately no significant

advantages were realized for the addition of steam to air ventilation even for wall jetting of steam interior to an offset air jet. In fact the addition of steam was seen to reduce the stability of the cavity for even moderate ventilation ratios, resulting in pulsations that reduced the overall length of the cavity due to large scale bubble pinch-off. Even for very low ventilation ratios in which some lengthening of the cavity was seen due to the increased inertia of the cavity contents stretching the cavity, the overall lengthening was only a small percentage of the overall cavity length and thus offers little improvement to air only ventilation. It is thus concluded that ACS cavity creation can be better optimized through more traditional techniques such as the addition of foils below the cavity to reduce cavity pulsation, the use of geometries to allow for smooth reattachment of the cavity to the surface, and careful control of the attitude of the hull relative to horizontal. The stability of the cavity was also dependent on upstream geometries, being minimized for a streamlined step which served to reduce destabilizing pulsations along the cavity interface.

Extension of these results to axisymmetric testing is difficult considering the creation of a cavity is here largely a result of ventilation gases being trapped along the solid surface by buoyant effects. This containment of the gases will not be possible for axisymmetric testing as the gases will be free to peel around the bottom surface of the device with ventilation on the top and sides being completely unconstrained in their upward buoyant deflection. This will also prevent the creation of stagnant, unventilated cavities save for the potential of a gaseous recirculation zone directly behind the cavitator

head. It was shown that continuous cavities could be maintained for low ventilation ratios with increasing ventilation ratios resulting in increasingly energetic entrainment of the air jet by the steam jet, leading to destruction of the cavity and the creation of a bubble filled wake. A similar trend is expected to hold for axisymmetric testing.

B. Axisymmetric Testing

Due to the limited applicability of flat plate test results to axisymmetric supercavitation, testing was performed with three axisymmetric cavitators in a higher velocity flow more indicative of actual supercavitation applications. The three cavitators were designed such that the proposed advantage of steam ventilation as a means by which non-condensable ventilation requirements could be reduced or altogether replaced could be tested. A common testing sequence was used for each cavitator and was as follows:

1. *Baseline testing for air only ventilation*
   1A. Determine minimum CA flowrate needed for attached and stable cavity
   1B-C. Test with CA only at 0.01/0.1 CFM
2. *Concurrent ventilation testing for minimum CA ventilation*
   2A-D. For CA flowrate determined in 1A, add steam at 2/4/6/8 CFM, reduce CA flowrate
   2E-H. For CA flowrate determined in 1A, reduce CA flowrate to hysteretic limit, add steam at 2/4/6/8 CFM, reduce CA flowrate
   2I-L. For CA flowrate determined in 1A, incrementally increase CA flowrate, add steam at 2/4/6/8 CFM, reduce CA flowrate
   2M. For CA flowrate determined in 1A, cycle through steam ventilation range
3. *Concurrent ventilation testing*
   3A-D. For CA flowrate at 0.01/0.1 CFM, add steam at 2/4/6/8 CFM, reduce CA flowrate
   3E-F. For CA flowrate at 0.01/0.1 CFM, cycle through steam ventilation range
   3G-J. For steam flowrate at 2/4/6/8 CFM, add air until cavity formation, reduce steam flowrate
   3K. Freely cycle through air and steam ventilation combinations
4. *Steam only ventilation*

Test case 1 allowed for a baseline comparison between the cavitators for the traditional use of non-condensable ventilation gasses. Determination of the critical ventilation flux for development of a stable attached cavity, stable in the sense that it was maintained at largely the same volume indefinitely, provided a measure of the overall susceptibility of each cavitator to generate an attached cavity. Discrete flowrates of steam were then added to this critical value in the hopes of evaluating whether or not steam could allow for the creation of larger cavities. As expected by supercavitation design theory, a hysteretic effect could be seen in which a higher ventilation flux was required for initial cavity development than that needed for its maintenance; the addition of steam was also tested at this hysteretic limit. An incremental increase of air above the critical ventilation rate before steam addition was also tested as the sensitivity of the cavity was decreased, alleviating the fear of modified cavity behavior by artifacts of the testing setup rather than by steam addition.

Test case 3 allowed for the effects of steam ventilation to be observed for larger cavities for which minute variations in the air flowrate were negligible. Cycling of the steam allowed for a much broader range of ventilation ratios to be tested then for discrete flowrates; cycling was done slowly enough to allow for changes in the cavity to be easily seen. The subsequent reduction of air following steam addition allowed for the evaluation of the proposition that concurrent ventilation would allow for reductions in the required air ventilation while maintaining cavity behavior. The behavior of concurrent ventilation was further investigated by freely cycling both the steam and air ventilation rates in

different sequences of addition. Test case 4 allowed for direct evaluation of the feasibility of pure steam ventilation.

Due to the nature of the set ventilation ranges, this study is in no way comprehensive as an infinite combination of ventilation scenarios exist. For unmixed, concurrent venting, the set ranges of air and steam flowrates correspond to approximate velocity ratios between $20<U_{steam}/U_{CA}<1600$. It is feared this ratio is much too large to allow for successful operation of the jetting cavitator as the air vent would be immediately entrained into the steam jet even for the lowest ventilation ratios, resulting in turbulent mixing and subsequent condensation of the steam. Test case 3K allowed for qualitative observations for ventilation outside of the measureable ranges, using vapor flowrates and air flowrates outside of the measureable range in the hopes of obtaining velocity ratios closer to and even receding below one. As previously mentioned, non-condensable mass fractions ranged from 0-100 percent for mixed, concurrent ventilation.

1. Test Case 1: Baseline Testing with Air Only Ventilation

For the jetting cavitator, stable, continuous, attached cavities required $Q_{air}>0.005$ *CFM* for initial formation while cavity formation occurred at flowrates below the measureable range of the rotameter bank for both the disc and film cavitators. A hysteric effect was seen in which the cavity would remain for small reductions in the minimum required air flowrate for both the disc and film cavitators; no noticeable hysteresis was seen for the departure point of attached cavitation at reduced air ventilation for the jetting cavitator.

Comparison of the size of the initial attached cavities suggests that the ventilated air has simply replaced the recirculation zone created by flow separation about the cavitator. This is supported by the observation of bubbles being captured in the wake, continually circulating without being swept downstream and thus outlining the recirculation zone which was seen to be much larger for the disc and film cavitators, even extending past the edge of the cavitator head into the flow. The larger recirculation zone following the sharp edged cavitator head resulted in a larger cavity upon initiation for the disc and film cavitators compared to the streamlined shape of the jetting cavitator.

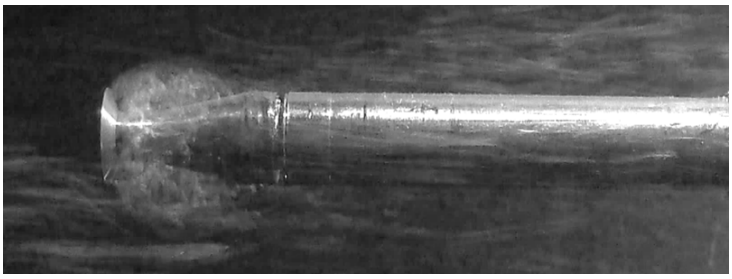

Figure 24. Disc cavitator with bubbles captured in recirculation zone following flow separation from the sharp edged disc. Zone can be seen extending past the disc edge into the flow.

Increasing the ventilation rate beyond the minimum value for successful cavity creation resulted in additional growth of the cavity, becoming larger than the recirculation zone. For the jetting cavitator, the cavity shape was rather planner, appearing as a sheet with the interface being largely tangent to the flow as seen in Figure 25 with a maximum diameter equal to that of the cavitator diameter itself irrespective of Q_{air}. Further increasing Q_{air} resulted in a lengthening of the cavity and subsequent

upward curvature due to buoyant effects but did not affect the average cavity diameter or general shape.

This cavity shape is vastly different from those formed by crosswise ventilation in which ventilation gases are carried into the flow by inertia after which they are turned back towards the body of the device resulting in the characteristic elliptic cavity shape as seen for the disc and film cavitators. Baseline testing of the disc and film cavitators at $Q_{air}=0.01\ CFM$ and $Q_{air}=0.1\ CFM$ allowed for the development of cavities with maximum diameters of roughly $2D$ and lengths of $\sim 4D$ and $\sim 7D$ respectively where D is the cavitator diameter. Further increasing the air ventilation rate past 0.1 CFM resulted in a cloudy supercavity as seen in Figure 26 for both the disc and film cavitator. This was a result of the air having increased momentum, being carried further into the flow beyond the smooth cavity interface at the azimuthal locations of the discrete ventilation ports; a continuous cavity was still maintained underneath the cloudy interface.

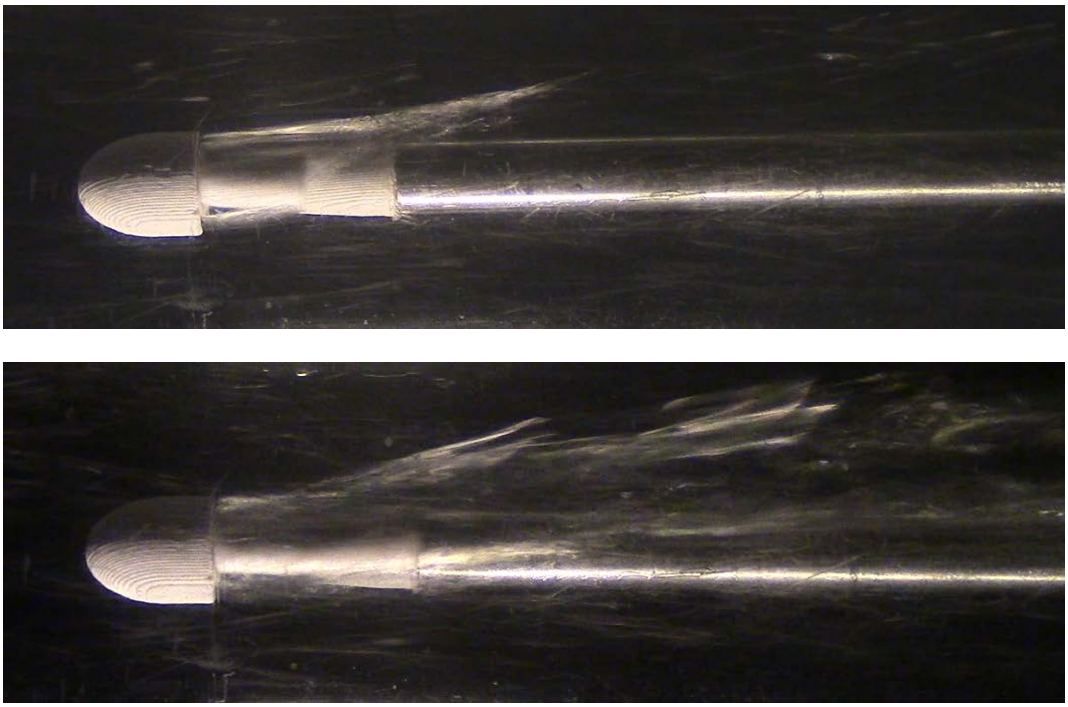

Figure 25. Jetting cavitator cavity shape for air only ventilation. Top figure for ventilation at 0.01 CFM; bottom figure for ventilation at 0.1 CFM. Flow at 4.5 mph left to right.

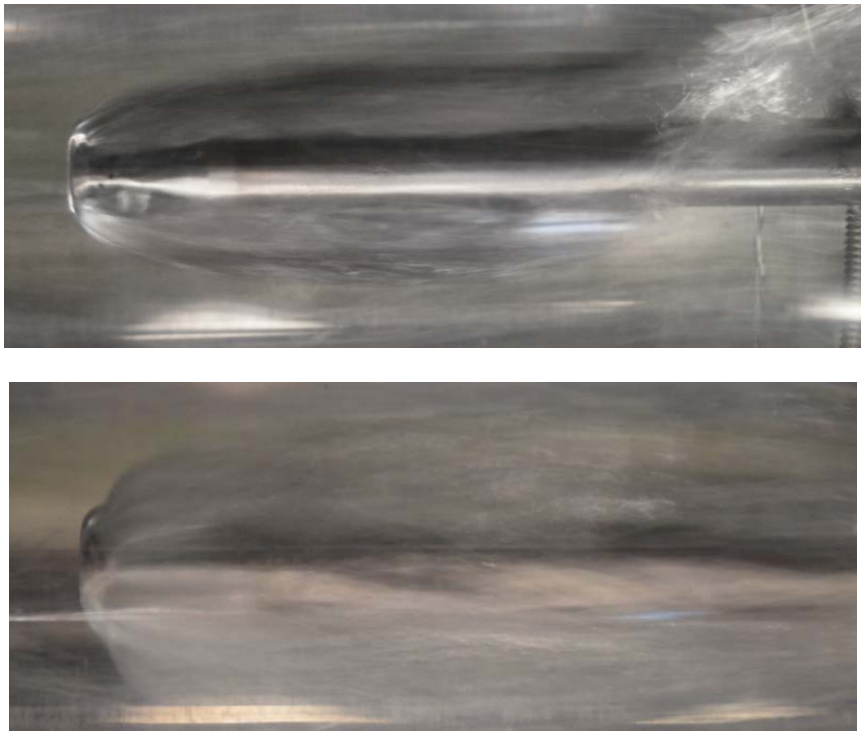

Figure 26. Air only ventilation of disc cavitator showing transition from clear to cloudy cavity as a result of excess ventilation disrupting free surface of the cavity. Similar results seen for film cavitator.

Figure 27. Disc cavitator for air ventilation at 0.01 CFM. Clear and smooth cavity can be seen. Similar cavity shapes were seen for ventilation at 0.1 CFM and for film cavitator.

Even for the differences in cavity shape, the overall cavity lengths were comparable amongst the various cavitators for similar Q_{air} values. As such, the cavities for the jetting

cavitator had significantly smaller volumes due to their largely planar shape. It is interesting that the cavity volume is significantly smaller for ventilation tangent to the flow and yet requires Q_{air} values comparable to ventilation off-tangent to the flow, suggesting the larger cavity allows for slower gas speeds within the cavity itself. Combining this observation with the replacement of the recirculation zone by ventilation gasses following flow separation in initial cavity creation and the off tangent ventilation configuration carrying the ventilation gasses into the flow where they are redirected suggests that there may in fact be a large recirculation zone within the cavity itself. This recirculation zone would alleviate the need for larger ventilation flowrates as expected for similar cavity lengths compared to the smaller volume cavities of the jetting cavitator as the ventilation would largely serve to maintain the outer cavity near the interface as this region would be characterized by an average velocity in the direction of the oncoming flow while the inner recirculation would require minimal ventilation to be sustained. This observation has no meaning to the present research but does suggest a significant aspect of ventilated cavitation behavior not found in the literature review.

For the water flowrate used during testing, significant gravity effects could be seen as shown in Figure 29. These effects were reduced for faster flow speeds which also showed a lengthening of the cavity for a given ventilation rate as to be expected for the corresponding reduction of the ventilated cavitation number. The resulting asymmetry resulted in earlier exposure of the lower support strut to the oncoming flow. This was very noticeable for the jetting cavitator due to its limited thickness. In fact, a large portion

of the cavity was actually above the centerline of the support strut for testing with the jetting cavitator as seen in Figure 25. Ventilation crosswise to the oncoming flow resulted in a much thicker cavity extending past the cavitator head into the flow for which the support strut remained interior for a larger proportion of the entire cavity length.

Cavity closure was by opposing hollow vortex tubes for all of the cavitators across all air ventilation ranges at flow speeds of 4.5 mph. Increasing the flow speed and ventilation flowrate for the disc and film cavitator resulted in transition to cavity closure by the pinching of off large bubbles due to large scale pulsations along the cavity interface. Further increases in Q_{air} or the addition of steam had no effect on the overall cavity length for this closure regime, resulting only in an increase in the pinch-off frequency. This transition was only seen for the higher water flowrates as the Froude effects were simply too large for the lower velocity water flows. This pinch off cycle can be clearly seen in Figure 28; the effect was not seen at all for the jetting cavitator regardless of ventilation or water flowrate, likely as a result of the limited thickness for which pulsations could propagate. As this region of cavity closure corresponds to excess ventilation, the addition of steam would be of no use; this cavity closure regime will not be considered further.

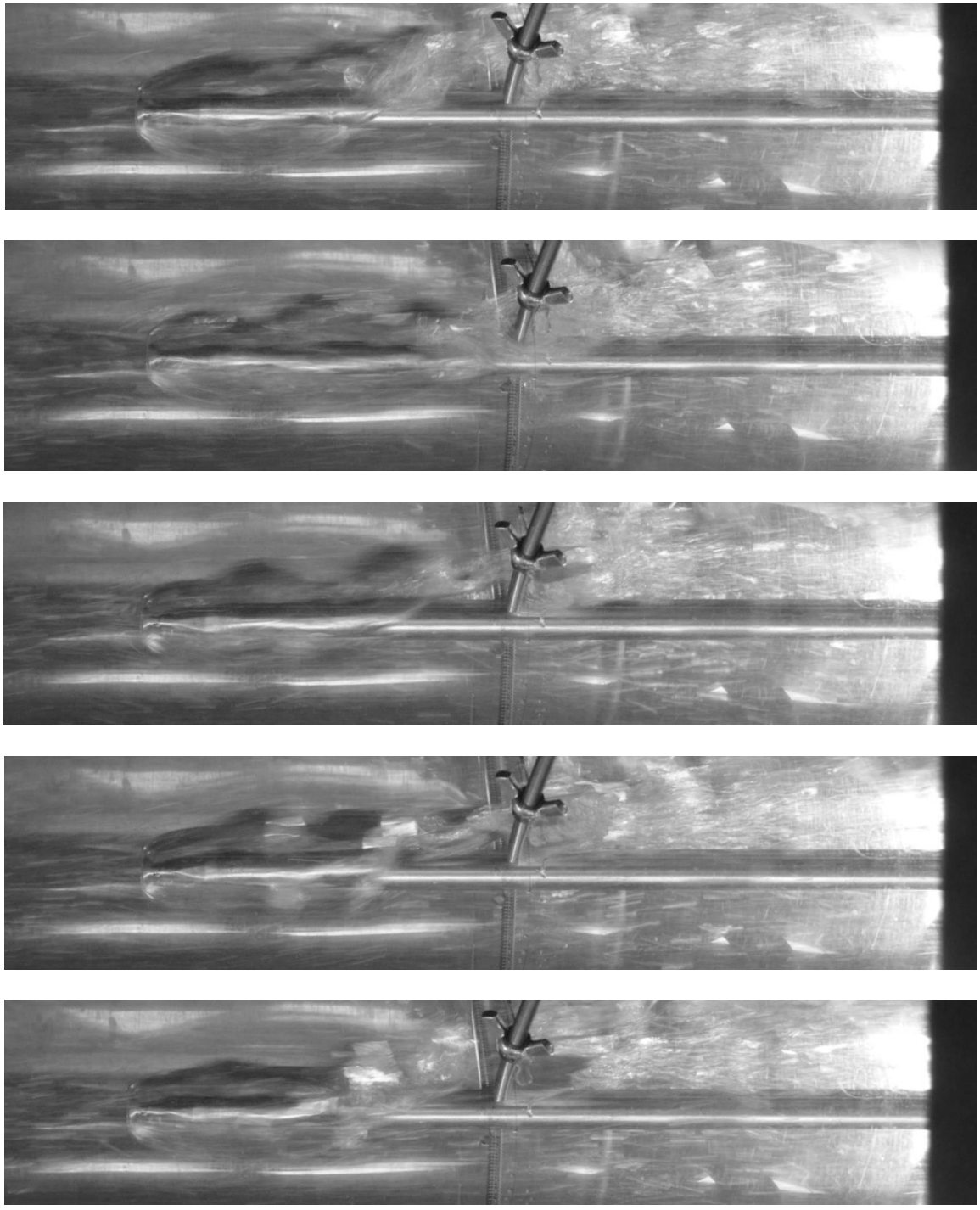

Figure 28. Sequence of photos showing the oscillatory behavior of the supercavity with periodic shedding occurring as seen by the dimpled appearance of the cavity. Flow velocity of ~ 7 mph.

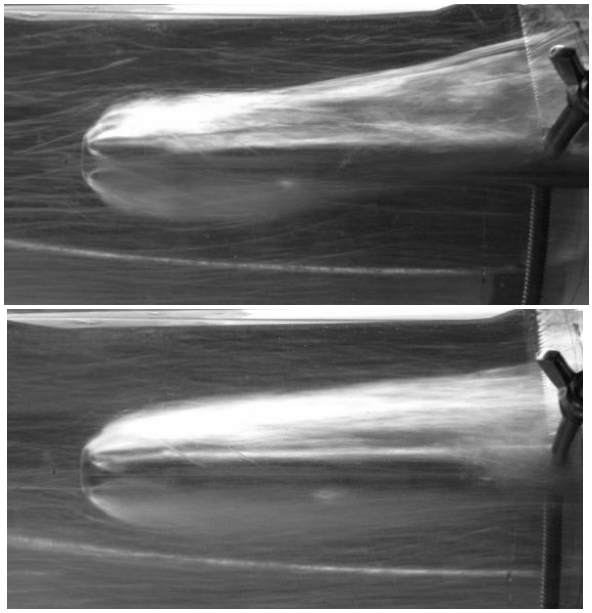

Figure 29. Comparison of cavity shape at various flow velocities for equivalent ventilation flux. Asymmetry of the cavity decreases for increasing flow speed while length increases. Left figure flow speed 4.5 mph; right figure flow speed 7 mph.

Fully developed and attached cavities were also observed on the supports when ventilation was performed as a result of the ventilation gases exiting the cavity, being entrained in the wake of the support members, and coalescing/growing to again form a continuous cavity. This occurred primarily for the support directly above the cavitator head as the ventilation gases were carried upward by buoyant forces. These cavitation structures were extremely unstable, forming and disappearing over the span of several seconds.

2. Test Case 2: Concurrent Ventilation Testing for Minimum Air Ventilation

The addition of steam at even the lowest measureable steam flux resulted in destruction of the air cavity for ventilation at both the unadjusted minimum and hysteric

minimum air flowrates for all specimen. The cavity volume was decreased as the steam was added, disappearing as or before steam ventilation reached 2 CFM. While the addition of steam required traversal of flowrates in which substantial condensation would occur, the gradual decrease in cavity volume suggests such condensation does not lead to the destruction in and of itself as the volumetric ventilation rate of liquid is negligible compared to the vapor volumetric flowrate even for ventilation rates well below 2 CFM. Similar destruction was seen for the addition of steam to a cavity created by an air flowrate incrementally larger than the critical rate although at a higher steam flowrate. As expected, the cavity was unable to reform upon cessation of steam ventilation for testing at the hysteretic limit.

For the jetting and film cavitator, cavity destruction was the result of entrainment of the air vent due to the ventilation ratio being considerably greater than one even for the smallest measured steam flowrates due to the very small air ventilation rates needed for initial cavity creation. The entrainment lead to the creation of a frothy wake comprised of bubbles with diameters on the order of 1mm. For the film cavitator, a small, largely continuous cavity remained upstream of the first row of steam vents while no such cavity remained for the immediate entrainment of air by the interior steam vent for the jetting cavitator. A slight increase in the cavity length ($<1D$) was actually seen for the initiation of steam ventilation for the film cavitator. This occurred for steam flowrates well below 2 CFM, suggesting the addition of steam may, in very specific circumstances allow for

increased cavitation potential without the need for increased non-condensable ventilation. No such effect was seen for the jetting cavitator.

Interpretation of this observation was difficult for the mixed ventilation testing of the disc cavitator as the addition of steam inherently lead to a reduction of the air flowrate, a reduction that could not here be accounted for as the critical air ventilation rate was below the measurable range. The usefulness of the result is thus rejected for the disc cavitator with the addition of steam to higher, measureable air flowrates providing more useful analysis. Even still, the destructive nature of steam ventilation on a minimally ventilated, gaseous cavity was seen for both the jetting and film cavitator for which air ventilation was maintained throughout steam addition.

3. Test Case 3: Concurrent Ventilation Testing

Concurrent ventilation at air flowrates of 0.01 CFM and 0.1 CFM exhibited very different behavior among the cavitators. For the disc cavitator in which the steam and air flows were mixed prior to ventilation, care was taken to simultaneously adjust the steam and air flowrates to ensure flowrates of 0.01/0.1 CFM were maintained for the addition of steam. For the addition of steam to a 0.01 CFM air flow, a significant lengthening was observed with transition from a clear to cloudy cavity being seen for steam flowrates above 4 CFM. This transition was seen for steam flowrates of approximately 2 CFM for air ventilation at 0.1 CFM. The lengthening and cavity interfacial transition show that the addition of steam serves to increase the net ventilation, and thus suggests the existence of a vaporous and gaseous cavity.

The addition of steam thus results in behavior similar to that seen for increased non-condensable flowrates, albeit at steam flowrates approximately an order of magnitude larger than the increase in air flowrates required for a similar effect. This highlights the substantial amount of condensation that is still occurring. While condensation is certainly occurring along the cavity interface and for the initial contact of the ventilation jet with the free flow, the composition of the cavity is unclear. It is interesting to note that pre-mixing of the air and steam flows prior to ventilation results in a reduction of the ventilation temperature due to the unheated air flow. This in turn reduces the sub-cooling value of the cavity relative to the water flow, consequently reducing the condensation potential of the ventilation mixture. The corresponding reduction of the partial pressure of the steam can actually result in a significant superheat of the steam as well, further reducing the condensation potential albeit the effect of superheating would be minimal considering the small Jakob number of water.

Testing was also performed in which the air ventilation rate was not maintained for the addition of steam as this allowed for a natural reduction in the air ventilation for steam addition, inherently testing the proposition that the addition of steam would allow for maintenance of a cavity at reduced non-condensable ventilation requirements. No such effect was seen as the cavity exhibited no lengthening as for the addition of steam while maintaining the air flowrate, and in fact was progressively reduced, eventually disappearing as the non-condensable mass fraction was reduced.

The very limited cavity volume and steam ventilation tangent to the flow made observance of any steam effects for the jetting cavitator difficult as it was not expected, or here seen, to result in a thickening of the cavity. As such, the addition of low flowrates of steam to an initial air cavity had no noticeable effect on the cavity shape. As the ventilation was tangent to the flow, the cavity appeared to have a higher inertia for very low steam flowrates (below 2 CFM), showing very high frequency oscillations along the cavity and a more energetic closure region. As Q_{steam} was increased, the air jet was entrained by the steam jet resulting in a collapse of the cavity; this entrainment increasing in energy for increasing steam flows.

Due to the jetting nature of this design, for ventilation ratios below one, the steam jet was actually entrained radially by the outer air jet, resulting in condensation along the cavity interface thus having minimal effect on the overall volume of ventilation gasses in the cavity. For ventilation ratios greater than one, entrainment is reversed, the air vent being entrained by the inner steam vent. For large ventilation ratios, this entrainment was energetic enough to result in complete mixing of the two jets, again resulting in condensation of the steam along the cavity interface. Even for ventilation ratios of approximately one for which entrainment has limited energy and a more gradual merging of the jets is to be expected, no increases in the cavity length were observed even though the net ventilation rate was theoretically increased. For air only ventilation, any increase in the ventilation rate resulted in a lengthening of the cavity, suggesting the inner steam vent is rapidly condensed for concurrent ventilation and thus adds nothing to the net

volumetric ventilation rate. This in turn suggests that the outer air jet is incapable of providing sufficient insulation to the inner steam jet as was hoped. Of course the thin nature of the largely planar cavity may result in condensation due to rapid heat transfer across the cavity thickness and even within the cavity itself regardless of the interaction of the two jets.

It should be understood that the above discussion has included ventilation ratios well below the measured range. Consequently these results rely on steam flowrates below the lowest measured value of 2 CFM, for which the quality at ventilation was expected to be below $x=0.5$. While the volume of vapor is considered to be much greater than the volume of liquid for qualities well below even $x=0.1$, the above conclusions require further testing for validation. Unfortunately, the repeated critical failure of several jetting cavitators prevented completion of the entire sequence of test cases; the above discussed results do however cover the greater portion of the test cases with similar behavior being expected for the remaining cases.

For the film cavitator, a modest change could be seen in the overall shape of the cavity for low steam fluxes. While the length and maximum diameter showed modest increases, asymmetry was significantly reduced. This is likely a result of the inertial energy of the steam vents downstream of the air vents increasing the overall inertia of the cavity, resulting in a faster ventilation gas speed within the cavity, allowing for the cavity contents to travel further downstream before deflection. Increases in the overall length were on the order of one cavitator. The reduction of asymmetry is not insignificant as it

resulted in the cavity covering a larger portion of the support strut and thus representing a further reduction in skin drag. This effect is expected to occur irrespective of ventilation gas and suggests a very useful design technique for ventilated supercavities at low Froude numbers in which asymmetry of the cavity could be significantly reduced through the use of small ventilation nozzles along the entire lower portion of the device; no such design was found in the literature or open source designs.

A waviness was also seen to develop along the cavity, reminiscent of the transition from a clear to cloudy cavity for excess non-condensable ventilation. As the waviness appears along the entire cavity, not just aft of the steam vents as would be expected if it was simply a result of the steam penetrating the inner smooth cavity, this suggests a successful increase in the net volumetric ventilation rate and subsequently, the useful addition of steam.

Further increases in the steam ventilation rate resulted in increasingly destructive entrainment of the air vent. Even still, a continuous cavity was maintained prior to the steam vents, with the entrainment of this cavity by the first row of downstream steam vents, resulting in very distinct bubble streaks corresponding to the individual vapor vents. These streaks exhibited a very stable, coherent structure, potentially even being continuous for several downstream diameters, the structures becoming less coherent for increasing steam ventilation rates. The secondary downstream vapor vents appeared to have no effect on these structures. While the composition of the bubbles was unable to be definitively known, comparison to the results of flat plate testing suggests they contain

both steam and air. The bubble diameter was on the order of 1 mm, being reduced in size for increasing steam ventilation fluxes as a result of the increased violence of the entrainment. While cavities were successfully created for the addition of air to steam at low ventilation ratios for all cavitators, the overall cavity behavior was identical to that seen for the addition of steam to an initially created air cavity.

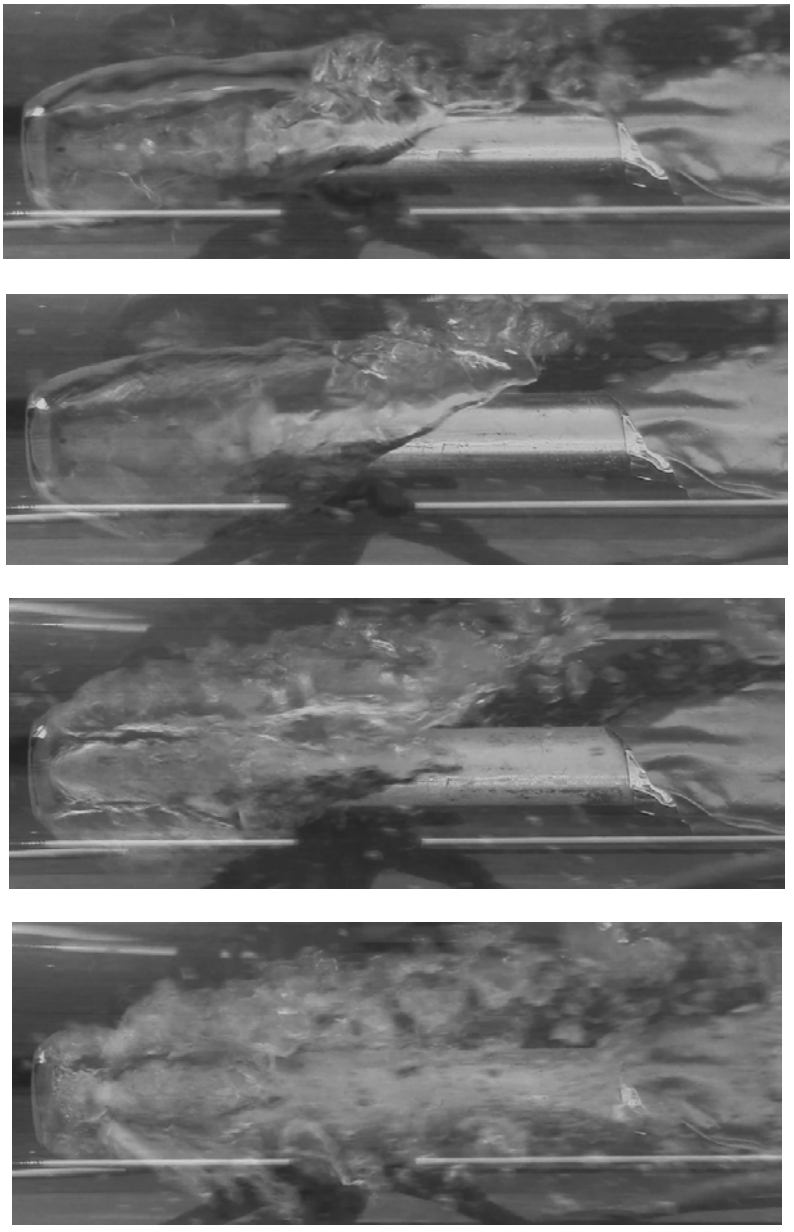

Figure 30. Transitions in cavity behavior for concurrent ventilation as seen for the film cavitator at a baseline ventilation of air at 0.01 CFM. From top to bottom: air only ventilation at 0.01 CFM. Addition of steam at flowrates less than 2 CFM showing development of waviness along the entire cavity. Entrainment of air vent by steam ventilation for increasing steam flowrates; continuous cavity remains underneath streaks. Bubble streaks for steam ventilation at flowrates above 4 CFM with continuous cavity remaining upstream of steam vents.

4. Test Case 4: Steam Only Ventilation

Steam only ventilation was incapable of generating a continuous attached cavity for all of the cavitator designs tested for steam flowrates up to and even exceeding 8 CFM. The condensation potential is simply too large to prevent condensation. Even if creation of purely vaporous ventilated cavities could be achieved at still larger steam flowrates and at significantly reduced sub-cooling, steam ventilation would at best require ventilation fluxes orders of magnitude above that need for non-condensable ventilation, significantly limiting any advantages of purely vaporous ventilation.

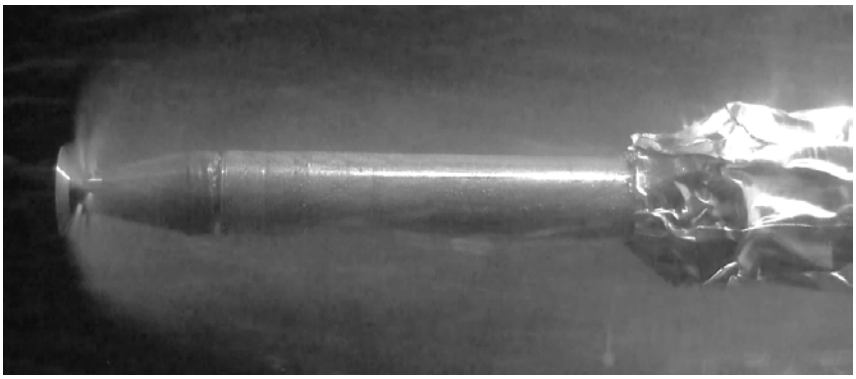

Figure 31. Steam only ventilation at 8 CFM for disc cavitator.

A steam plume could be clearly seen upon exit of the steam from the discrete vents as expected by DCC theory for both the sharp edged disc and film venting cavitator. The maximum plume length was on the order of 0.1mm for the highest steam flowrates tested, being of no consequence to overall cavity development. A denser region of steam could be seen upon exit of the steam channel for the jetting cavitator suggesting successful circumferential mixing within the channel and the creation on an annular vent. In all cases, the steam region quickly breaks down, forming a frothy mixture of very small

bubbles of $d << 0.1$mm which are swept downstream, the bubbles forming streaks corresponding to the azimuthal orientation of their origin vent for the disc and film cavitators with no radial signature for the jetting cavitator. Although it is assumed these bubbles are largely vaporous, they may also be the result of desorption of gasses from the flow due to the increased turbulence and temperature in the venting region as mentioned by Ayodeji et al. [85].

CHAPTER 5. CONCLUSIONS

The potential for use of steam as a ventilation gas in supercavitation design has been both theoretically and experimentally evaluated. Interestingly, no references to the use of a condensable ventilation gas were found in the open literature or free press releases of applied supercavitating devices suggesting this study is the first of its kind. Consequently, the theoretical feasibility analysis relied on extension of theories relevant to cases in which a vapor is directly inserted into a bulk liquid or liquid flow. The sole use of steam for cavity creation was quickly realized to be improbable due to the extreme condensation potential encountered by the steam, resulting in nearly instantaneous condensation even for ventilation flowrates well above those expected to be realistic for self-contained steam generation.

The significant reduction of heat transfer rates and corresponding reductions in condensation seen for the addition of non-condensable gasses to a steam flow suggested the potential of concurrent, mixed ventilation where a non-condensable boundary layer might develop, serving as an insulating boundary to the steam. It was feared that the development of this layer would require longer time scales than possible for the traversal of ventilation gasses along the length of the cavity. Consequently, the concept of concurrent, unmixed ventilation in which steam is inserted interior to air ventilation was proposed, this case being similar to offset and wall jetting. The mixing length and overall length scale of interfacial instabilities serve as the limiting factors for this concept.

Experimental testing was then performed, first through low fidelity testing with ventilation below a horizontal surface in a water flow of 15 in/s; this case being indicative of ACS applications. Thickening of the cavity was seen for the addition of modest steam flowrates to cross-wise air ventilation as a result of the steam successfully increasing the net volumetric flowrate into the cavity. Ventilation tangent to the flow resulted in a reduction of the cavity aspect ratio due to the increased inertia for concurrent ventilation, resulting in a lengthening of the cavity on the order of 10% of the overall cavity length. Concurrent ventilation at high ventilation ratios resulted in destruction of continuous cavities as a result of entrainment and mixing of the steam and air flows for all cases, leading to condensation throughout the cavity. As expected from the theoretical analysis, steam only ventilation was incapable of generating a continuous cavity. Considering the modest gains in cavity thickness and length, the usefulness of steam ventilation in ACS applications is limited, especially when compared to alternative optimization methods.

Final testing was performed using axisymmetric cavitators to test mixed, concurrent ventilation as well as unmixed, concurrent ventilation with specimen designed to test the artificial creation of a non-condensable boundary layer underneath which steam ventilation occurred in the hopes of reducing the required non-condensable flowrate while maintaining supercavitating behavior. Again, modest gains were seen for low ventilation ratios in which the cavity length exhibited lengthening on the order of one cavitator diameter. These gains occurred for steam ventilation flowrates orders of

magnitude larger than the increases in non-condensable ventilation that would be needed for similar lengthening. Steam ventilation at increasingly higher flowrates actually had a detrimental effect on the cavity, resulting in cavity destruction by entrainment of the air flow by the steam flow, leading to the generation of bubble filled wakes. Again, the successful creation of continuous cavities by steam only ventilation was not seen even for steam flowrates several orders of magnitude above the minimum required non-condensable rate. Considering all of these results, it appears that the partial or complete replacement of non-condensable gases for ventilation by steam is not a viable supercavitation design method.

WORKS CITED

[1] P. Eisenberg, Cavitation, N.p., N.d..

[2] R. T. Knapp, J. W. Daily and F. G. Hammitt, Cavitation, New York: McGraw-Hil, 1970.

[3] O. Kreisher, "Underwater Express," *Sea Power: Military & Government Collection,* vol. 50, no. 2, pp. 24-26, 2007.

[4] D. R. Stinebring, R. B. Cook, J. E. Dzielski and R. F. Kunz, "Highspeed supercavitating vehicles," in *Proccedings of AIAA Guid. Navigation. Control Conference Exhibition*, 2006.

[5] I. Kirscher, T. Gieseke and R. Kuklinski, "Supercavitation research and development," Undersea Defense Technologies, Waikiki, 2001.

[6] K. Matveev, T. Burnett and A. Ockfen, "Study of the air-ventilated cavity under the hull on water surface," *Ocean Engineering,* vol. 36, pp. 930-940, 2009.

[7] H. Mokhtarzadeh, G. Balas and R. and Arndt, "Effect of cavitator on supercavitating vehicle dynamics," *IEEE Journal of Oceanic Engineering,* vol. 37, no. 2, pp. 156-165, 2012.

[8] J. Franc and J. Michel, "Attached cavitation and the boundary layer: Experimental investigation and numerical treatment," *Journal of Fluid Mechanics,* vol. 154, pp. 63-90, 1985.

[9] C. Brennen, Cavitation and Bubble Dynamics, New York: Oxford University Press, 1995.

[10] J. Franc and J. Michel, Fundamentals of Cavitation, Dordrecht: Kluwer Academic Publishers, 2004.

[11] V. Carey, Liquid-Vapor Phase-Change Phenomena, Washington: Hemisphere Publishing Corporation, 1992.

[12] F. G. Hammitt, Cavitation and Multiphase Flow Phenomena, New York: McGraw-Hill, 1980.

[13] E. Harvey, W. McElroy and A. Whiteley, "On cavity formation in water," *Journal of Applied Physics,* vol. 18, pp. 162-172, 1947.

[14] C. Brennen, "The dynamic behavior of and compliance of a stream of cavitation bubbles," *Journal of Fluid Engineering,* vol. 95, no. 1, pp. 533-541, 1973.

[15] S. Kelly, S. Segal and J. Peugeot, "Simulation of cryogenics cavitation," *AIAA Journal,* vol. 49, no. 11, 2011.

[16] Zhang, X., Wei, Y., Zhang, J., Wan, C., and Yu, K., "Experimental research on the shape characters of natural and ventilated supercavitation," *Journal of Hydrodynamics,* vol. B19, no. 5, pp. 564-571, 2007.

[17] A. Armstrong, *Abrupt and smooth separation in plane and axisymmetric flow,* 1953, pp. 22-63.

[18] V. Arakeri, "Viscous effects on the position of cavitation separation from smooth bodies," *Journal of Fluid Mechanics,* vol. 68, pp. 779-799, 1975.

[19] L. Briancon-Marjollet, J. Franc and J. Michel, "Transient bubbles interacting with an attached cavity and the boundary layer," *Journal of Fluid Mechanics,* vol. 218, pp. 355-376, 1990.

[20] D. de Lange and G. de Bruin, "Sheet cavitation and cloud cavitation re-entrant jet and three-dimensionality," *Applied Scientific Research,* vol. 58, pp. 91-114, 1998.

[21] E. Kawakami and R. Arndt, "Investigation of the behavior of ventilated supercavities," *Journal of Fluids Engineering,* vol. 133, 2011.

[22] M. Hoekstra, "The myth of the re-entrant jet," in *WIMRC 3rd International Cavitation Forum*, UK, 2011.

[23] A. Kubota, H. Kato and H. Yamaguchi, "A new modeling of caviating flows: A numerical study of unsteady cavitation on a hydrofoil section," *Journal of Fluid Mechanics,* vol. 240, pp. 59-96, 1992.

[24] F. Avellan, P. Dupont and I. Ryhming, "Generation mechanism and dynamics of cavitation vortices downstream of a fixed leading edge cavity," in *Proc. 17th Symp. Naval Hydrod.*, Washington, 1988.

[25] V. Buyvol, "Slender cavities in flows with perturbations," *Nauvoka Dunka Ed.,* 1980.

[26] I. Kirshner and S. Arzoumanian, "Implementation and extension of Paryshev's model of cavity dynamics," in *International Conference on Innovative Approaches to Further Increase Speed of Fast Marine Vehicles, Moving Above, Under And In Water Surface, SuperFAST'2008*, Saint-Petersburg, 2008.

[27] E. Paryshev, "Theortical investigation of stability and pulsations of axisymmetric cavities," in *Trudy TsAGI No. 1970*, 1978.

[28] S. Ashley, "Warp drive underwater," *Scientific American,* pp. 70-79, 2001.

[29] N. Nouri, M. Riahi, A. Valipour, M. Raeyatpishe and E. Molavi, "Analytical and experimental study of hydrodynamic and hydroacoustic effects of air injection flowrate in ventilated supercavitation," *Ocean Engineering,* vol. 95, pp. 94-105, 2015.

[30] S. Ceccio, "Friction drag reduciton of external flows with bubble and gas injection," *Annual Review Fluid Mechanics,* pp. 183-203, 2010.

[31] C. Winter, "This stealth attack boat may be too innovative for the Pentagon," 21 August 2014. [Online]. Available: http://www.businessweek.com/articles/2014-08-21/juliet-marines-ghost-boat-will-be-hard-sell-to-u-dot-s-dot-navy. [Accessed 23 September 2014].

[32] M. Wosnik, T. J. Schauer and R. E. Arndt, "Experimental study of a ventilated supercavitating vehicle," in *Fifth International Symposium on Cavitation*, Osaka, 2003.

[33] L. A. Epstein, "Methods of the dimensional analysis and similarity theory in problems in ship hydromechanics," Leningrad, 1970.

[34] W. Swanson and J. O'Neill, "The stability of an air-maintained cavity behind a stationary object in flowing water," Hydrodynamics Laboratory, California Institute of Technology, Pasadena, 1951.

[35] E. Amromin and S. Kovinskaya, "Selection of gas-based drag reduction technology," Mechmath, LLC, Prior Lake, 2006.

[36] E. Kawakami and R. Arndt, "Investigation of the behavior of ventilated supercavities," *Journal of Fluids Engineering,* vol. 133, 2011.

[37] R. Arndt, W. Hambleton, E. Kawakami and E. Amromin, "Creation and maintenance of cavities under horizontal surfaces in steady and gust flows," *Journal of Fluids Engineering,* vol. 131, 2009.

[38] K. Matveev, "On the limiting parameters of artificial cavitation," *Ocean Engineering,* vol. 30, pp. 1179-1190, 2003.

[39] K. Matveev, "Reply to "Discussion of 'Study of air-ventilated cavity under model hull on water surface' by K.I. Matveev, T.J. Burnett, and A.E. Ockfen," *Ocean Engineering,* vol. 37, p. 1392, 2010.

[40] M. Gurevich, "Jet Theory," Moscow, 1979.

[41] A. Butuzoz, "Artificial cavitation flow behind a slender wedge on the lower surface of a horizontal wall," *Fluid Dymanics,* pp. 56-58, 1967.

[42] M. Wosnik, T. J. Schauer and R. E. Arndt, "Expreimental study of a ventilated supercavitating vehicle," in *Fifth International Symposium on Cavitation*, Osaka, 2003.

[43] J. Ping, C. Wang and Y. Wei, "Numerical simulation of artificial ventilated cavity," *Journal of Hydrodynamics,* vol. B18, no. 3, pp. 273-279, 2006.

[44] E. Alyanak, R. Grandhi and R. Penmetsa, "Optimum design of a supercavitating torpedo considering overall size, shape, and structural configuration," *International Journal of Solids and Structures,* vol. 43, pp. 642-657, 2005.

[45] R. Waid, "Cavity shapes for circular disks at angles of attack," Hydrodynamics Laboratory California Instituite of Technology, Pasadena, 1957.

[46] Y. Savchenko, Y. Vlasenko and V. Semenenko, "Experimental studies of high-speed cavitated flows," *International Journal of Fluid Mechanics Research,* vol. 26, no. 3, pp. 365-374, 1999.

[47] A. Vasin, "The principle of independence of the cavity sections expansion (Logvinovich's principle) as the basis forinvestigation on cavitation flows," in *RTO AVT Lecture Series on Supercavitating Flows. North Atlantic Treaty Organization*, Brussels, 2001.

[48] A. May, "Water entry and the cavity-running behavior of missiles," Navsea Hydroballistics Advisory Committee, Arlington, 1975.

[49] X. Chen, C. Lu, J. Li and Z. Pan, "The wall effect on ventilated cavitating flows in closed cavitation tunnels," *Journal of Hydrodynamics,* vol. B20, no. 5, pp. 561-566, 2008.

[50] T. Wu, A. Whitney and C. Brennen, "Cavity-flow wall effect and correction rules," *Journal of Fluid Mechanics,* vol. 29, pp. 223-256, 1971.

[51] C. Brennen, "A numerical solution of axisymmetric cavity flow," *Journal of Fluid Mechanics,* vol. 37, no. 4, pp. 671-688, 1969.

[52] V. P. Karlikov and G. Sholomovich, "Method of approximate account for the wall effect in cavitation flow around bodies in water tunnels," *Journal of Fluid Dynamics,* vol. 1, no. 4, pp. 61-64, 1966.

[53] H. Cohen and R. C. Difrima, "Wall effects in cavitating flows," in *Second Symposium on Naval Hydrodynamics*, Washington, 1958.

[54] Y. Savchenko, "Supercaviating object propulsion," Ukrainian National Academy of Sciences - Institute of Hydromechanics, Kiev, 2001.

[55] J. Castano and R. Kuklinski, "High-speed Supercavitating Underwater Vehicle". US Patent 6,739,266 B1, 25 May 2004.

[56] S. Fox, "DARPA readies an ultra-fast mini-sub," Popular Science, 28 July 2009. [Online].

[57] S. Cho, S. Chun, W. Baek and Y. Kim, "Effect of multiple holes on the performance of sparger during direct contact condensation of steam," *Experimental Thermal and Fluid Sciences,* vol. 28, pp. 629-638, 2004.

[58] A. de With, R. Calay and G. de With, "Three-dimensoinal condensation regime diagram for direct contact condensation of steam injected into water," *International Journal of Heat and Mass Transfer,* vol. 50, pp. 1762-1770, 2007.

[59] A. de With, "Steam plume length diagram for direct contact condensation of steam injected into water," *Internatoinal Journal of Heat and Mass Transfer,* vol. 30, pp. 971-982, 2009.

[60] K. Harby, S. Chiva and J. Munoz-Cobo, "An experimental investigation on the characteristics of submerged horizontal gas jet in liquid ambient," *Experimental Thermal and Fluid Science,* vol. 53, pp. 26-39, 2014.

[61] W. Minkowycz and E. Sparrow, "Condensation heat transfer in the presence of noncondensables, interfacial resistance, superheating, variable properties, and diffusion," *International Journal of Heat and Mass Transfer,* vol. 9, pp. 1125-1144, 1966.

[62] T. Karapantsios, M. Kostoglou and A. Karabelas, "Local condensation rates of steam-air mixtures in direct contact with a falling liquid film," *International Journal of Heat and Mass Transfer,* vol. 38, no. 5, pp. 779-794, 1995.

[63] S. Oh and S. Revankar, "Experimental and theoretical investigation of film condensation with non-condensable gas," *International Journal of Heat and Mass Transfer,* vol. 49, pp. 2523-2534, 2006.

[64] B. Ren, H. Xu, J. Cao and Z. Tao, "Experimental study on the condensation of steam/air mixture in a horizontal tube," *Experimental Thermal and Fluid Science,* vol. 58, pp. 145-155, 2014.

[65] S. Park, M. Kim and K. Yoo, "Condensation of pure steam and steam-air mixture with surface waves of condensate film on a vertical wall," *Internation Journal of Multiphase Flow,* vol. 22, no. 5, pp. 893-908, 1996.

[66] G. Tang, H. Hu, Z. Zhuang and W. Tao, "Film condensation heat transfer on a horizontal tube in presence of a noncondensable gas," *Applied Thermal Engineering,* vol. 36, pp. 414-425, 2012.

[67] R. Kuklinski, "Boiling Heat Transfer Torpedo". US Patent 6962121 B1, 2005.

[68] Y. Wang, X. Sun, Y. Dai, G. Wu, Y. Cao and D. Huang, "Numerical investigation of drag reduction by heat-enhanced cavitation," *Applied Thermal Engineering,* vol. 75, pp. 193-202, 2015.

[69] N. Gao, C. Ching, D. Ewing and J. Naughton, "Flow and heat transfer measurements in a planar offset attaching jet with a co-flowing wall jet," *International Journal of Heat and Mass Transfer,* vol. 78, pp. 721-731, 2014.

[70] X. Wang and S. Tan, "Experimental investigation of the interaction between a plane wall jet and a parallel offset jet," *Experiments in Fluids,* vol. 42, pp. 551-562, 2007.

[71] Z. Li, W. Huai and Z. Yang, "Interaction between wall jet and offset jet with different velocity and offset ratio," in *2012 International Conference on Modern Hydraulic Engineering*, 2012.

[72] N. Bunderson and B. Smith, "Passive mixing control of plane jets," *Experiments in Fluids,* vol. 39, pp. 66-74, 2005.

[73] C. Nath, S. Voropayev, D. Lord and H. Fernando, "Offset of turbulent jets in low-aspect ratio cavitites," *Journal of Fluids Engineering,* vol. 136, 2014.

[74] Y. Taitel and A. Dukler, "A model for predicting flow regime transitions in horizontal and near horizontal gas-liquid flow," *AIChE J.,* vol. 22, pp. 47-55, 1976.

[75] R. Figliola and D. Beasley, Theory and Design for Mechanical Measurements, 5th ed., Hoboken: John Wiley and Sons, Inc., 2011.

[76] K. Matveev, "Air-ventilated hulls," [Online].

[77] E. Amromin, G. Karafiath and B. Metcalf, "Ship drag reduction by air bottom ventilated cavitation in calm water and in waves," *Journal of Ship Research,* vol. 55, no. 3, pp. 196-207, 2011.

[78] S. Ekkad, Y. Lu and H. Nasir, "Film condensation from a row of holes embedded in transverse slots," in *Proceedings of GT2005*, Reno-Tahoe, 2005.

[79] S. Waye and D. Bogard, "High resolution film cooling effectiveness measurements of axial holes embedded in a transverse trench with various trench configurations," *Journal of Turbomachinery,* vol. 129, no. 2, pp. 294-302, 2006.

[80] Y. Lu, A. Dhungel, S. Ekkad and R. Bunker, "Effect of trench width and depth on film cooling from cylindrical holes embedded in trenches," *Journal of Turbomachinery,* vol. 131, no. 1, 2008.

[81] R. Goldstein, E. R. Eckert and F. Burggraf, "Effects of hole geometry and density on three-dimensional film cooling," *International Journal of Heat and Mass Transfer,* vol. 17, pp. 595-607, 1974.

[82] S. Ekkad and J. Han, "A review of hole geometry and coolant density effect on film cooling," in *Proceedings of the ASME 2013 Heat Transfer Summer Conference*, Minneapolis, 2013.

[83] M. Wosnik, T. J. Schauer and R. E. Arndt, "Experimental study of a ventilated supercavitating vehicle," in *Fifth International Symposium on Cavitation*, Osaka, 2003.

[84] A. Sotiriadis, R. Thorpe and J. Smith, "Bubble size and mass transfer characteristics of sparged downwards two-phase flow," *Chemical Engineering Science,* vol. 60, pp. 5917-5929, 2005.

[85] J. Ayodeji, B. Asante and B. Ross, "Steam bubbling regimes and direct contact condensation heat transfer in highly subcooled water," *Chemical Engineering Science,* vol. 45, no. 3, pp. 639-650, 1990.

[86] T. Na and I. Pop, "Flow and heat transfer over a longitudinal circular cylinder moving in parallel or reversely to a free stream," *Acta Mechanical,* vol. 118, pp. 185-195, 1996.

[87] I. Huhtiniemi and M. Corradini, "Condensation in the presence of noncondensable gases," *Nuclear Engineering and Design,* vol. 141, pp. 429-446, 1993.

[88] W. Minkowycz and E. Sparrow, "The effect of superheating on condensation heat transfer in a forced convection boundary layer," *International Journal of Heat and Mass Transfer,* vol. 12, pp. 147-154, 1969.

[89] C. Chan and C. Lee, "A regime map for direct contact condensation," *International Journal of Multiphase Flow,* vol. 8, no. 1, pp. 11-20, 1982.

[90] Q. Xu, L. Guo, S. Zou, J. Chen and X. Zhang, "Experimental study on direct contact condensation of stable steam jet in a vertical pipe," *International Journal of Heat and Mass Transfer,* vol. 66, pp. 808-817, 2013.

[91] D. Hasson and D. N. U. Luss, "An experimental study of steam condensation on a laminar water sheet," *International Journal of Heat and Mass Transfer,* vol. 7, pp. 983-1001, 1964.

[92] Y. Xu, "Direct contact condensation with and without noncondensable gas in a water pool," Purdue University, 2004.

[93] W. Yi, J. Tan and T. Xiong, "Investigations on the drag reduction of high-speed natural supercavitation bodies," *Modern Physics Letters,* vol. B23, no. 3, pp. 405-408, 2009.

[94] B. Saranjam, "Experimental and numerical investigation of an unsteady supercavitating moving body," *Ocean Engineering,* vol. 59, pp. 9-14, 2013.

[95] S. Mimouni, M. Boucker, J. Lavierville and D. Bestion, "Modeling and computation of cavitation and boiling bubbly flows with the Neptune_CFD code".

[96] G. Siamas, X. Jiang and L. Wrobel, "Numerical investigation of a perturbed swirling annular two-phase jet," *International Journal of Heat and Fluid Flow,* vol. 30, pp. 481-493, 2009.

APPENDICES

Appendix A. Stream Measurement Procedure

The flowrate of steam was determined through application of the phenomenological Darcy-Weisbach equation,

$$\Delta p = f_f \frac{L}{d_H} \frac{\rho U^2}{2} \tag{20}$$

or, solving for the velocity corresponding to a given pressure drop,

$$U = \sqrt{\Delta p \frac{2 f_f}{\rho} \frac{d_H}{L}} \tag{21}$$

where d_H is simply the inner diameter for a circular pipe. The friction factor is determined either through use of the Moody diagram or calculation according to the Colebrook equation, both of which are functions of the Reynolds number. A pressure drop is first measured across a known length of pipe and the flow density is determined according to the pressure and temperature of the flow. An iterative procedure then follows in which a flowrate is first assumed, allowing for calculation of the Reynolds number according to,

$$\mathrm{Re}_{D_H} = \frac{\rho U D_H}{\mu} = \frac{Q D_H}{\upsilon A} \tag{22}$$

and corresponding computation of the friction factor from which a flowrate can be determined. The initial guess is then corrected until convergence of the solution and the initial guess is reached, generally requiring only several iterations.

The Darcy-Weisbach relation assumes fully developed, steady state, and incompressible flow. Compressible effects can be accounted for with the addition of a

correction factor but were neglected for the present study. Laminar and turbulent effects are accounted for in determination of the friction factor allowing for much greater versatility then laminar flow elements. Measurement uncertainties arise in determination of the flow density, which is itself dependent on the pressure and temperature measurement, diameter, friction factor, and pressure drop. A significant random uncertainty was also seen for calibration efforts as no standard for measurement was available in the laboratory. Considering these uncertainties and the largely qualitative focus of the present research, an error analysis was forgone with steam flowrates being given as general ranges or as orders of magnitude.

While the above process may seem cumbersome, it is manageable when only several discrete flowrates are needed with the flowrate range only limited by the pressure measurement device. Other than specialized steam measurement systems, which were cost prohibitive for the current project, laminar flow elements were infeasible due to the potential for condensation within the lamina, a critical flaw considering the extreme sensitivity of LFEs to changes in the flow area. Orifice meters would have provided a cost effective alternative but would still be limited by their turndown ratio as a wide range of flowrates were investigated. The pressure drop pipe thus provided the cheapest, quickest, and most versatile steam measurement technique.

Appendix B. Justification for Axisymmetric Steam Ventilation Ranges

Due to the inability to ensure steam ventilation remained at a sufficient vapor quality at ventilation by direct measurement, heat transfer calculations were required to estimate the required flowrates needed to prevent condensation. Unfortunately no relations were found for turbulent, longitudinal flow along a cylinder. The relations of Na and Pop for laminar, longitudinal flow were thus adapted through several assumptions [86].

A flow at 2 m/s of 20°C water (Pr=7) over the 0.76 m long stainless steel support tube through which steam flowed served as the simplified flow model. The stainless pipe (k=16 W/mK) had inner and outer diameters of 3.175E-3 and 4.673E-3 meters respectively. Then using the relations of Na and Pop,

$$\xi = \bar{x} = 4\frac{\left(x / \mathrm{r}_o\right)}{\mathrm{Re}_\infty} \tag{23}$$

where we are concerned with an estimate of the average heat transfer coefficient so x=L and the Reynolds number based on L gives a value of 1.5E6 denoting turbulent flow conditions. As the relations of Na and Pop are for laminar flow, comparison to flat plate heat transfer relations were made in the hopes of determining an approximate scaling factor for conversion of the heat transfer correlations from laminar to turbulent conditions. It was found that $\overline{Nu}_{turb} \approx 6\overline{Nu}_{lam}$. As the laminar relations for longitudinal flow were only several times larger than flow over a flat plate, it was assumed that the overall scaling would be similar and was thus used, allowing for a correction to turbulent

flow upon solving for laminar flow. Taking the parameter λ as zero in accordance with the model for no motion of the cylinder, ξ = 4.2E-4.

While this was well below the smallest tabulated solution given, a plot of –q'(ξ,0) vs. ξ showed great linearity and it was thus extrapolated that the –q'(ξ,0) value could simply be taken as the y-intercept of the –q'(ξ,0) vs. ξ graph. Noting the large uncertainty in the overall relations, the results for *Pr*=10 were used, giving –q'(ξ,0) = 1.47. The average heat transfer coefficient was then found according to,

$$\bar{h} = \frac{\overline{Nu}k}{L} = \frac{1}{x}\int_0^L h_x dx = 1.47\frac{k}{L}\left(\frac{U_\infty}{\upsilon}\right)^{1/2}\int_0^L \frac{dx}{x^{1/2}} = 2(1.47)\,\mathrm{Re}_\infty^{\,1/2}\left(\frac{k}{L}\right) \tag{24}$$

where *Nu* is given by,

$$Nu = \frac{-q'(\xi,0)}{\sqrt{1-\lambda}}\sqrt{\mathrm{Re}_\infty} \tag{25}$$

to give $\bar{h}_{lam}$=2771.4 W/m^{2}K. Then adjusting for turbulent effects, $\bar{h}_{turb}$=16.6 kW/m^{2}K. Then solving for the total heat transfer according to,

$$q = \frac{T_{steam} - T_\infty}{\dfrac{1}{2\pi r_0 L\bar{h}} - \dfrac{\ln(\mathrm{r}_o/\mathrm{r}_i)}{2\pi kL}} \tag{26}$$

where T_{steam} was taken as 122°C gave q=12.9kW. Using the thermal capacity of the steam, the required mass flowrate to prevent condensation was found by,

$$\dot{m} = \frac{q}{Cp\Delta T} \tag{27}$$

for Cp=2000 J/kgK, giving a required steam flowrate of $\dot{m}=290$ g/s, a value much larger than that capable for the steam generator. Due to the large volume difference between steam and liquid water, it was realized that $Q_{vapor}>>Q_{liquid}$ even for relatively small vapor qualities. Recalculation of the required mass flowrate for ventilation at $x=0.5$ was then performed according to,

$$\dot{m} = \frac{q}{Cp\Delta T + [\mathrm{h}_g - (\mathrm{h}_f + \mathrm{x}\mathrm{h}_{fg})]} \tag{28}$$

resulting in an increase in the minimal required ventilation flowrate to $\dot{m}=10$ g/s, a value at the maximum upper range capable of being provided with the current experimental setup and for which the steam generator pressure would not be maintained, severely limiting the length of useful testing.

Two layers of ¼" double faced foil insulation with an R-value of 8 (2.82 m^2K/W) were then added to the support tube, increasing the average radius of the insulation layer to 11.113E-3m. Recalculating the thermal resistance network according to,

$$q = \frac{T_{steam} - T_\infty}{(\frac{1}{2}\pi(r_o + 0.0127)\,\mathrm{L}\,\bar{h}) + (R_{insulation}\,2\pi(11.113\,\mathrm{E}-3)\,\mathrm{L}) + (\frac{\ln(\mathrm{r}_o/\mathrm{r}_i)}{2\pi kL})} \tag{29}$$

gave q=633W, a 95% reduction in the overall heat transfer. Recalculating the required flowrates according to Eq. (28) gave $\dot{m}=14$ g/s and $\dot{m}=2.3$ g/s for ventilation at $x=1$ and $x=0.9$ respectively. These values were much more appropriate for testing with further reductions being allowed for lower vapor qualities. This analysis has been highly

speculative but was conservative as a superheat was assumed to remain along the entire length of the steam supply path and the laminar to turbulent correction was also rounded up to the nearest integer. Visualization throughout testing appeared to support the analysis however, as ventilation below $\dot{m}=1$ g/s, which corresponded to $x=0.5$, showed limited to no vapor plumes and even some chugging action for very low steam flowrates, suggesting prohibitive condensation had occurred.

Appendix C. Direct Contact Condensation

Direct contact condensation (DCC) refers to the condensation of a vapor injected directly into a bulk liquid, such as the injection of steam through a submerged nozzle into a water pool. DCC has been largely investigated with regard to industrial two-phase systems such as boilers and condensers due to its extreme heat transfer capabilities. Results of DCC research for steam injected through a fully submerged nozzle into water shows great correlation among researchers, resulting in general trends as presented below.

Examining the injection of steam through a submerged nozzle, the steam forms a plume extending into the flow upon exiting the nozzle. The plume is generally modeled as a pure steam region surrounded by an interface at which condensation occurs through convective heat transfer and mass diffusion. The interface is externally surrounded by a hot water layer comprised of temperature and momentum induced eddies; this is a two-phase layer at a temperature close to the saturation temperature of the steam and may include bubbles of uncondensed steam. The bulk flow surrounds these layers and directly affects the interface shape through turbulent effects and heat transfer.

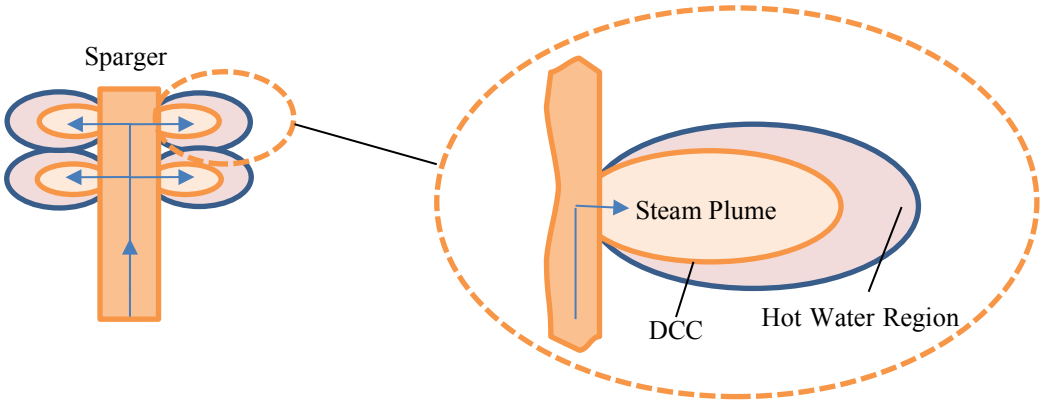

Figure 32. Schematic showing steam plumes for a multiple nozzle sparger design and associated detail view of a single plume with DCC regions. Arrows show path of steam.

The steam plume will take on a variety of shapes depending on the vapor flowrate and water sub-cooling relative to the steam, generally increasing in length and volume for increasing injection fluxes and decreasing sub-cooling. At very high injection rates and low condensation potentials, the plume will exhibit a certain amount of stability, becoming less stable for decreasing flowrates and increasing condensation potentials, eventually exhibiting chugging action wherein condensation occurs in the nozzle itself and liquid periodically fills the nozzle. Between chugging and jetting, bubbling occurs which is characterized by the periodic formation and detachment of bubbles. For high enough steam inflow rates and minimal water sub-cooling, the steam will exhibit behavior similar to a non-condensable gas [58]. The detached bubbles are convected away from the injector and condense in the bulk flow, creating a trail of smaller steam bubbles in the downstream flow.

The culmination of much DCC research can be seen in the creation of regime maps as seen in Figure 33. It appears that a similar regime map holds for injection into a flow when compared to the stagnant pool case although adjustments of the values will be necessary as the turbulent mixing in the outer DCC layers will affect the heat transfer behavior.

The size of the steam plume is directly related to the rate of condensation of the steam, and is thus maximized for minimal sub-cooling of the water relative to the steam. In other words, as expected by fundamental heat transfer theory, the total heat transfer will increase for increasing temperature differences between the steam and pool temperatures, or, as the saturated steam temperature is proportional to pressure, for increasing ventilation pressure [87]. The local temperature around the steam-water interface is actually the most important factor affecting the dynamics of condensation rather than the mean temperature of the sub-cooled water [57]. Of course these two regions cannot be completely uncoupled as the bulk water temperature will affect heat transfer from the interfacial region and thus the temperature of the region itself, explaining the use of the more easily quantified pool temperature when describing condensation potential.

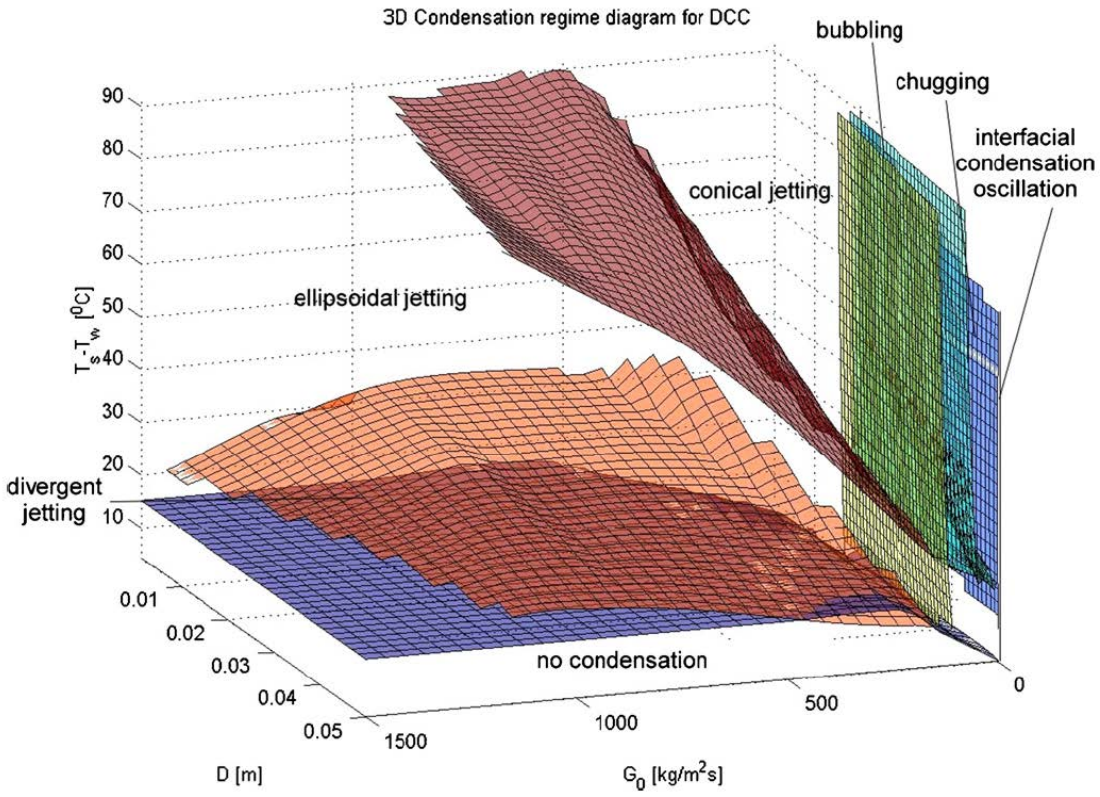

Figure 33. 3D regime map for DCC of steam injected into water with water sub-cooling, nozzle diameter, and steam influx serving as the axis variables. Taken from de With et al. [58].

Superheating also serves to increase the heat transfer through the same mechanism. The effect of superheating is also dependent on the amount of sub-cooling, having a larger effect for smaller temperature differences and converging to saturated heat transfer values for increasing T_{sat}-T_w values. It has also been shown that the effect of superheating in forced convection flow is less than that for gravity-induced convection [88]. It is generally accepted that the effect of superheat is negligible for pure steam as the Jakob number is much less than one for sub-cooling less than several hundred degrees; extension of this assumption results in the secondary assumption that sensible heat

transfer is often considered negligible relative to latent heat transfer for DCC [62]. Of course the increased heat transfer due to superheating does not inherently correspond to increased condensation potential as sensible rather than latent heat transfer will still occur initially.

As expected, the largest steam plume lengths occur for high Reynolds numbers of the injection steam and low condensation potentials [59]. Inertial effects become less important for increasing condensation potentials and decreasing injection Reynolds numbers such as in the case of subsonic venting where inertial gains are small [89]. This shows the general dominance of condensation effects over inertial effects in determining the steam plume length. Inertial gains are also opposed by increases in the interfacial area as well as increasing film velocity at the DCC interface which both serve to increase the overall heat transfer [65].

Dynamic motion of the pool also has an effect as the steam plume length is decreased by 60-65% for injection into a flow when compared to stagnant pool for steam at similar Reynolds numbers [59]. Xu et al. and de With both attribute this to the increased heat transfer resulting from the constant supply of cooler water and added turbulence at the interface as a result of the flow itself [90, 59]. The increased turbulence of the interfacial layer serves to minimize the temperature of the two phase region, thus increasing the thermal gradient and subsequently the heat transfer [90].

The above discussion assumes a single nozzle. Cho et al., however, investigated DCC for varying sparger designs and found that the interaction of various steam vents significantly impacts DCC behavior. The interaction decreases the kinetic energy of the individual steam jets, which, as this energy is largely responsible for thermal mixing with the surrounding water, decreases thermal mixing, resulting in larger temperature increases in the local region around the sparger and corresponding decreases in the condensation potential. This interaction increases for smaller pitch to hole diameter ratios (P/D) and a staggered configuration of the vents. For sufficiently small P/D ratios, the coalescence and interaction of the neighboring jets results in the formation of larger and more stable bubbles than for a single vent hole [57]. This behavior could be expected for an axisymmetric arrangement of ventilation ports around a cavitator as such a configuration is nearly identical to a sparger.

As for the effect of non-condensable gases in the steam flow, convection and momentum carries steam, and the associated non-condensable gas, towards the condensation interface where the steam subsequently condenses. The non-condensables, however, are incapable of condensation and thus remain at the interface. Removal of the non-condensable gases is then by diffusion which requires a sufficient gradient in order to occur, resulting in the formation of a boundary layer of non-condensable gas along the interface. This in turn reduces the partial pressure of vapor at the interface and thus the saturation temperature, resulting in a reduction of heat transfer due to a reduction of temperature differences between the plume and hot water layer [61]. This can also be

explained from a thermal resistance standpoint, in which the air concentration layer effectively increases the thermal resistance at the interface [91].

This has been shown by several authors including Xu who applied thermodynamic and mass transfer principles to model the presence of non-condensables in bubble development for steam injected into a pool, obtaining a decreasing trend in heat transfer for increasing non-condensable concentrations [92]. The effect of superheating is also accentuated for increasing non-condensable concentrations, resulting in an increase in heat transfer for increasing superheat such that the effect of non-condensables in reducing the heat transfer is partially negated. The overall effect of the non condensables is still maintained, however, such that there is a net reduction in the heat transfer in the case of non-condensable gas [61].

Appendix D. Other Considerations for Testing

There were no possibilities for testing at the speeds required for natural cavitation using pre-existing facilities at Clemson such as water tables or flowloops even if a vacuum were used to reduce the local pressure [4]. The use of a fluid other than water, which would allow for the potential of cavitation at lower velocities at roughly room temperature was also infeasible due to the scale of testing desired. A vertical water drainage system was also considered; this setup would allow for repeated testing at minimal cost and could potentially use existing materials for fabrication. Unfortunately, desired flowrates would be difficult to maintain with available pumps.

The possibility of towing was also disregarded as no pre-existing facilities allowed for the lengths required for acceleration and meaningful testing. Rotational tests in a large pool were also considered but were again found infeasible, especially for ventilation; the rotation would also distort the cavity, reducing the usefulness of any data that would be collected. Ultimately, the flow loop as described in Chapter III. was chosen as it allows for control, repeatability, and adaptability at a low cost while allowing for the test specimen to be easy observed throughout the experiment.

In terms of evaluation of the design concepts, CFD simulation may be beneficial to achieve an understanding of the coupled thermal and fluid interactions. According to several researchers a coupled multiphase, unsteady Reynolds averaged Navier-Stokes-model coupled with a six-degree-of-freedom rigid body motion model (URANS–6DOF dynamics model) can be used to numerically model supercavitation with reasonable

accuracy [93, 94]. Similarly, Ping et al. have modeled supercavitation within Fluent and using NEPTUNE as done by Mimouni et al. [43, 95].

Appendix E. Mechanical Drawings of Test Specimen

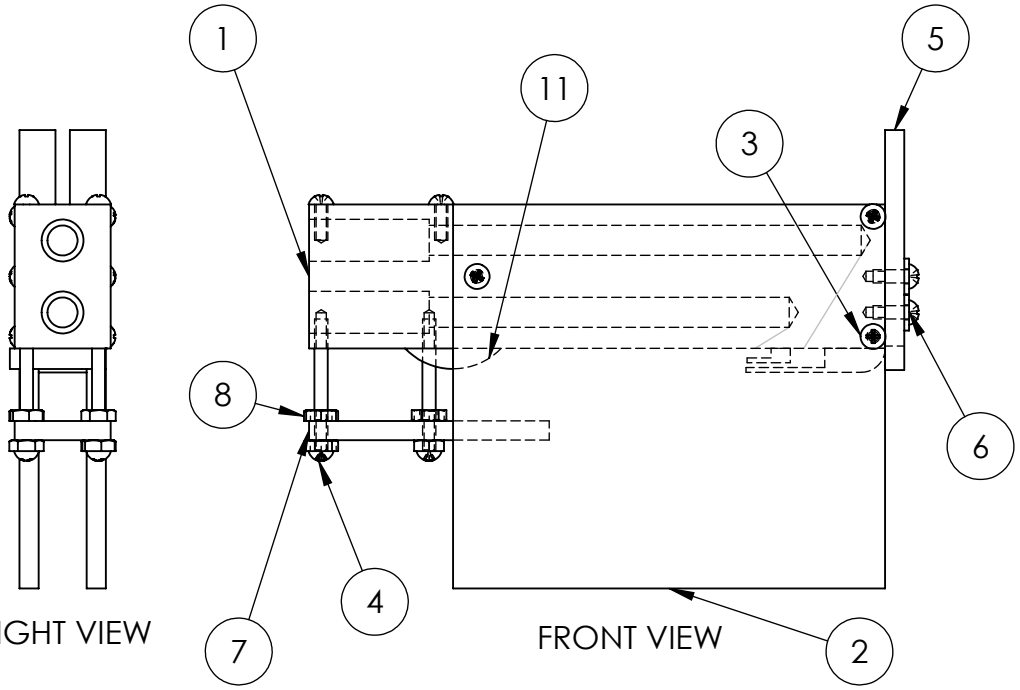

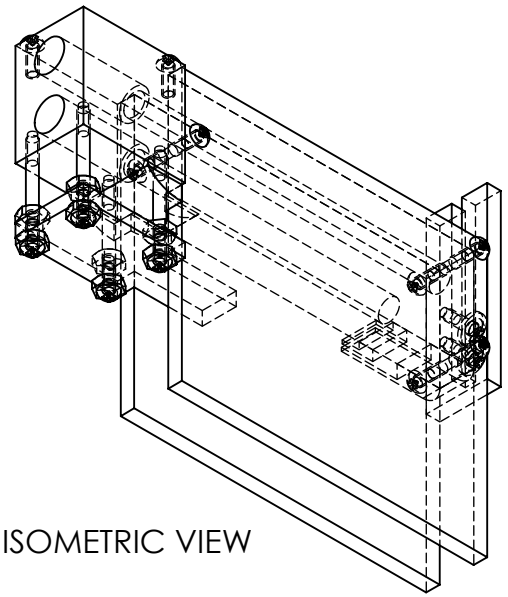

ISOMETRIC VIEW

ITEM NO.	PART NUMBER	QTY.
1	WATER TABLE TEST SPECIMEN	1
2	VIEWING WINDOWS	2
3	#6-32 x0.375 SCREW	10
4	#6-32 x1.375 SCREW	4
5	FLOW CHANNEL GATE	1
6	#6-32 WASHER	2
7	PULSATION PLATE	1
8	#6-32 NUT	8
9	VENTILATION NOZZLE 1	1
10	VENTILATION NOZZLE 2	1
11	CAVITY CLOSURE INSERT	1

UNLESS OTHERWISE SPECIFIED:

ALL EDGES SQUARE
DIMENSIONS ARE IN INCHES
TOLERANCES:
TWO PLACE DECIMAL ±0.01
THREE PLACE DECIMAL ±0.01

MATERIAL: UNSPECIFIED

COMMENTS:

TITLE:

WATER TABLE TESTING ASSEMBLY

SIZE	OWNER	DATE
A	AUSTIN CULBERSON	1/4/15

SCALE: 1:3 | WEIGHT: - | SHEET 1 OF 1

5 4 3 2 1

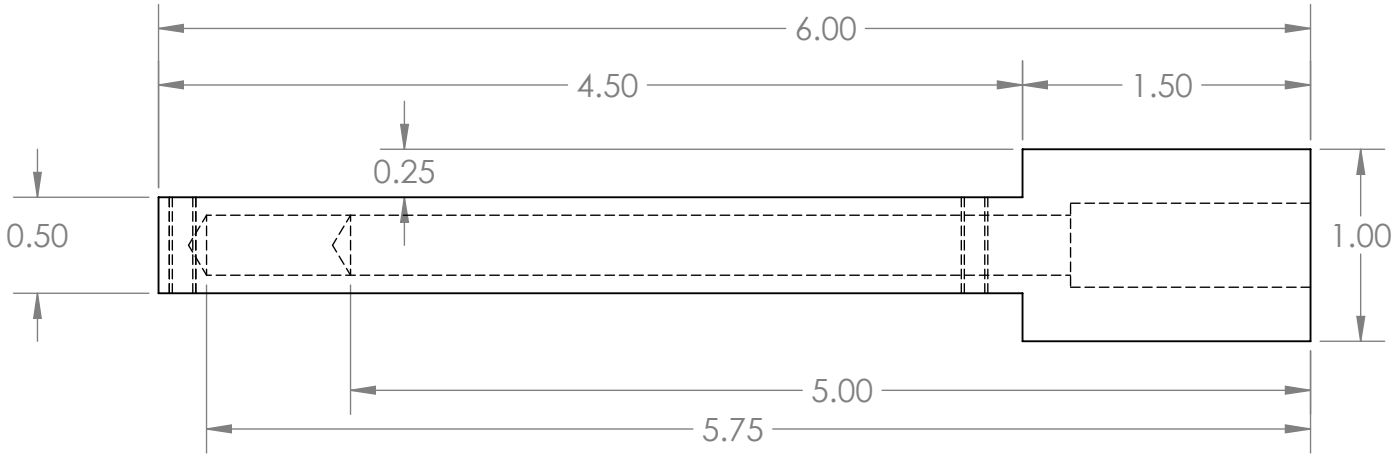

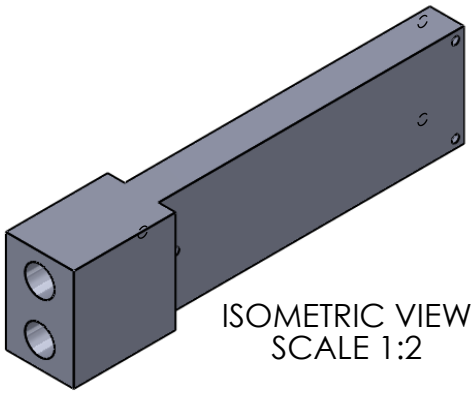

ISOMETRIC VIEW
SCALE 1:2

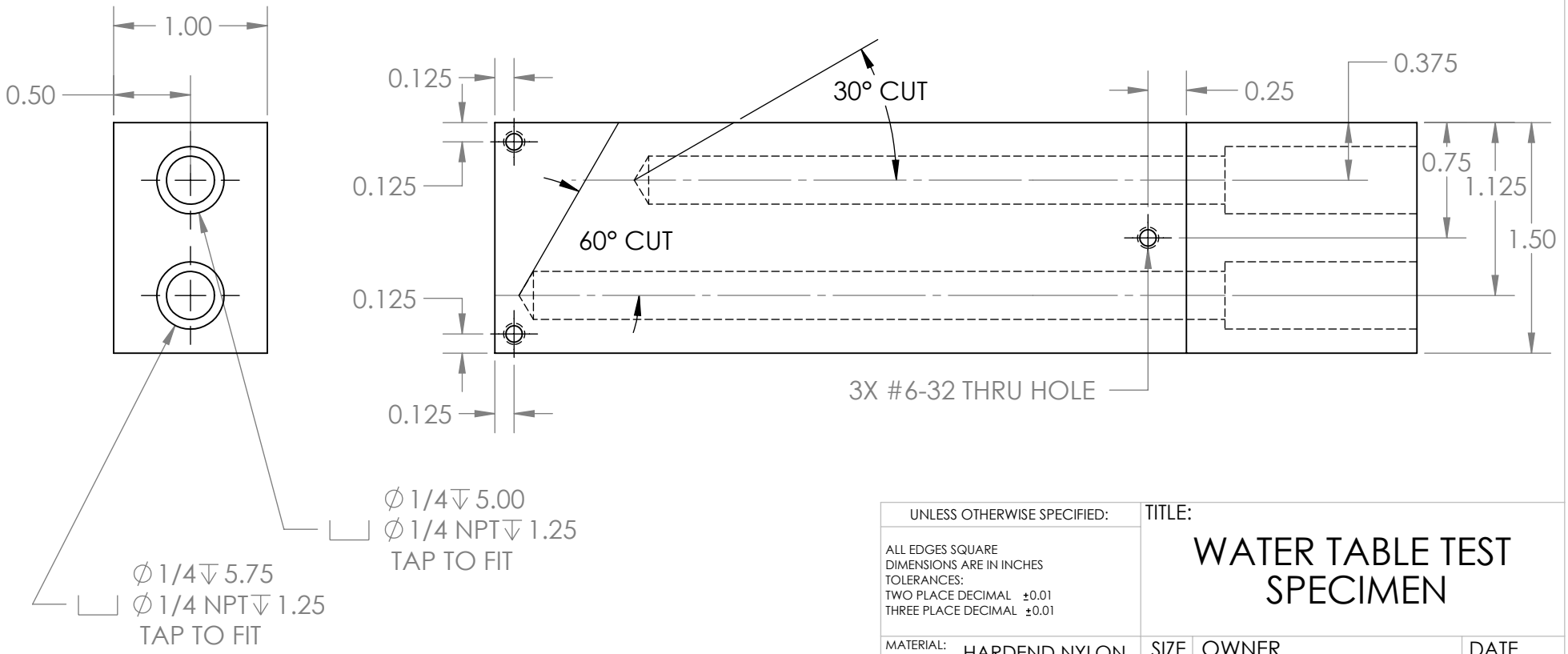

60°(OR 90°) AND 30° (OR 45°) CUT THICKNESS IS NOT CRITICAL

UNLESS OTHERWISE SPECIFIED:	TITLE: WATER TABLE TEST SPECIMEN
ALL EDGES SQUARE DIMENSIONS ARE IN INCHES TOLERANCES: TWO PLACE DECIMAL ±0.01 THREE PLACE DECIMAL ±0.01	
MATERIAL: HARDEND NYLON	SIZE A / OWNER AUSTIN CULBERSON / DATE 12/15/14
COMMENTS:	SCALE: 1:1 / WEIGHT: - lb. / SHEET 1 OF 1

5 4 3 2 1

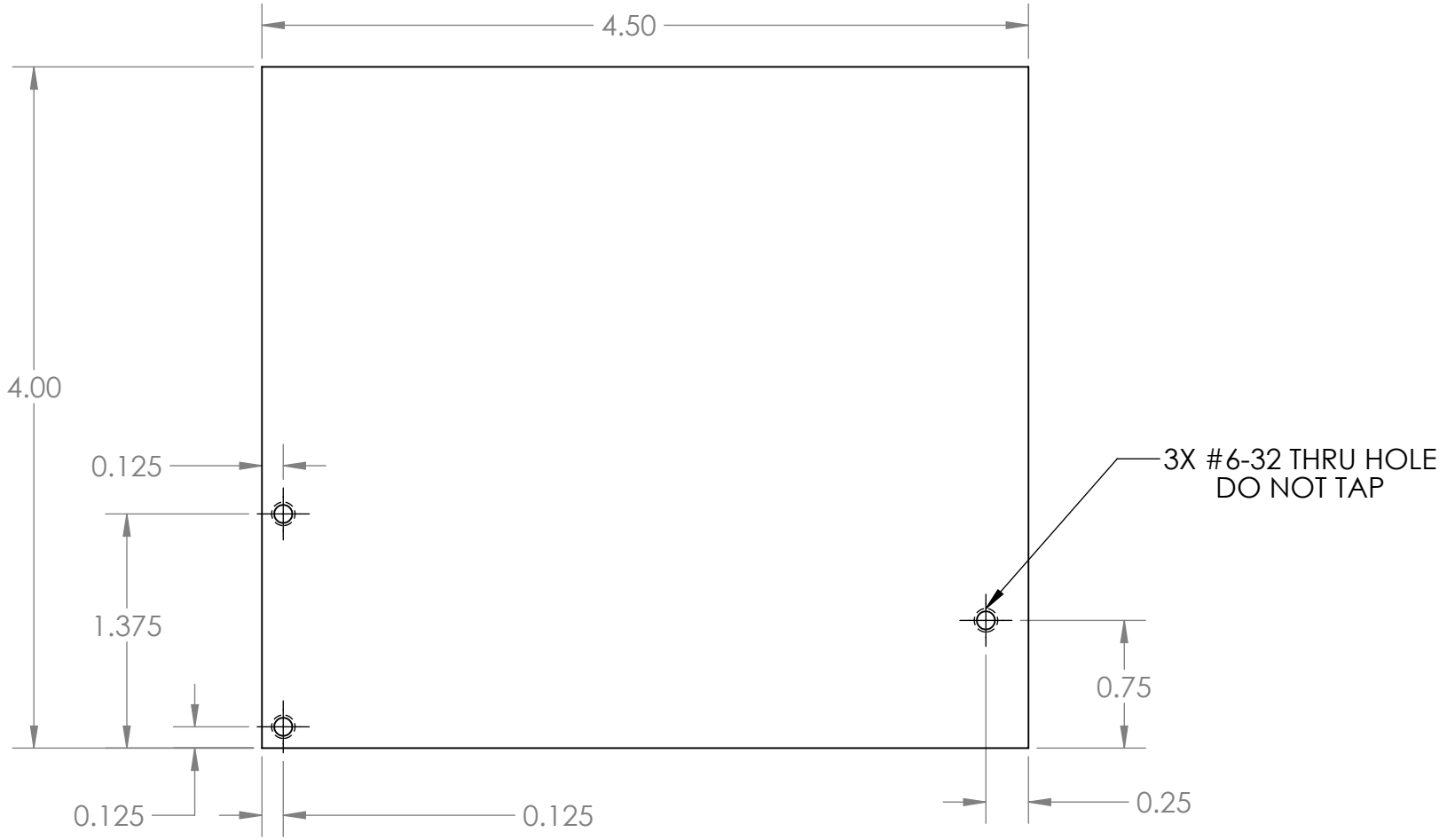

UNLESS OTHERWISE SPECIFIED: ALL EDGES SQUARE DIMENSIONS ARE IN INCHES TOLERANCES: TWO PLACE DECIMAL ±0.01 THREE PLACE DECIMAL ±0.01	TITLE: WATER TABLE VIEWING WINDOW		
MATERIAL: PLASTIC	SIZE A	OWNER AUSTIN CULBERSON	DATE 12/17/14
COMMENTS:	SCALE: 1:1	WEIGHT: - lb.	SHEET 1 OF 1

SUPPLIED PLASTIC DEFINES THICKNESS

5 4 3 2 1

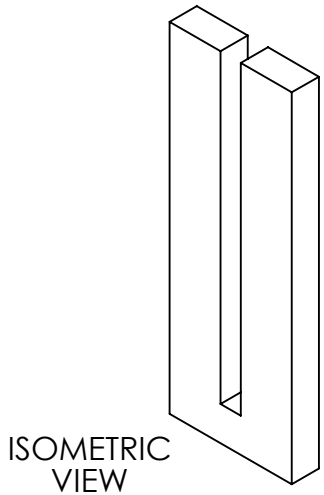

ISOMETRIC VIEW

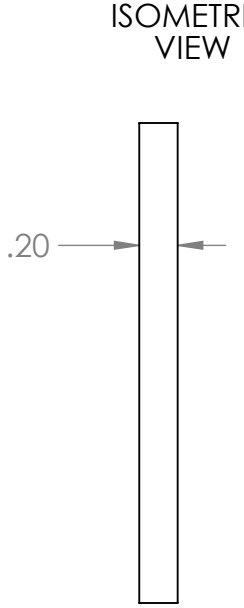

RIGHT VIEW

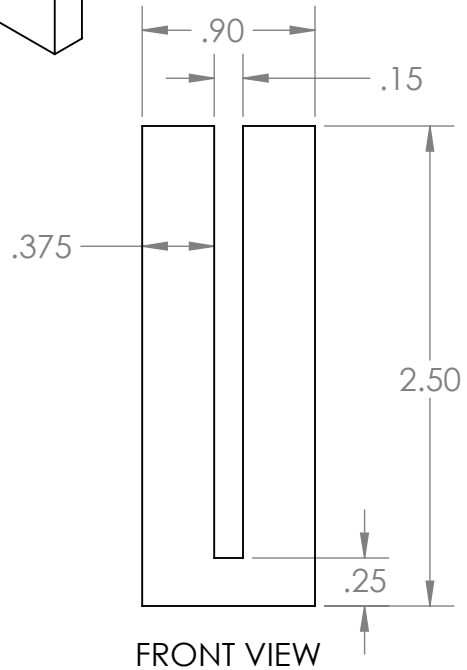

FRONT VIEW

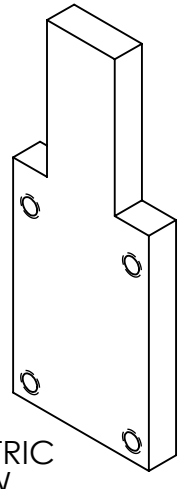

ISOMETRIC VIEW

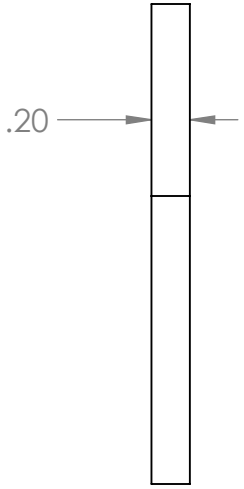

RIGHT VIEW

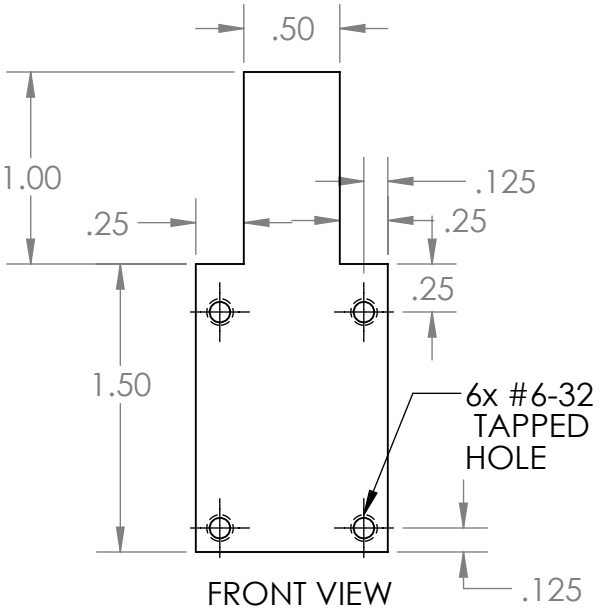

FRONT VIEW

UNLESS OTHERWISE SPECIFIED: ALL EDGES SQUARE DIMENSIONS ARE IN INCHES TOLERANCES: TWO PLACE DECIMAL ±0.01 THREE PLACE DECIMAL ±0.01	TITLE: FLOW CHANNEL GATE/ PULSATION PLATE		
MATERIAL: UNSPECIFIED	SIZE A	OWNER AUSTIN CULBERSON	DATE 1/4/15
COMMENTS:	SCALE: 1:1	WEIGHT: -	SHEET 1 OF 1

5 4 3 2 1

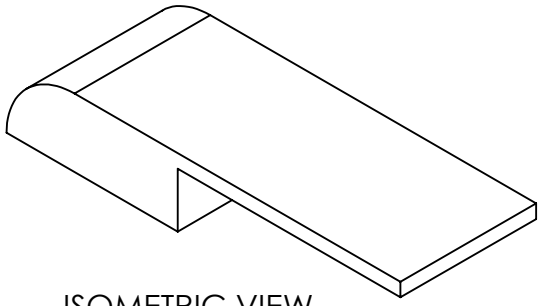

ISOMETRIC VIEW

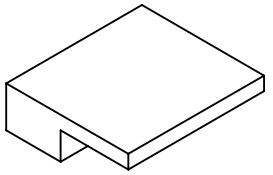

ISOMETRIC VIEW

TOP VIEW

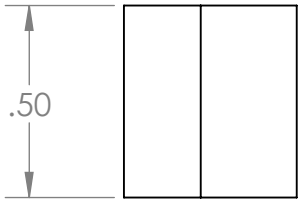

TOP VIEW

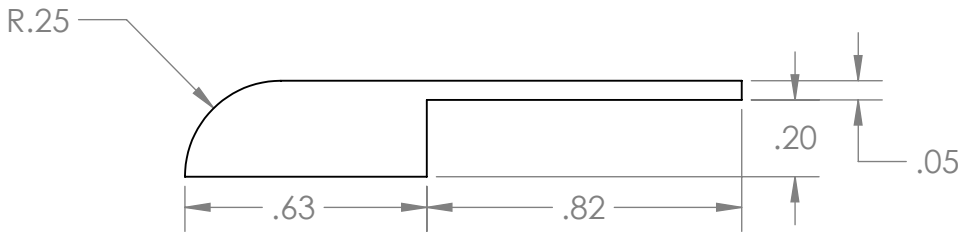

FRONT VIEW

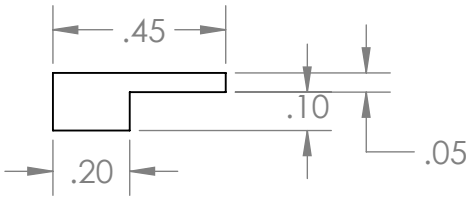

FRONT VIEW

UNLESS OTHERWISE SPECIFIED: ALL EDGES SQUARE DIMENSIONS ARE IN INCHES TOLERANCES: TWO PLACE DECIMAL ±0.01 THREE PLACE DECIMAL ±0.01	TITLE: FLATE PLATE TESTING VENTILATION NOZZLES		
MATERIAL: UNSPECIFIED	SIZE A	OWNER AUSTIN CULBERSON	DATE 1/5/15
COMMENTS:	SCALE: 2:1	WEIGHT: -	SHEET 1 OF 1

5 4 3 2 1

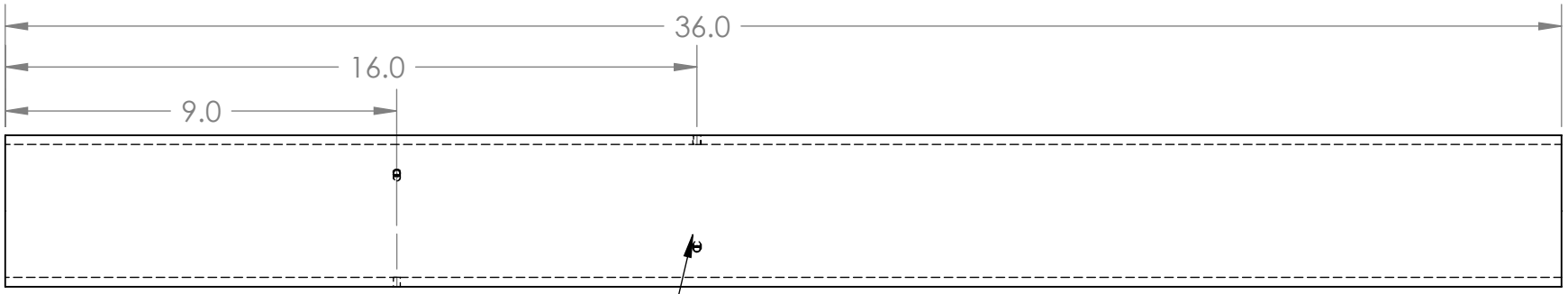

6X #10-32 Tapped Hole

SIDE VIEW
SCALE 1:4

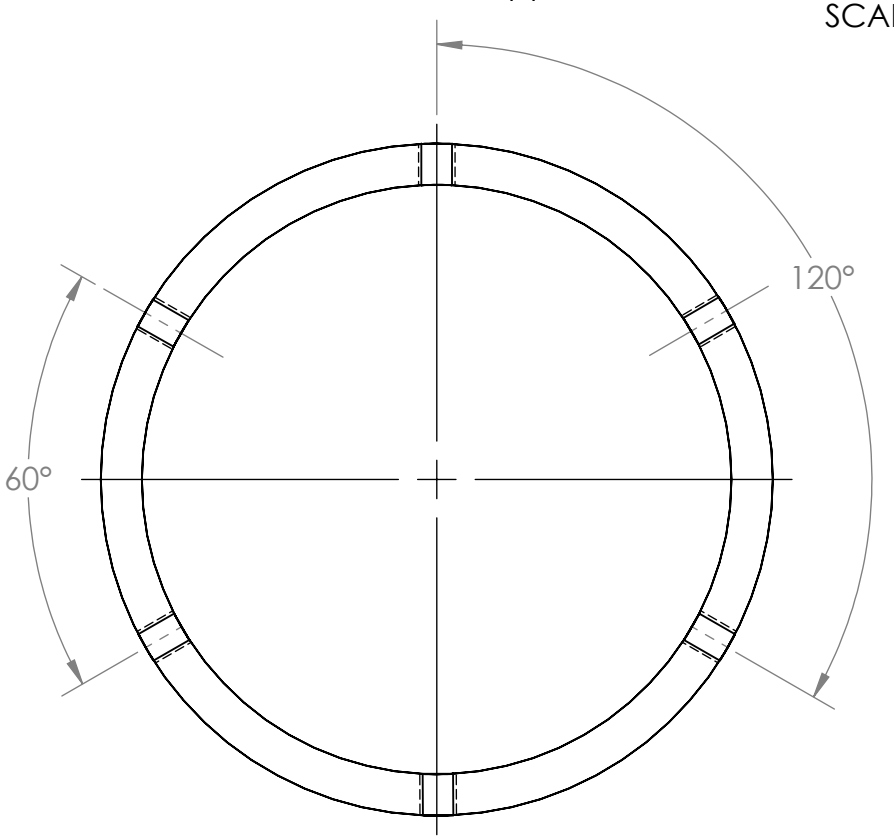

FRONT VIEW
SCALE 1:1

HOLES ARE SPACED 120° WITH 60° OFFSET BETWEEN ROWS

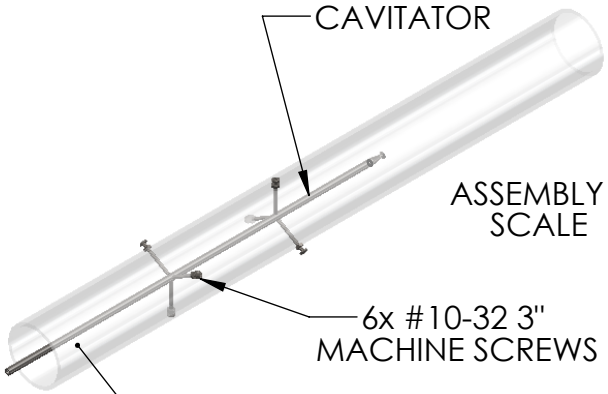

ASSEMBLY VIEW
SCALE 1:9

UNLESS OTHERWISE SPECIFIED: ALL EDGES SQUARE DIMENSIONS ARE IN INCHES TOLERANCES: TWO PLACE DECIMAL ±0.01 THREE PLACE DECIMAL ±0.01 ANGLES ±1°	TITLE: TEST SECTION VIEWING TUBE		
MATERIAL: ACRYLIC	SIZE A	OWNER AUSTIN CULBERSON	DATE 4/2/14
COMMENTS: TUBE IS STOCK 3" SCH. 40	SCALE: N/A	WEIGHT: N/A	SHEET 1 OF 1

5 4 3 2 1

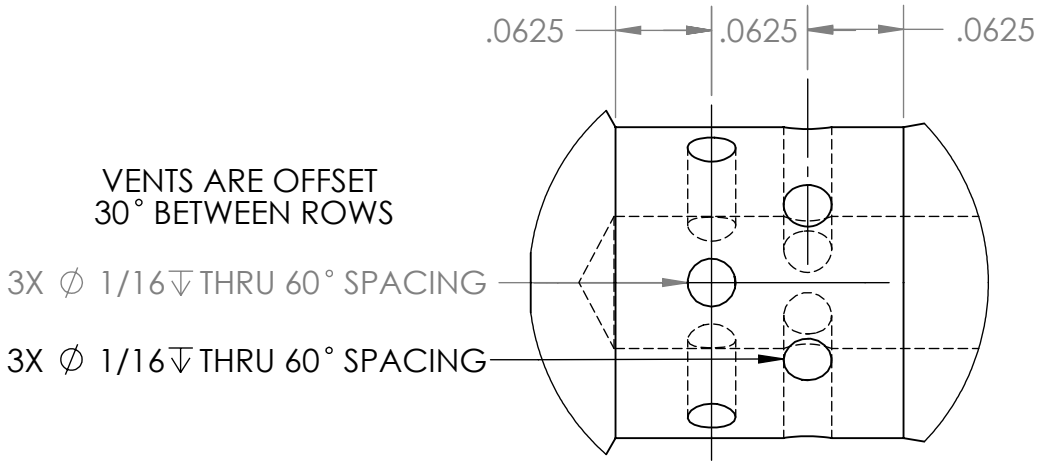

DETAIL A
SCALE 8 : 1

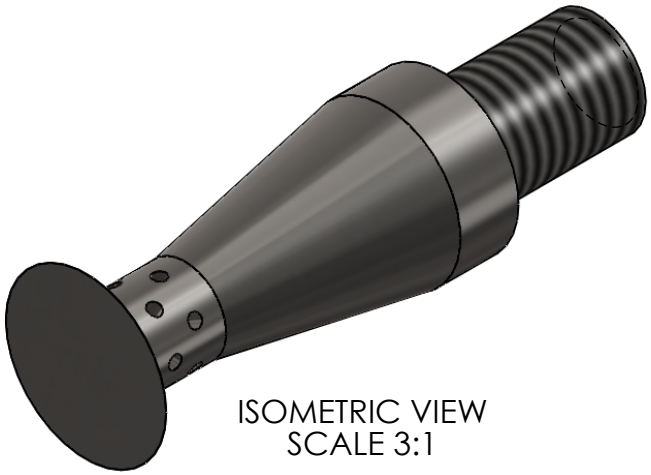

ISOMETRIC VIEW
SCALE 3:1

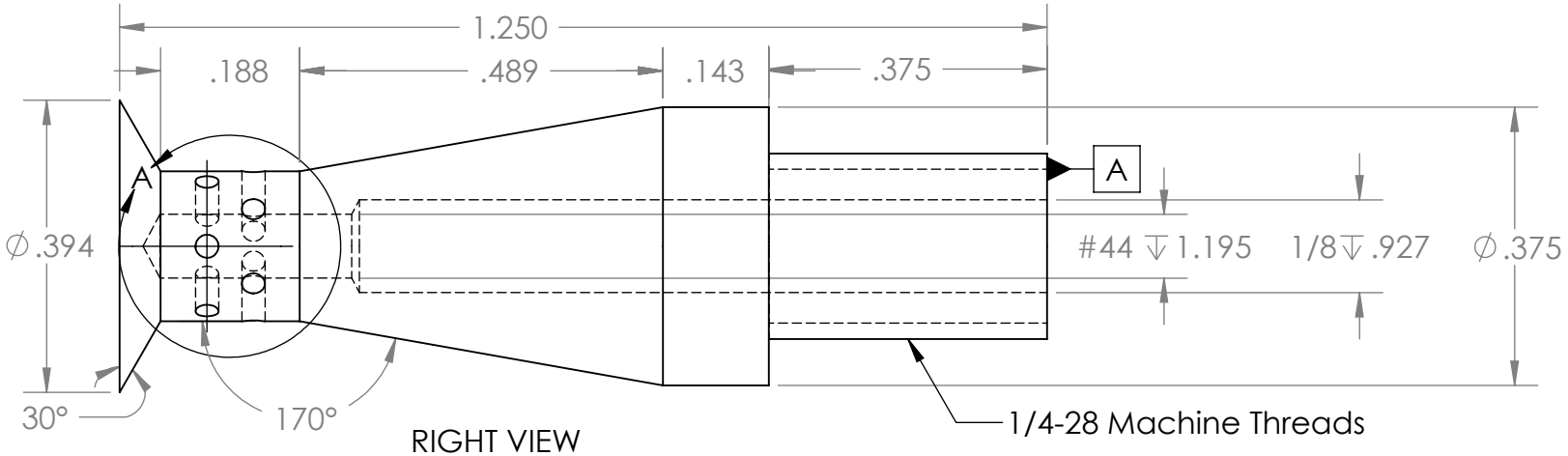

RIGHT VIEW
SCALE 4:1

CAVITATOR IS DESIGNED TO INTERFACE WITH A 3/8" OUTER VENTILATION AND SUPPORT TUBE WITH 1/4-28 INTERIOR THREADS

UNLESS OTHERWISE SPECIFIED: ALL EDGES SQUARE DIMENSIONS ARE IN INCHES TOLERANCES: TWO PLACE DECIMAL ±1/64 THREE PLACE DECIMAL ±1/64 ANGLES ±0.5°	TITLE: 1 CM DISC CAVITATOR
MATERIAL: STAINLESS	SIZE A | OWNER AUSTIN CULBERSON | DATE 3/14/14
COMMENTS: HOLE DEPTHS TAKEN FROM DATUM SURFACE A	SCALE:N/A | WEIGHT: N/A | SHEET 1 OF 1

5 4 3 2 1

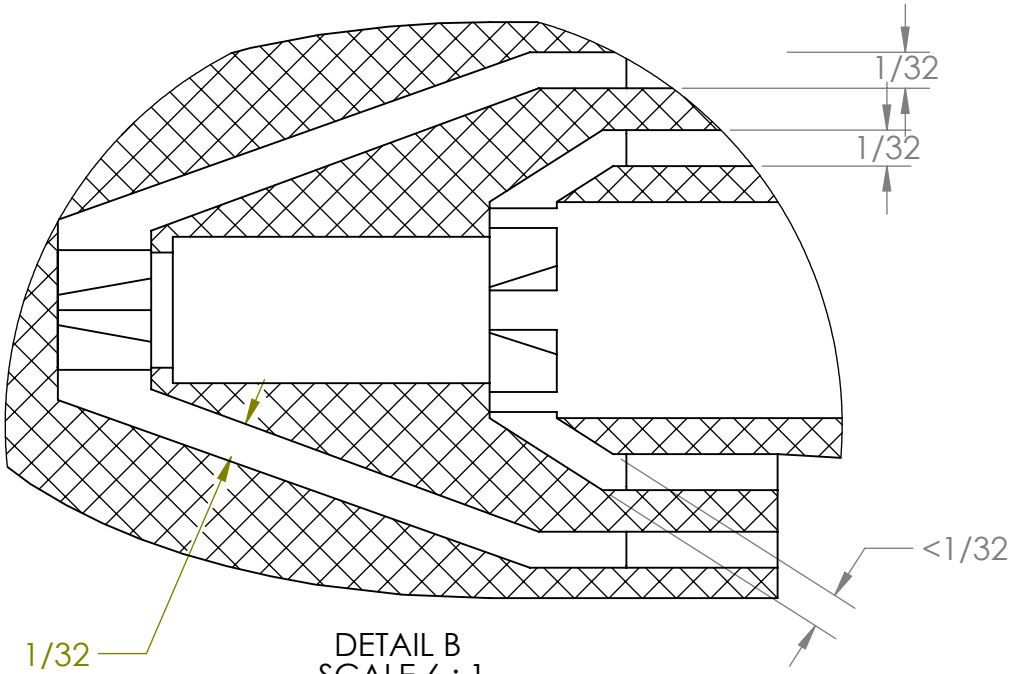

DETAIL B
SCALE 6 : 1

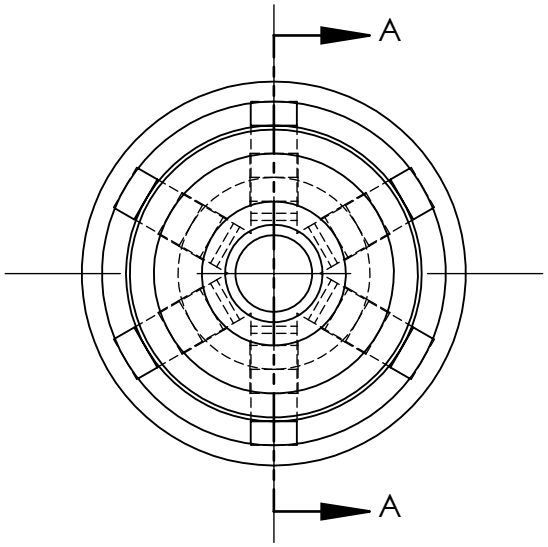

REAR VIEW
SCALE 4:1

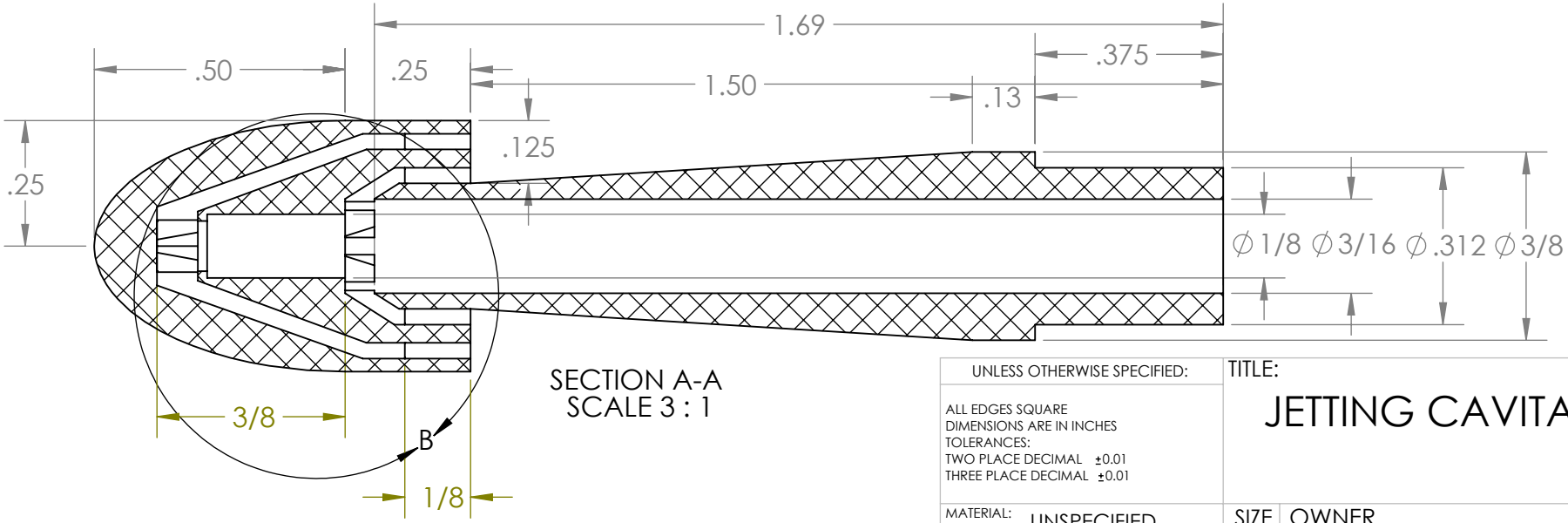

SECTION A-A
SCALE 3 : 1

UNLESS OTHERWISE SPECIFIED: ALL EDGES SQUARE DIMENSIONS ARE IN INCHES TOLERANCES: TWO PLACE DECIMAL ±0.01 THREE PLACE DECIMAL ±0.01	TITLE: JETTING CAVITATOR		
MATERIAL: UNSPECIFIED	SIZE A	OWNER AUSTIN CULBERSON	DATE 3/13/15
COMMENTS:	SCALE: -	WEIGHT: - lb.	SHEET 1 OF 1

5 4 3 2 1

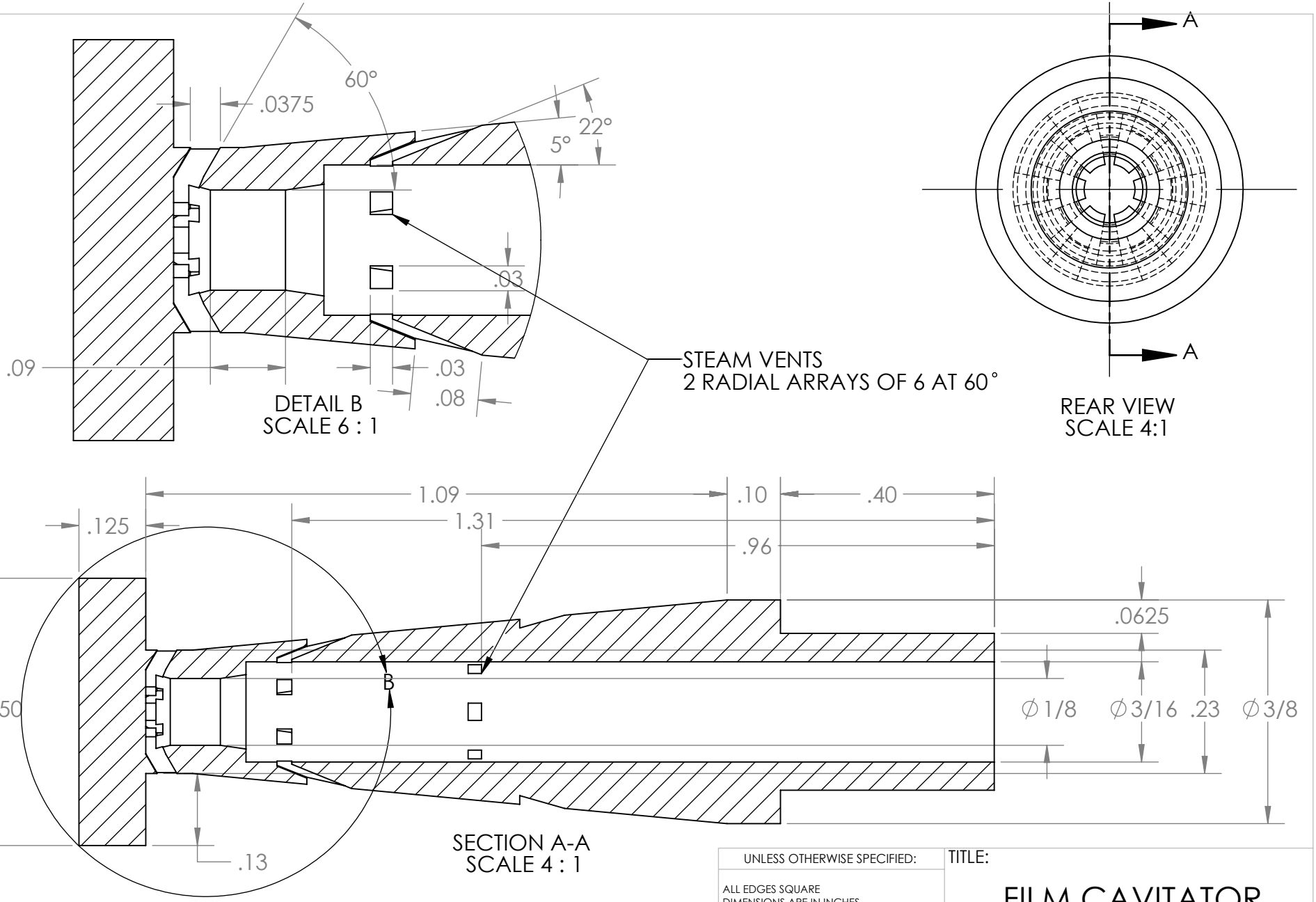

UNLESS OTHERWISE SPECIFIED:	TITLE: FILM CAVITATOR		
ALL EDGES SQUARE DIMENSIONS ARE IN INCHES TOLERANCES: TWO PLACE DECIMAL ±0.01 THREE PLACE DECIMAL ±0.01			
MATERIAL: UNSPECIFIED	SIZE: A	OWNER: AUSTIN CULBERSON	DATE: 4/2/15
COMMENTS:	SCALE: -	WEIGHT: -	SHEET 1 OF 1

ALL VENTILATION HOLES ARE CUT 0.03 x 0.03. STEAM VENTS ARE CUT 18° RELATIVE TO CAVITATOR OUTER SURFACE

5 4 3 2 1